Proto-planetary disc evolution and dispersal

Giovanni Pietro Rosotti

München 2014

Proto-planetary disc evolution and dispersal

Giovanni Pietro Rosotti

Dissertation
an der Fakultät für Physik
der Ludwig–Maximilians–Universität
München

vorgelegt von
Giovanni Pietro Rosotti
aus Monza, Italien

München, den 28. August 2014

Contents

Zusammenfassung

Planeten entstehen innerhalb einer Gas- und Staubscheibe, die um einen Protostern rotiert. Dabei bestimmt die Lebensdauer der protostellaren Scheibe die Zeitskala für die Bildung von Planeten. Die charakteristischen Eigenschaften eines neu gebildeten Planetensystems werden von der Dynamik der Gas-Staubscheibe vorgegeben.

Aufgrund zahlreicher Beobachtungen können protostellar Scheiben klassifiziert und unterschiedlichen Klassen zugeordnet werden. Die sogenannten "Übergangsscheiben" mit einem staubfreien inneren Scheibenbereich bilden dabei eine eigene Klasse. Hinsichtlich ihrer dynamischen Entwicklung wird angenommen, dass die Übergangsscheiben das Endstadium der Scheibenentwicklung repräsentieren. Numerische Simulationen von Übergangsscheiben können dazu beitragen, die für die Scheibendynamik dominanten physikalischen Prozesse herauszuarbeiten. Bisher wurden die Planetenentstehung und die Photoevaporation durch hochenergetische Röntgenphotonen als dominierender physikalischer Prozess bei der Bildung von Übergangsscheiben separat untersucht. Die simultane Berücksichtigung beider Prozesse und ihre wechselseitige Einflussnahme wird im ersten Teil dieser Arbeit betrachtet.

In dieser Arbeit wird auch der Einfluss eines Jupiterähnlichen Planeten auf die Lebensdauer der Übergangsscheibe untersucht. Es wird gezeigt, dass durch einen Jupiterähnlichen Planeten die Lebensdauer maßgeblich verkürzt wird, indem die inneren Scheibenregionen von den äußeren Scheibenregionen und somit vom Massenreservoir getrennt werden. Dies führt im Vergleich mit dem Photoevaporationsprozess zu größeren (Gas)Lücken in den Übergangsscheiben bei gleicher Massenakkretionsrate. Durch die Berücksichtigung jupiterähnlicher Planeten lassen sich somit die durch Beobachtungen dokumentierten Übergangsscheiben mit großen Lücken erklären. Bei zusätzlicher Berücksichtigung eines als "thermal sweeping" genannten Prozesses durchläuft die Übergangsscheibe eine Instabilität, die die Zerstörung der Scheibe innerhalb von 10 000 Jahren zur Folge hat. Dieser Prozess kann - da auch die äußeren Scheibenbereiche nur über sehr kleine Zeitskalen ausgebildet werden (in Abhängigkeit von der Röntgenquelle) - als ein Erklärungsversuch für die geringe Anzahl beobachteter Übergangsscheiben mit vernachlässigender Massenakkretion dienen. "Thermal sweeping" scheint jedoch nicht effizient genug zu sein, um den Beobachtungsstatistiken zu genügen.

Als weiterer Teil dieser Arbeit, wird am Beispiel des Photoevaporationsprozesses zwanglos die anhand von Beobachtungsergebnissen nachgewiesene Korrelation zwischen der Protosternmasse und der Massenakkretionsrate nachvollzogen. Somit kommt dem Photoevap-

orationsprozess (durch hochenergetische Röntgenphotonen) gegenüber anderen möglichen Prozessen eine herausgehobene Stellung zu.

Als weiterer Prozess wird in dieser Arbeit die dynamische Wechselwirkung von protostellaren Scheiben und vorbeifliegenden Sternen wurde untersucht. Zu diesem Zweck wurde ein Modell entwickelt, dass den Einfluss der Stellardynamik auf die protostellaren Scheiben im Muttercluster analysiert. Dabei wurden erstmals Stellar- und Scheibendynamik simultan modelliert. Die Simulationsergebnisse belegen, dass "close encounters" zwar nicht einen signifikanten Einfluss auf die Scheibenmasse, wohl aber auf die Größe der protostellaren Scheiben haben und eine obere Grenze definieren.

Eine Untersuchung, inwiefern auch über die Lebensdauer protostellarer Scheiben hinaus eine Neuausbildung von Scheiben möglich ist, schließt die vorliegende Arbeit ab. Sobald sich der Stern in einem Gebiet aktiver Sternentstehung befindet, ist es für ihn möglich, Materie aus dem interstellaren Medium zu akkumulieren und eine Scheibe auszubilden. Abschätzungen ergaben, dass durch diesen Prozess einige Sterne (im Prozentbereich) in Sternentstehungsgebieten eine Scheibe der zweiten Generation ausbilden, die in Zusammenhang mit den beobachteten "old accretors" stehen könnten.

Abstract

Planets form from gas and dust discs in orbit around young stars. The timescale for planet formation is constrained by the lifetime of these discs. The properties of the formed planetary systems depend thus on the evolution and final dispersal of the discs, which is the main topic of this thesis.

Observations reveal the existence of a class of discs called "transitional", which lack dust in their inner regions. They are thought to be the last stage before the complete disc dispersal, and hence they may provide the key to understanding the mechanisms behind disc evolution. X-ray photoevaporation and planet formation have been studied as possible physical mechanisms responsible for the final dispersal of discs. However up to now, these two phenomena have been studied separately, neglecting any possible feedback or interaction. In this thesis we have investigated what is the interplay between these two processes.

We show that the presence of a giant planet in a photo-evaporating disc can significantly shorten its lifetime, by cutting the inner regions from the mass reservoir in the exterior of the disc. This mechanism produces transition discs that for a given mass accretion rate have larger holes than in models considering only X-ray photo-evaporation, constituting a possible route to the formation of accreting transition discs with large holes. These discs are found in observations and still constitute a puzzle for the theory. Inclusion of the phenomenon called "thermal sweeping", a violent instability that can destroy a whole disc in as little as 10^4 years, shows that the outer disc left can be very short-lived (depending on the X-ray luminosity of the star), possibly explaining why very few non accreting transition discs are observed. However the mechanism does not seem to be efficient enough to reconcile with observations.

In this thesis we also show that X-ray photo-evaporation naturally explains the observed correlation between stellar masses and accretion rates and is therefore the ideal candidate for driving disc evolution.

Another process that can influence discs is a close encounter with another star. In this thesis we develop a model to study the effect of stellar dynamics in the natal stellar cluster on the discs, following for the first time at the same time the stellar dynamics together with the evolution of the discs. We find that, although close encounters with stars are unlikely to change significantly the mass of a disc, they can change substantially its size, hence imposing an upper limit on the observed disc radii.

Finally, we investigated in this thesis whether discs can be reformed after their dispersal.

If a star happens to be in a region that is currently forming stars, it can accrete material from the interstellar medium. This mechanism may result in the production of "second generation" discs such that in a given star forming region a few percent of stars may still possess a disc, in tentative agreement with observations of so called "old accretors", which are difficult to explain within the current paradigm of disc evolution and dispersal.

Chapter 1

Introduction

1.1 The cartoon of star and planet formation

Stars form from the gravitational collapse of dense clumps of molecular gas. As clumps are observed to be rotating, angular momentum conservation dictates that the star will be surrounded by a disc. The outskirts of the original clump are left in the so-called "envelope", which slowly accretes onto the protostar. Depending on the masses of disc and envelope, protostars have been empirically divided in classes, ranging from 0 to III. The most relevant for the purposes of this thesis is the class II, where the envelope has become negligible but the protostar is still surrounded by a disc. It is at this stage that the disc is normally called "proto-planetary disc". According to the theory of core accretion, small dust grains collide, stick together and thus grow, until they become planetesimals (bodies held together by gravity) and finally planets. Finally, class III is the last phase where the star (still finishing to contract before arriving on the main sequence) is mostly "naked", and the only materials left orbiting it are planetesimals and planets.

The main relevance of proto-planetary discs is that planet formation is happening in them. Until recently, we were aware of the existence of only 8 planets, the ones comprising the Solar System. A major breakthrough in the development of planet formation came in 1995, when Mayor & Queloz (1995) discovered the first exoplanet around a main sequence star. Since that first discovery, we know nowadays almost 2000 exoplanets. These observations are now able to put constraints on the exoplanet population, and we now think that more than 50% of all stars host at least a planet around them (Mayor et al., 2011; Fressin et al., 2013). The most striking aspect of these exo-planets is that they are very different from our own solar System: exo-planets show a huge variety of eccentricities, radii, masses and densities. Whole classes of planets which do not even exist in the solar system are present, like super Earths and hot Jupiters, just to name a few. This has caused a big revolution in planet formation theories, which were before focused in explaining the formation of the solar system only. Planet formaton theories predict (Pollack et al., 1996) that planet formation is a slow process, taking some Myrs. This is roughly the same timescale as the lifetime of proto-planetary discs. Therefore, understanding disc evolution is fundamental

to have a coherent and complete picture of planet formation; we expect that, depending on when exactly disc dispersal happens, and the exact way in which it proceeds, this can have a big impact on the properties of the planetary systems. Admittedly, we are still far from this final objective of understanding in detail the correlations between the evolution of discs and those of planetary systems and such a daunting task is outside the scope of this thesis. Nevertheless, we will show in this thesis how planet formation, especially in the case of giant planets, and X-ray photoevaporation, one of the main processes leading to disc dispersal, have a deep interplay that leaves imprints on the discs.

1.2 Proto-planetary discs: basic facts from observations

1.2.1 The existence of proto-planetary discs

The very fact that proto-planetary discs exist is a consequence of the fundamental law of angular momentum conservation. Let us take the Solar System as an example.

We can estimate the angular momentum of the Sun as

$$J_\odot = k M_\odot R_\odot^2 \Omega, \tag{1.1}$$

where k is a constant of order unity. Since the Sun rotational period is ~ 25 days, the total angular momentum of the Sun is roughly $\simeq 3 \times 10^{49} k$ cm^2 g s^{-1}. The angular momentum in a point mass in Keplerian rotation around the Sun is given by

$$J_p = M_p \sqrt{G M_\odot a_p}, \tag{1.2}$$

which evaluated for Jupiter gives $\simeq 2 \times 10^{50}$ cm^2 g s^{-1}. This shows how most of the angular momentum of the Solar System is not in the Sun, but rather in the planets. Still, the angular momentum in the Solar System is much less than the one in a molecular cloud core (the progenitor of a star). Typical values, knowing that cores typically have a rotational kinetic energy which is $1-2$ % of their gravitational energy, for a $1 M_\odot$ core are of order of $J_{core} = 9 \times 10^{53}$ cm^2 g s^{-1}. It is true that young stars are faster rotators than the Sun, but the difference is at most 2 orders of magnitude (Soderblom et al., 2013) (as the maximum speed is limited by the breakup velocity) and cannot account for the missing angular momentum. As the collapse cannot create or dissipate angular momentum, this shows that during the collapse a structure must have formed where the angular momentum was stored. It also points out that some mechanism must have happened later in this structure that has dissipated (i.e., transported somewhere else) this angular momentum. The most straightforward hypothesis is that the angular momentum is accumulated in a rotationally supported, thin structure: a proto-planetary disc. The issue of the transport of angular momentum will be addressed in the next section.

It is also possible to estimate the size of discs. The (average) specific angular momentum of a parcel of gas is: $j = J/M \simeq 4 \times 10^{20}$ cm s^{-1}. If we assume that the specific angular

Figure 1.1: HST compilation of proplyds images. The bright part of the proplyd is due to gas that is ionized from the high energy photons of nearby massive stars. Instead, the black part is tracing the bulk of the disc, where the dust makes it optically thick and thus visible in absorption against the bright background.

momentum of the material that is going to form the disc is conserved during the collapse, then we can use Kepler laws to find the radius of circularization: $r_{circ} = j^2/(GM) \simeq 100 \; AU$.

Consistently with this picture, observations indeed indisputably prove that discs exist. Some of the most spectacular images of discs come from Hubble Space Telescope (HST) images of the Orion Nebula Cluster (ONC), shown in figure 1.1, where the discs can be seen in silhouette (due to their high optical depth at optical wavelengths) on top of the reflection nebula behind (O'dell et al., 1993a). The images also show that they have a flattened structure.

More in general, two are two characteristic signatures of the presence of proto-planetary discs. Discs are composed by gas (which constitutes the bulk of their mass) and a small amount of dust (typically 1 %) by mass. Despite the fact that most of the mass is in the gas, it is the dust that provides most of the opacity of a disc, making it usually optically
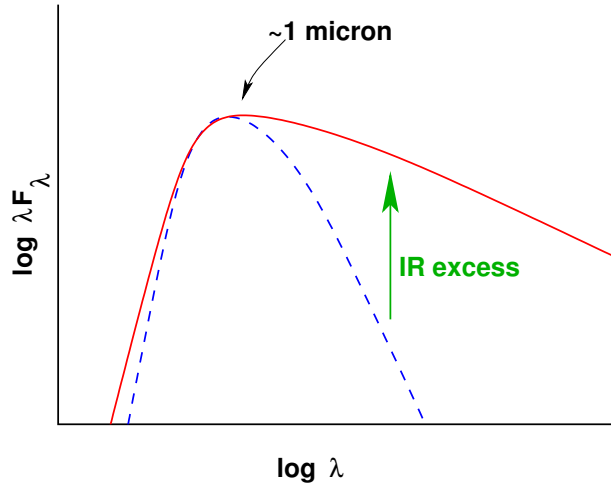
Figure 1.2: Sketch of an SED of a proto-planetary disc. The blue dashed line shows the photosphere of the star, while the red solid line is the total emission. Both the IR and UV excess discussed in the text are visible. From Armitage (2007).

thick at all wavelenghts smaller than the far infra-red (FIR). The dust intercepts and absorbs the radiation from the central star, which heats it to temperatures ranging from tens (in the outskirts) to thousands (at the dust destruction radius, some fractions of AU from the star) of K. The corresponding thermal emission from the dust ranges from the near infra-red (NIR) to the sub-mm. If we are not able to spatially resolve the disc-star system, this emission sums up with the one of the star when looking at the spectral energy distribution (SED) of the source. With respect to a "naked" star, the disc contributes at any wavelength longer than the NIR, giving rise to the so called IR excess (see figure 1.2). Also the presence of an envelope, which reprocesses the light emitted by the star, causes an IR excess. Therefore, we can use the IR excess as a signature of a proto-star. More specifically, the slope of the SED in the NIR, defined as:

$$\alpha_{IR} = \frac{d \log \lambda F_\lambda}{d \log \lambda}, \tag{1.3}$$

depends on the relative importance of the envelope and of the disc. This is the origin of the classification in classes (Lada & Wilking, 1984) of proto-stars. Class IIs (that is, star+disc systems) are characterized by a slope $-1.6 < \alpha_{IR} < -0.3$.

In addition, class II sources are also known to show an ultra violet (UV) excess. This emission comes from the innermost radii of the disc, where the material is falling onto the star. In the magneto-accretion paradigm (Ghosh & Lamb, 1979a,b; Koenigl, 1991; Shu et al., 1994), the magnetic field of the star is strong enough to truncate the disc at a few stellar radii. Inside this radius, the material falls onto the star following the magnetic field lines at almost free-fall velocities. When this material impacts on the surface, it shocks and heats up. The typical temperatures are expected to be around $10^4 K$, so that the material is ionized. It will then emit thermally at UV wavelengths and show strong recombination lines, of which the most important is the $H\alpha$ line. Observations in the UV band or of
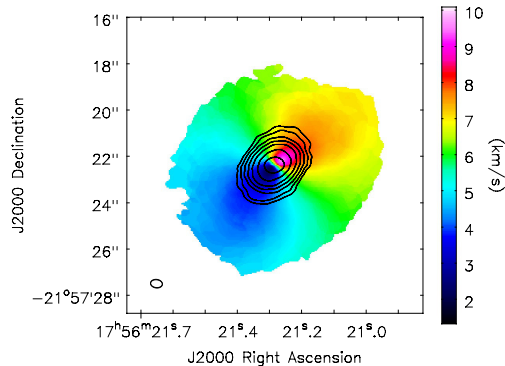
Figure 1.3: ALMA image of the disc around star HD 163296 (de Gregorio-Monsalvo et al., 2013). The black contours show the continuum emission, while the colours show the CO molecule emission. Different colours correspond to different speeds along the line of sight. The "butterfly" pattern in the image is typical of keplerian rotation.

the recombination lines are thus a probe of this accretion process. The reason why the accreted material has to become luminous can be understood regardless of the details of how the accretion takes place. In order to accrete onto the star, this material has to get rid of its energy, so that it can become bound to the star. The energy that must be lost to bring an amount of material m from infinity down to Keplerian rotation around a star of mass M_* and radius R_* is $\Delta E = \frac{1}{2}\frac{GM_*m}{R_*}$, and therefore the luminosity emitted is given by:

$$L = \frac{1}{2}\frac{GM_*\dot{M}}{R_*}. \tag{1.4}$$

Note that the surface of the star is not in keplerian rotation, and thus the energy emitted in the accretion process is actually higher than what given by equation 1.4. Also, this is the total energy emitted, and how much exactly is emitted at each wavelength depends on the details of how the accretion happens. Nevertheless, we can model these processes and estimate from the amount of UV excess the mass accretion rate onto the star $\dot{M}$.

Despite the name, the IR excess is actually present at all wavelengths longer than the NIR, since the Rayleigh-Jeans tail of the dust will always sum up with the emission of the photosphere of the star. There are two advantages that can be achieved when observing at longer wavelengths, in the mm regime:

1. the disc is usually optically thin at wavelengths longer than some hundreds of μm, allowing us to measure its mass (provided that the opacity of the dust is known);

2. the technique of interferometry allows us to achieves an angular resolution high enough to resolve the disc and detect features in it.

These techniques were first exploited to measure disc masses (Weintraub et al., 1989) and provide evidence, using the rotational transition of the CO molecule as a tracer, that the discs are in Keplerian rotation around their stars (Sargent & Beckwith, 1987). The field

of sub-mm astronomy saw major improvements in the last years, and such measurements are now routinely possible with modern facilities. At the moment of writing the Atacama Large Millimeter Array (ALMA) is being finalised, providing a major breakthrough in unprecedented sensitivity and spatial resolution.

Summarising, the main evidences of the existence of discs and the most important methods to detect and study them are:

- Shadows behind a bright background in the optical;

- IR excess;

- UV excess and recombination lines;

- Resolved images in the sub-mm.

1.2.2 Disc properties: observational findings

Proto-planetary discs are very well studied objects (a search on ADS for the word "proto-planetary discs" in the abstract returns more than 7000 results), and it is impossible to summarise all the observational findings in the few pages of this thesis. Excellent reviews are available in the literature, particualrly Williams & Cieza (2011a) that focuses on the observational aspect, and the reviews of the *Protostars and Planets* conference series. Here, we summarise only the findings that are useful for the purposes of this thesis, namely the ones concerning the topic of disc evolution and dispersal.

1.2.2.1 Mass accretion rates

As explained before, the UV excess allows to measure the mass accretion rate through the relation:

$$L = k\frac{GM_*\dot{M}}{R_*},\tag{1.5}$$

where the coefficient k is of order unity and takes into account the fact that the material is coming from the radius at which the disc is truncated by the magnetic fields of the star. A commonly used value is 0.8 (Gullbring et al., 1998).

Observationally, what we measure is the total luminosity, the one coming from accretion and the intrinsic one from the star. Therefore, it is necessary to have an independent knowledge of the star intrinsic properties to be able to disentangle the two. Theoretical models of stellar evolution (D'Antona & Mazzitelli, 1994; Siess et al., 2000) can provide us with a stellar template spectrum and give knowledge on the mass and the radius of the star, which is needed to convert the accretion luminosity into an accretion rate. Unfortunately these measures are complicated by extinction, which severely affects the UV wavelengths (star forming regions can be characterised by high extinctions if the sources are still embedded in the natal cloud). Typical values of the mass accretion rates are in the range 1×10^{-11}–1×10^{-7} (Gullbring et al., 1998).
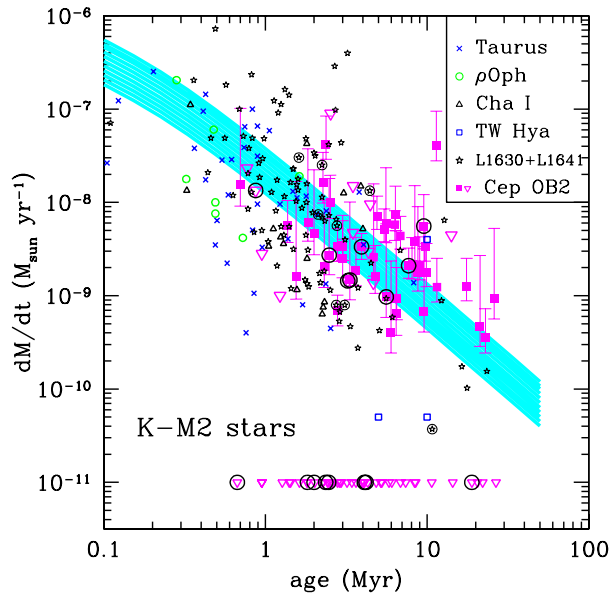
Figure 1.4: Dependence of the mass accretion rate with the stellar age for a compilation of sources from different star forming regions. From Sicilia-Aguilar et al. (2010).

Empirically, the mass accretion rate measured in the UV is found to correlate with the intensity of recombination lines in the spectrum of the star at optical and NIR wavelengths (Muzerolle et al., 1998; Calvet et al., 2004; Natta et al., 2004; Herczeg & Hillenbrand, 2008a). The most used ones are the Hα and Paβ lines. This has the advantage of being able to measure the mass accretion rates even for very obscured objects, where the UV is not visible or is contaminated. In addition, it is less time consuming. As with every empirical correlation, one should remember however of the intrinsic scatter of the relation. In addition, these lines do not trace only the accretion, but also the activity of the star taken in itself, and care should be put in separating the two contributions.

Measurements of the mass accretion rates are interesting to understand disc evolution when they are combined with the age of the star. Measuring the ages of a single star is usually done by placing them on a Herspting Russell (HR) diagram and fitting their position using theoretical tracks of stellar evolution. This is the same procedure that also provides the star mass and radius. However, ages are notoriously very uncertain to constrain, mainly due to theoretical uncertainties in the calculation of evolutionary tracks. The interested reader can consult the recent review by Soderblom et al. (2013) for more information. Despite these uncertainties, the mass accretion rates are found to have a very good correlation with the age of the star (Hartmann et al., 1998), as figure 1.4 shows. The mass accretion rate declines with age, and it can be fitted with a power-law with an exponent of -1.5. This is an important constraint that observations put for any theory of disc evolution.

Another finding of the observations is that the mass accretion rate, albeit with much spread, correlates with the mass of the star, a result reported by many authors (Muzerolle
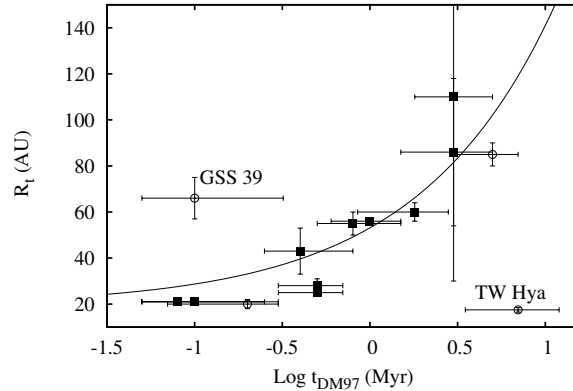
Figure 1.5: Disc size versus age of the host stars (Isella et al., 2009). Despite the big uncertainties, there is a positive correlation between the two quantities.

et al., 2003; Calvet et al., 2004; Mohanty et al., 2005; Natta et al., 2006; Herczeg & Hillenbrand, 2008a; Antoniucci et al., 2011; Biazzo et al., 2012; Manara et al., 2012a). The slope of the correlation was found by earlier investigations to be 2; current works usually estimate it to be around 1.7. While it is natural to expect more massive stars to accrete more material, a task left to the theory is to explain what is the exact mechanism producing the observed slope. This thesis contains an interpretation based on the framework of X-ray photo-evaporation.

1.2.2.2   Disc sizes

Measuring the disc size is a much more difficult task than measuring the mass accretion rate, and indeed it is known for a much smaller sample of discs. The task requires obviously high spatial resolution, but also to look at the right wavelength. As the outer parts of the discs are cold, these regions are not emitting in the NIR or MIR, and their emission starts to be important only at FIR and mm wavelengths. In practice, this forces this kind of observations to use sub-mm interferometry, which is the only technique in this range of the spectrum able to give the required spatial resolution. The only exception is the ONC, where the bright background allows us to see the discs in silhouette even at optical wavelengths, where we can take advantage of the high spatial resolution of HST. However, it should be kept in mind that the discs in the ONC are shaped by the high energy radiation from the massive stars of the Trapezium, so that results based on them cannot be easily generalised to all discs. In what follows, we restrict ourselves to studies that have used sub-mm interferometry.

Unfortunately, the sample for which these measurements are possible is small and the errors on these measures big, so that it is difficult to draw strong conclusions. Nevertheless, the results of these works is that the disc size has a positive correlation with the disc age (Isella et al., 2009; Guilloteau et al., 2011a), that is, older discs are also bigger, as shown in figure 1.5. As it will be explained in the next section, this is a natural result in the
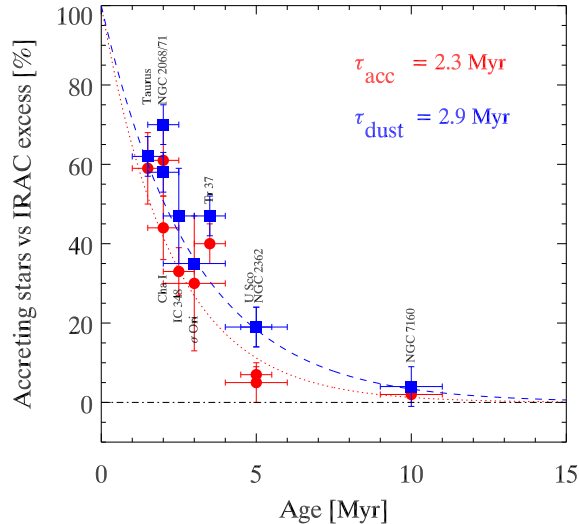
Figure 1.6: The fraction of stars that possess a disc (defined either through H*alpha* emission line, red dotted line, either through IR excess, blue dashed line) for different star forming regions as a function of their age. The decline with age, with a characteristic time-scale of $3 Myr$, is particularly evident. From Fedele et al. (2010a).

context of the theory of viscous discs.

1.2.3 Disc lifetimes

1.2.3.1 Nearby star forming regions

The two indicators that we have discussed so far show that discs evolve with time. However, they do not directly constrain what is the lifetime of a disc. A powerful observational probe of disc lifetimes comes from measuring the fraction of stars in a cluster that show IR or UV excess. We have already commented on the difficulties in estimating ages due to the uncertainties in pre-main sequence tracks. Looking at clusters has the advantage that, apart for the age spread inside the cluster, all stars are coeval. In addition, while it is also not without uncertainties, the age of a cluster is more solid than the age of a single star, as we can put together different clues and pieces of evidence. In theory, estimating the fraction of sources with an excess is as simple as counting how many sources are present, and how many of them show an excess. In practice, things can be much more complicated as assessing the completeness is not a simple task, and it is difficult to confirm or disprove the membership for sources in the same field of view. Despite these problems, a very strong result of this kind of studies (Haisch et al., 2001; Mamajek, 2009; Fedele et al., 2010a; Ribas et al., 2014) is that the disc fraction decreases with age, as figure 1.6 shows. The data is also good enough to allow to measure the disc lifetime, which is found to be on average of 3 Myr. This is the basic constraint coming from observations that any theory of disc dispersal must reproduce.

More in detail, the decline of the disc fraction is approximately exponential with time.

In addition, the IR and the UV excess disappear almost at the same time, so that there are very few sources that show only one of the two excesses. The exceptions exist, however, and a very important class of objects is the one of transition discs, usually discs that show UV excess but no IR excess. This class will receive much attention in the next parts of this thesis. The other class, discs with IR excess but no UV excess, are actually even more, as can be seen by comparing the two fractions. However, to the best of our knowledge they have not been studied extensively yet. One should also keep in mind that they could be just the result of a lower sensitivity in detecting the UV excess, and therefore they might just be old discs (therefore having a low mass accretion rate).

1.2.3.2   The problem of *old accretors*

The observational result on the disc lifetime we have discussed up to now was found when looking at nearby star forming regions, where detailed measurements of the two excesses are possible. It is usually not possible to push further away the measurements of the mass accretion rate, that usually need spectroscopy and are therefore time consuming. De Marchi et al. (2010) developed an innovative method for measuring accretion rates using only photometry. This relaxes the constraints on the measurements of mass accretion rates and makes it possible to study much more distant sources. In particular, De Marchi and collaborators studied extensively the star formation happening in the Magellanic Clouds (Beccari et al., 2010a; De Marchi et al., 2011a,e, 2013b). Their most striking finding is that accretion in these regions seems to persist for much longer than in the nearby star forming regions. Many of the observed accretors are found to be as old as $30 - 40$ Myr, and still accreting at high rates. This result was confirmed for many different regions.

Unfortunately, no other group has followed up yet these observations. It is important that these results get an independent confirmation, possibly through the use of an another method (but keep in mind the constraints due to the distance), as the results are difficult to reconcile within the current framework of disc evolution. It should be noted however that the old population is spatially more extended than the young one (De Marchi et al., 2011c), strengthening the validity of the age attribution; in addition, some of the old accretors also show IR excess (De Marchi et al., 2013b), which strengthens the interpretation that they possess discs. In this thesis, we will show that it is possible to envisage a theoretical scenario that can account for the presence of these discs.

1.3   Proto-planetary discs: basic theory of viscous discs

Having introduced the basic observational facts that discs exist and the constraints that are available on their evolution, we can now proceed to introduce the equations that are required to model them. Proto-planetary discs are an example of accretion discs, a structure that can be found in many different physical environments (around black holes, neutron stars, white dwarves,...) and much of what follows in this section can be applied in contexts outside star and planetary formation.

Before diving into the equations, it is worth to think why a disc can accrete. In the case of a test particle in orbit around a central mass, no accretion can happen: the test particle will continue to orbit forever. In order to accrete, the semi-major axis has to be reduced, and thus the angular momentum must decrease. However, the gravitational force is a central force - its torque vanishes, and angular momentum is a conserved quantity. Other forces must be present to reduce the angular momentum and allow accretion.

Since an accretion disc is a fluid structure, other forces do exist. Note however that internal forces cannot modify the total angular momentum. What they can do is to redistribute the angular momentum between the fluid elements - we will see later that this is done by viscosity that, thanks to the shear caused by differential rotation, transfers the angular momentum outwards. The approach we will follow is to write down the equations including the effects of viscosity, and show *a posteriori* that this actually leads to accretion.

We will make the assumption that the disc is thin, that is, its thickness H is much smaller than the distance from the star R. We will show that the thin disc approximation coincides with the condition that the sound speed c_s is much less than the rotational velocity v_ϕ. We will request also that the accretion is slow, namely that the radial velocity v_r is much less than both the sound speed and the rotational velocity. We have then an ordering of velocities given by:

$$v_r \ll c_\mathrm{s} \ll v_\phi. \tag{1.6}$$

The consistency of this ordering will be shown in due course.

Let us adopt a cylindrical coordinate system centered on the central object. The reference frame chosen is such that the $z = 0$ plane coincides with the disc plane. We will use R to label the spherical distance from the origin and $\boldsymbol{e}_R$ for the corresponding unit vector, while we will use r for the cylindrical coordinate and $\boldsymbol{e}_r$ for the corresponding unit vector. We assume azimuthal symmetry, so that quantities do not depend on the azimuthal coordinate ϕ.

Let us introduce the surface density $\Sigma(r, t)$:

$$\Sigma(r, t) = \int_{-\infty}^{+\infty} \rho(r, z, t)\mathrm{d}z, \tag{1.7}$$

where ρ is the volume density. We can rewrite the continuity equation in cylindrical coordinates using this new quantity:

$$\frac{\partial \Sigma}{\partial t} + \frac{1}{r}\frac{\partial}{\partial r}(r\Sigma v_r) = 0, \tag{1.8}$$

We assume that the disc is axisymmetric and thus we neglect the dependence on the ϕ angle. Since also the radial velocity appears as an unknown, we need another equation, which is supplied by the Navier-Stokes equation,

$$\frac{\partial \boldsymbol{v}}{\partial t} + (\boldsymbol{v} \cdot \boldsymbol{\nabla})\boldsymbol{v} = -\frac{1}{\rho}(\boldsymbol{\nabla} P - \boldsymbol{\nabla} \cdot w) - \boldsymbol{\nabla}\Phi, \tag{1.9}$$

Here $-\boldsymbol{\nabla}\Phi$ is the gravitational force (per unit mass) and w is the (shear) stress tensor (we neglect bulk viscosity), which in cartesian coordinates is given by:

$$w_{ij} = \eta \left[\frac{\partial v_i}{\partial x_j} + \frac{\partial v_j}{\partial x_i} - \frac{2}{3}(\boldsymbol{\nabla} \cdot \boldsymbol{v})\delta_{ij} \right], \tag{1.10}$$

where η is the dynamical viscosity coefficient. We can introduce also the kinematic viscosity coefficient $\nu = \eta/\rho$. In a purely circular flow, where the velocity is written as:

$$\boldsymbol{v} = v_\phi(r)\boldsymbol{e}_\phi, \tag{1.11}$$

where $\boldsymbol{e}_\phi$ is the azimuthal unit vector, it can be shown that the only non-vanishing component of the stress tensor in cylindrical coordinates is $w_{r\phi}$, and thus, expanding the tensor divergence in cylindrical coordinates, viscosity acts only in the tangential direction, due to the differential rotation that causes different annuli to shear with each other. It can be shown that for such a flow this component is given by:

$$w_{r\phi} = \rho\nu r \frac{\mathrm{d}\Omega}{\mathrm{d}r}, \tag{1.12}$$

and thus it scales linearly with the derivative of angular velocity. Note that it vanishes for a rigidly rotating flow. Actually, our flow is not purely circular, since also a small component of the radial velocity is present, but we can safely neglect this small contribution.

For simplicity, we make here the assumption that the gravitational potential is generated only by the central object, and we neglect the disc self-gravity. This assumption corresponds to stating that the disc mass is much less then the central object mass.

Thanks to the approximation done, the gravitational force is simply

$$-\boldsymbol{\nabla}\Phi = -\frac{GM}{R^2}\boldsymbol{e}_R, \tag{1.13}$$

so that the rotational velocity for circular orbits in the disc plane is the keplerian speed:

$$v_\phi^2 \simeq V_{\mathrm{k}}^2 = \frac{GM_{\mathrm{BH}}}{r}, \tag{1.14}$$

while the angular velocity is given by the third Kepler law:

$$\Omega_{\mathrm{k}}^2 = \frac{GM_{\mathrm{BH}}}{r^3}. \tag{1.15}$$

A relevant timescale, the dynamical time, can then be introduced:

$$t_{\mathrm{dyn}} = \frac{1}{\Omega_{\mathrm{k}}} = \sqrt{\frac{r^3}{GM_{\mathrm{BH}}}}. \tag{1.16}$$

We will see later on that the rotational speed has actually a small correction due to pressure gradients.

We now turn to examine the components of the vector equation (1.9).

1.3.1 Vertical structure: hydrostatic equilibrium

Since the vertical component of velocity is small, we can neglect the left hand-side of equation (1.9), and viscosity vanishes in the vertical direction. This component of Navier-Stokes equation then simply expresses the condition of hydrostatic equilibrium:

$$\frac{1}{\rho}\frac{\partial P}{\partial z} = -\frac{d\Phi}{dz}. \tag{1.17}$$

Neglecting self-gravity, we have to consider only the gravity of the central object. Since the disc is thin we can approximate the gravity force with:

$$-\frac{GM_{\mathrm{BH}}}{R^2}\boldsymbol{e}_R \cdot \boldsymbol{e}_z = -\frac{GM_{\mathrm{BH}}}{r^2+z^2}\boldsymbol{e}_R \cdot \boldsymbol{e}_z \sim -\frac{GM_{\mathrm{BH}}}{r^2}\frac{z}{r}, \tag{1.18}$$

so that we obtain a differential equation for the density:

$$\frac{c_{\mathrm{s}}^2}{\rho}\frac{\partial \rho}{\partial z} = -\frac{GM_{\mathrm{BH}}z}{r^3} = -\Omega_{\mathrm{k}}^2 z, \tag{1.19}$$

where we make the assumption of a barotropic fluid, for which the sound speed is defined as $c_{\mathrm{s}}^2 = \partial P/\partial \rho$. We have not yet specified the equation of state, a task that we will do later.

The equation can be integrated, giving the vertical density profile:

$$\rho(z) = \rho_0 \exp\left(-\frac{\Omega_K^2 z^2}{2c_{\mathrm{s}}^2}\right) = \rho_0 \exp\left(-\frac{z^2}{2H^2}\right). \tag{1.20}$$

The vertical profile is then a gaussian, with mid-plane density ρ_0 and scale-height H given by

$$H = \frac{c_{\mathrm{s}}}{\Omega_{\mathrm{k}}}. \tag{1.21}$$

Equation (1.21) gives a simple relation between the disc height, the sound speed and the angular velocity, that will turn out to be very useful. We can also compute the aspect ratio:

$$\frac{H}{r} = \frac{c_{\mathrm{s}}}{V_{\mathrm{k}}} \tag{1.22}$$

so that for the thin disc condition to be valid, the rotational velocity has to be much greater than the sound speed, that is $V_{\mathrm{k}} \gg c_{\mathrm{s}}$. The condition (1.22) expresses the fact that the disc height depends on temperature: the disc tends to expand in the vertical direction due to thermal motions, counteracting gravity.

1.3.2 Radial direction: centrifugal balance

Let us now consider the radial component of equation (1.9). The Eulerian derivative of velocity is small, since we assume slow accretion, and we can safely neglect it (remember our

ordering of velocities (1.6)). The advection term of velocity, once evaluated in cylindrical coordinates, gives the well known centripetal term $-v_\phi^2/r$. On the right hand side, the non vanishing terms are gravity and the pressure term, that we can express making use of the definition of the sound speed:

$$\frac{1}{\rho}\frac{\partial P}{\partial r} = \frac{c_s^2}{\rho}\frac{\partial \rho}{\partial r} \sim -\frac{c_s^2}{r} \tag{1.23}$$

and thus this term is small compared to the centrifugal term, but still greater than the radial velocity term; if we consider it, this leads to a small correction to the rotation curve with respect to a purely Keplerian curve. Thus a fluid disc has a slightly different rotation curve from a disc composed only by test particles, an effect caused by pressure. The force balance equation reads:

$$v_\phi^2 = \frac{GM_{\rm BH}}{r} + c_s^2\frac{{\rm d}\log\rho}{{\rm d}\log r} = v_{\rm k}^2 + c_s^2\frac{{\rm d}\log\rho}{{\rm d}\log r}. \tag{1.24}$$

Since usually the density decreases with radius, the actual rotation curve is slightly sub-Keplerian. In particular, if one assumes a power-law dependence for density $\rho \propto r^{-\beta}$:

$$v_\phi = V_{\rm k}\left[1 - \beta\left(\frac{c_s}{V_{\rm k}}\right)^2\right]^{1/2}. \tag{1.25}$$

The departure from a Keplerian rotation curve is usually a second order effect when one is interested in the gas dynamics of an accretion disc. However, it is very important in the context of planet formation. The dust particles in the disc do not feel the gas pressure, but rather the gas drag, a force whose magnitude is proportional to the difference of velocity between the gas and the dust:

$$F_{drag} \propto (\mathbf{v}_{\rm gas} - \mathbf{v}_{\rm dust}). \tag{1.26}$$

The proportionality constant depends on the dust grain size and on the density of the gas. Since the dust particles do not feel the gas pressure, they orbit at keplerian speed. As the gas is rotating slower than them, the dust particles feel a force that opposes to their rotation, causing them to loose angular momentum. The net effect is that the semi-major axis of the dust orbit reduces with time, and the dust eventually drifts onto the star. It can be shown that this effect is most important for particles that for typical conditions are around $1m$ big at $1AU$ from the central star (Weidenschilling, 1977a). This is the reason why this problem has been called "meter-sized problem". In the framework of core accretion, dust particles collide and stick together, growing from nm to km sizes. However, if once they reach a certain size they are removed by this drift onto the star, the whole process stops; planetesimals, and thus planets, cannot form. This is still an open problem and, although many solutions have been proposed (e.g., Youdin & Shu, 2002; Varnière & Tagger, 2006; Johansen et al., 2009; Pinilla et al., 2012c), a single one has not emerged yet.

1.3.3   Azimuthal direction: the mass diffusion equation

Due to the axial symmetry, pressure gradients and the gravitational force vanish in the tangential direction. Thus the only non vanishing force is the viscosity, until now neglected in the other directions.

Integrated in the vertical direction, the Navier-Stokes equation reads:

$$\Sigma \left(\frac{\partial v_\phi}{\partial t} + \frac{v_r v_\phi}{r} + v_r \frac{\partial v_\phi}{\partial r} \right) = \frac{1}{r^2} \frac{\partial}{\partial r} \left(r^2 T_{r\phi} \right), \tag{1.27}$$

where we introduced the tensor $T = \int_{-\infty}^{+\infty} w \mathrm{d}z$. The relevant component, $T_{r\phi}$, is given by $T_{r\phi} = \nu \Sigma r \Omega'$, where $\Omega' = \mathrm{d}\Omega/\mathrm{d}r$. Combining this expression with the continuity equation (1.8) gives:

$$\frac{\partial}{\partial t} \left(\Sigma r v_\phi \right) + \frac{1}{r} \frac{\partial}{\partial r} \left(r v_r \Sigma r v_\phi \right) = \frac{1}{r} \frac{\partial}{\partial r} \left(r^2 T_{r\phi} \right). \tag{1.28}$$

This can be regarded as the continuity equation for the angular momentum per unit surface $\Sigma r v_\phi$. The first term is the time derivative of the angular momentum in an annulus (apart for a factor 2π), while the second term expresses *advection* due to the presence of a radial velocity. The right-hand side expresses the angular momentum flux due to viscous forces, since on every annulus they exert a torque given by:

$$G(r) = -2\pi r^2 T_{r\phi} = -2\pi \nu \Sigma r^3 \Omega'. \tag{1.29}$$

As anticipated, viscosity is then effectively capable of transporting angular momentum.

Finally, we can substitute V_k for v_ϕ; using again the continuity equation (1.8) we obtain an equation for the density evolution of the disc, that reads:

$$\frac{\partial \Sigma}{\partial t} = \frac{3}{r} \frac{\partial}{\partial r} \left[r^{1/2} \frac{\partial}{\partial r} \left(\nu \Sigma r^{1/2} \right) \right]. \tag{1.30}$$

.

This is a diffusion (parabolic) partial differential equation, where the diffusion coefficient is regulated by the ν viscosity coefficient. If we set $\nu = 0$, no diffusion occurs: the density is constant and no accretion happens.

It is instructive to recast the equation by a simple change of variables. If we introduce $X = 2r^{1/2}$ and $f = \frac{3}{2}\Sigma X$, the equation reads

$$\frac{\partial f}{\partial t} = D \frac{\partial^2 f}{\partial X^2}, \tag{1.31}$$

where we have introduced $D = 12\nu/X^2$ and we have further made the assumption that ν does not depend on r (otherwise ν would be inside the derivative). This makes it clear that the underlying structure of the equation is that of a diffusion equation (the same structure of the heat equation). It also allows us to introduce a characteristic time-scale, that is, X^2/D. In physical units, this corresponds to $t_\nu \simeq r^2/\nu$. This is a fundamental quantity for an accretion disc, usually called the viscous time. Any evolution of the disc due to viscosity is going to happen on this characteristic time-scale.

Until now we have not specified a functional form for ν, and we cannot thus solve the equations. In general, ν is a function of all the other fluid quantities, and this makes the equation non-linear. We will now briefly discuss the origin of this viscosity.

1.3.4   The origin and magnitude of viscosity

Up to now, we did not specify anything about viscosity besides its existence. In terrestrial experiments we can measure directly fluid viscosities, and indeed when this is done it is found that they agree reasonably well with the molecular viscosity. In this picture, the origin for viscosity lies in the random thermal motions of molecules composing the gas; through collisions they transfer momentum between different parts of the fluid. In particular, when dealing with a shearing flow, molecules which move by random thermal motion from a higher mean velocity region toward a lower mean velocity region carry more angular momentum than those moving in the opposite direction, resulting in a net transfer of angular momentum that at a macroscopic level we call viscosity. The relevant coefficient can be computed using the kinetic theory of gases. See however Clarke & Pringle (2004) for some subtleties related to the circular nature of this shear flow.

However, while molecular viscosity generally explains the viscosity seen in terrestrial fluids, this is not the case for accretion discs. It can be shown that, if we assume that proto-planetary discs are viscous because of molecular viscosity, the viscous time-scale would be longer than a Hubble time! This is clearly in contrast with the observational fact that discs are accreting.

This means that another process must be at play. Although there is no theory that can fully describe all the details of the viscous processes happening in the disc, the most plausible candidate is the magneto rotational instability (MRI) (Balbus & Hawley, 1991a). The interested reader should consult the recent review on the topic by Turner et al. (2014). The mechanism requires a weak vertical magnetic field in order to operate. In a nutshell, as in the ideal MHD limit the magnetic flux is frozen in the fluid, the magnetic field opposes to the shearing rotation and tries to impose an uniform angular velocity. If we perturb a fluid element and move it slightly outwards, the magnetic field will try to keep the same rotation speed as before. This means that the forces on the fluid element are not in equilibrium in the radial direction. The excess centrifugal force drives the fluid element further outwards, and the process runaways. For the mechanism to work, the disc must be ionized enough to be coupled to the magnetic field. However, proto-planetary discs are cold, so that thermal ionization is usually not able to provide the required ionization (except for the very inner region of the disc, at sub-AU distance from the star). Other sources of ionization come from the high energy radiation from the star, from cosmic rays and from the radioactive decay of unstable nuclei in the disc itself. Detailed calculations (e.g., Gammie, 1996; Ilgner & Nelson, 2006; Turner & Drake, 2009; Bai, 2011; Mohanty et al., 2013), which also must take into account the effects of non ideal MHD, show that there are regions of the disc where the ionization is not high enough. It is expected that these regions have a much lower viscosity than the rest of the disc, and they are usually called "dead-zones" as they are inactive from the accretion point of view. Although the exact locations vary depending

on the model taken into account, typically dead zones are found to be at several AUs from the star.

Traditionally, the uncertainties related to the transport properties of the disc have been bypassed, through the use of a very effective parametrisation introduced by Shakura & Sunyaev (1973a). Dimensionally, the viscosity coefficient can be expressed as:

$$\nu = \alpha c_{\mathrm{s}} H, \tag{1.32}$$

where α is a dimensionless quantity. We can put some constraint on α by requiring that $\alpha < 1$, since it is unlikely that turbulent velocities are supersonic (in this case they would cause shocks in the gas and rapidly dissipate their energy) and since an upper limit for the largest turbulent eddies is given by the disc thickness H (assuming an isotropic turbulence). Of course this is not a theory for accretion disc viscosity: we simply moved our ignorance from the ν coefficient to the α parameter. The further assumption that is usually made is that α is a constant. There is no physical reason why this should be the case; for example, if dead zones are present we expect α to vary in the disc. Lacking however a better theory, this assumption has the advantage to allow us to parametrize the results and decouple the phenomenon we want to investigate from the issue of the origin of the viscosity. Indeed, most of the studies of disc evolution follow this approach. This is also the assumption that we will use in the rest of this thesis. Typical values of α computed with MRI models in the ideal MHD limit are $\alpha \sim 10^{-2}$.

1.3.5   Self-similar solutions

Equation 1.30 admits in general no analytical solution, and one needs to numerically integrate it in the general case. There are however special cases where analytical solutions are available, and allow one to get a handle on the behaviour of a viscously evolving accretion disc. A class of solution is the so-called "self-similar solutions", which have a power-law varying viscosity:

$$\nu = \nu_1 \left(\frac{r}{r_1}\right)^{\gamma}. \tag{1.33}$$

Lynden-Bell & Pringle (1974) showed that the equation then admit the following time-varying surface density as a solution:

$$\Sigma(\tilde{r}, T) = \frac{C}{3\pi\nu_1\tilde{r}^{\gamma}} T^{-(5/2-\gamma)/(2-\gamma)} \exp\left[-\frac{\tilde{r}^{(2-\gamma)}}{T}\right], \tag{1.34}$$

where $\tilde{r} = r/r_1$, C is a normalization constant and we have introduced a dimensionless time parameter T given by $T = 1 + t/t_s$, where t_s is to order of unity the viscous time-scale introduced previously and is given by:

$$t_s = \frac{1}{3(2-\gamma)^2}\frac{r_1^2}{\nu_1}. \tag{1.35}$$
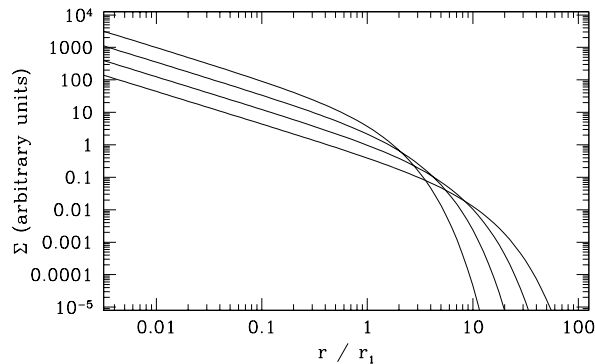
Figure 1.7: Self-similar solution at different times for the case $\nu \propto r$. The curves are plotted at $T = 1$ (that is, $t = 0$), $T = 2$, $T = 4$ and $T = 8$, where T is the dimensionless parameter defined in the text. From Armitage (2007).

Note that a power-law has no relevant spatial scale, so that r_1 has no special meaning for what concerns the functional form of the viscosity. It does have however a meaning when looking at equation 1.34: if we set $t = 0$, r_1 is the length-scale of an exponential cut-off in the surface density (that is, the surface density quickly tends to vanish for radii greater than r_1). There are several interesting feature of this solution that are worth noting. First of all, this cut-off radius r_d is not a constant, but evolves with time due to $1/T$ factor. The evolution is given by:

$$r_d(t) = r_1 T^{1/(2-\gamma)}. \tag{1.36}$$

As T is an increasing function of time, the cut-off radius increases with time (unless $\gamma > 2$). This is often called "viscous spreading" and expresses the fact that, as time passes, viscosity redistributes the angular momentum in the disc, moving it to the outer regions; the excess angular momentum makes them expand. From the observational point of view, we can identify this cut-off radius with the physical size of a proto-planetary disc.

The other fact to note is that the only other part depending on time is the factor $f_{depl} = T^{-(5/2-\gamma)/(2-\gamma)}$. This is always a decreasing function of time. We can then divide the disc in two regions:

- regions that are initially at a radius $r < r_1$ are unaffected by the change of the scaling radius. The surface density here decreases in time as a power-law (strictly speaking, a power-law for T, but note that this is also a power-law for t provided $t \gg t_s$) due to the factor f_{depl};

- regions that are intially at a radius $r > r_1$ have initially strongly suppressed surface densities due to exponential cut-off. Eventually, the disc will expand enough to reach these regions, so that the surface density will increase and the exponential factor will become unimportant. From now on, the evolution of the surface density will follow the same power-law evolution as the other regions.

Figure 1.7 shows that the behaviour of the solution is indeed the one that was described.

Note that, since the outer part of the disc is expanding, this means that the net radial velocity of the gas there is outwards. Therefore, strictly speaking the disc is *accreting* (that is, matter is being transferred inwards) only in the inner region; the outer one is *decreting*. For each given radius r, however, accretion will eventually happen; if we wait enough time, the disc will always expand enough to bring this radius in the inner region of the disc.

Finally, other quantities of interest are the mass of the disc and the mass accretion rate onto the star. The disc transfers materials to the star, and thus its mass must decrease with time. As the mass in the disc decreases and the disc expands, there is increasingly less mass available near to the star, so that we expect also the mass accretion rate to decrease with time. Indeed, it can be shown (Hartmann et al., 1998) that the mass decreases in time as $T^{-1/[2(2-\gamma)]}$, whereas the mass accretion rate decreases as $T^{-(5/2-\gamma)/(2-\gamma)}$. It should be noted that the power-law exponent of these relations does not depend on the total value of the viscosity, but only on its radial dependence. This is not to say however that the absolute value of the viscosity is irrelevant; the initial value of the mass accretion rate is, to order unity, $\dot{M}(t=0) = M_d(t=0)/t_\nu$. Increasing the viscosity has the effect to increase, for a given disc mass, the mass accretion rate onto the star. However, the way this accretion rate declines with time does not depend on the magnitude of the viscosity.

1.4   Comparison with observations: limitations of pure viscous evolution

We have seen in the previous sections that the viscous evolution of a disc leads to mass accretion on the star, and consequently to a reduction in time of the mass of the disc. These predictions can be directly compared to the results of observations. As mentioned in section 1.2.2.1, Hartmann et al. (1998) found that the mass accretion rate onto the star decreases roughly as $t^{-1.5}$. This decline is consistent with the relations derived in the previous section, and in particular it implies that $\gamma \sim 1$. From the theoretical point of view, this result is appealing, as indeed $\gamma \sim 1$ can be found by simple assumptions. If we fix α to be a constant, the slope of ν depends only on the temperature profile of the disc, which enters through the sound speed and the vertical scale-height. In particular, we can rewrite equation 1.32 as $\nu \propto c_s^2/\Omega_k \propto T(r)r^{3/2}$, where $T(r)$ is the temperature profile of the disc. If $T(r) \propto r^{-1/2}$, we get the observed scaling. Indeed, Kenyon & Hartmann (1987) showed that this is exactly the scaling expected by a flared disc - that is, a disc whose aspect ratio increases with radius.

The observations can also approximately constrain the values of α if also the mass and sizes of the discs are available. Hartmann et al. (1998) finds that the data is reproduced by models with $\alpha \sim 10^{-2}$, consistently with the predictions of MRI models. Newer observational results (e.g., Andrews et al., 2010) have not changed significantly this original estimate.

This result should not be overinterpreted however; more accurate models of the temperature profile (Chiang & Goldreich, 1997; D'Alessio et al., 1998; Dullemond et al., 2007a)

find slightly different power-law exponents, and it should be remembered that there are huge observational uncertainties, particularly in the age determination. Nevertheless, the fact that we are able to reproduce approximately this observational result shows that viscous evolution is one of the main mechanisms driving disc evolution.

However, we note that at each finite time the mass of a disc in the self-similar solution is always non zero, that is, only in the limit of an infinite time the disc disperses completely. While this is the mathematical behaviour of the solution, what is relevant in comparison with observations is for how long a disc would be observable, that is, what mass is required to have an optically thick disc. Let us assume that the disc has initially a mass of $0.01 M_\odot$ and a scale radius of $30 AU$. This means that the surface density at, say, $1 AU$ is approximately $10^3 g cm^{-2}$. Adopting for the dust an opacity of $100 g^{-1} cm^2$, this means that we need to deplete the surface density of a factor 10^5 before we transition to the optically thin regime. The depletion factor for the $\gamma = 1$ case is given by $T^{-3/2}$, so that we would need to wait approximately 2×10^3 viscous time-scales. With a typical value of the viscous time scales of 10^5 yr, the transition cannot happen before 10^8 yr in the most optimistic case. As was reported in section 1.2.3.1, observations instead typically find a mean disc lifetime of $\sim 3 Myr$. This simple argument thus shows that viscous models cannot provide alone a complete description of disc evolution. While we might be tempted to increase the level of viscosities to make the discs lifetimes shorter, the room for play is limited, since the previous mentioned observations of disc masses and accretion rates put constraints on the maximum amount of viscosity. Therefore, while the Lynden-Bell & Pringle (1974) solution is a very powerful and simple instrument, it certainly cannot fully describe disc evolution. This leads to the possible scenarios:

- Another process, other than viscous evolution, is at play.

- Viscosity must not be a constant, that is, it must increase with time. This is indeed likely in the MRI scenario; as the discs age, the relative importance of the magnetic field becomes more important with respect to the gas dynamics, and the viscosity can potentially increase. However, it is far from obvious that the increase is big enough to satisfy the constraints. To the best of our knowledge, this is a route that has been explored very little to explain disc evolution, but see Armitage et al. (2013) for a recent paper that considers this effect. Their finding is that indeed the increase is not really relevant, although they find discs winds (which were not considered in this thesis) to be potentially important for disc evolution.

- The optical properties of discs change with age, that is, the opacity of discs must decrease as they age, so that they transition to optically thin at earlier ages than what our simple calculation before assumed. Indeed, this is known to happen due to grain growth. As grains stick together and coagulate, they become bigger and bigger, and increasingly less opaque at a given wavelength. However, this argument is likely to fail in practice, as it will be shown in the next section.
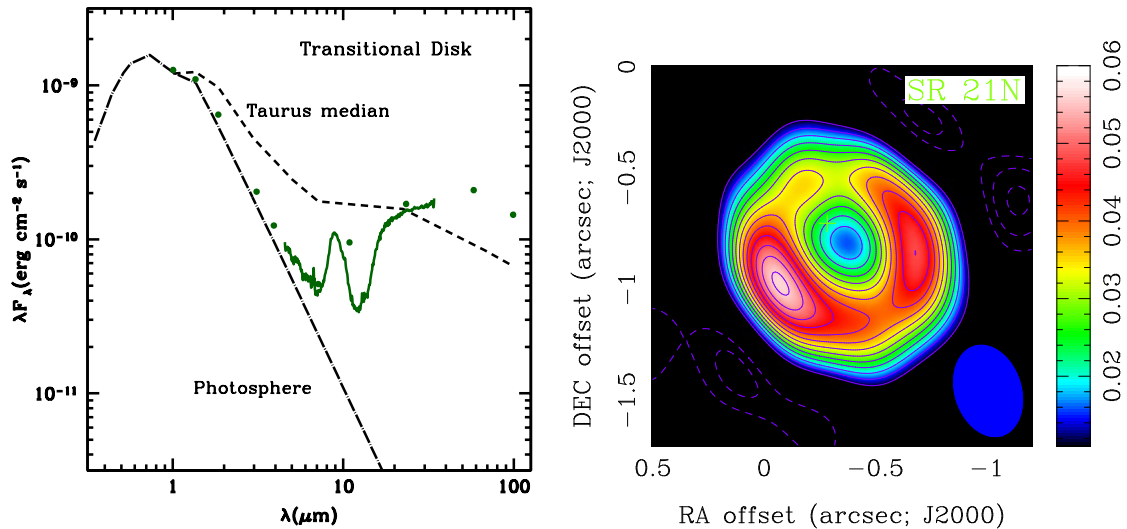
Figure 1.8: Two examples of transition discs. The left panel shows the SED of GM Aur (Calvet et al., 2005a). For reference, the figure also reports the median SED in Taurus, showing the lack of emission in the transition disc up to $\sim 20\mu m$ wavelengths. The SED thus declines and then rises again at longer wavelengths, in contrast with the SED of a full disc that is always declining. The right panel shows a sub-mm image of SR21 taken with the Submillimeter Array (SMA) (Brown et al., 2009). The hole has a size of 33 AU.

1.5 Other constraints from observations: transition discs

Luckily, other constraints necessary to develop a theory of disc dispersal come from the observational class of transition discs (Strom et al., 1989a; Skrutskie et al., 1990a). Although different authors use different definitions, colloquially they are discs that lack IR excess at the NIR/MIR wavelengths. An example transition disc SED is shown in the left panel of figure 1.8. In order to explain this puzzling behaviour, one has to assume that they show a hole of some AU in size in the dust distribution. This hole is responsible for the lack of warm dust, and therefore the lack of emission at the corresponding wavelengths. While for a more than a decade observations had to rely only on SEDs for their modelling (e.g., Kenyon & Hartmann, 1995; Calvet et al., 2005a; Currie & Kenyon, 2009; Muzerolle et al., 2010; Lada et al., 2006; Cieza et al., 2010; Espaillat et al., 2010a), sub-mm interferometry reached in the last years the necessary spatial resolution to investigate more closely these objects (e.g., Piétu et al., 2006; Brown et al., 2009; Andrews et al., 2011; Isella et al., 2012). All these observations have found that transition discs do indeed posses big holes at mm wavelengths, as shown in the right panel of figure 1.8. The cavities can be very big in some cases (approaching 100 AU) and they are usually very sharp and clean in the inside, as far as the resolution and sensitivity of the current observing facilities can tell. For a recent review of all the observational results on transition discs, the interested reader can consult Espaillat et al. (2014).

In a theoretical framework for disc evolution, transition discs are considered to be the last phase in a lifetime of a proto-planetary disc. Indeed, many authors consider them as the intermediate phase between the class II and the class III stage. Theoretically, this interpretation is supported by the fact that they show accretion rates which are on average a factor of 10 smaller than the whole class II population, and therefore they should be older objects. One should be careful however in interpreting this result, as the class of transition discs is not homogeneous; some transition discs have accretion rates that are indistinguishable from the ones found in classical T Tauri stars. Their fraction is roughly 10% of the whole disc population. If we assume that all discs go through this phase, this means that the transition disc phase must be relatively short-lived, of order several $10^5 \ yr$. This behaviour has often been referred to as "two-timescale behaviour", as discs are normally evolving on a timescale of several 10^6 years, but then they are quickly destroyed.

Transition discs thus provide the theory with other constraints about disc evolution that must be satisfied. Viscous evolution, in the way as we formulated it in the previous section , cannot provide an explanation for them as it predicts an homogenous depletion of the disc. However, viscous evolution already complies with the previous mentioned constraints, and so all the models for transition discs invoke the presence of another process, in addition to viscous evolution, rather than proposing a completely different theory. As already mentioned, the class of transition discs is not homogenous. It has a huge spread in mass accretion rates and disc masses. For this reason, Owen & Clarke (2012a) has proposed that transition discs are actually composed of two different families, depending on their millimeter flux (that is, their mass). If this interpretation is correct, note that more than one additional process might be at play. Depending on which is the relevant one, a disc might take a different evolutionary path and become a different kind of transition disc.

In the next section, we explore a plausible additional mechanism for the purposes of this thesis that regulates disc evolution, photo-evaporation. We will concentrate in particular on which of the constraints coming from observations photo-evaporation can satisfy, and which ones cannot. In the following section we will briefly touch about other mechanisms (particularly dynamical encounter, which is also important for the purposes of this thesis), which are important for disc dispersal (not necessarily only for transition discs).

1.6   Photo-evaporation

1.6.1   Basics

We can ask ourselves how important is the contribution of the thermal energy to the total energy of a parcel of gas. To answer, it is instructive to introduce the gravitational radius:

$$R_g = \frac{GM_* \mu m_p}{kT} \sim 100 \left(\frac{T}{1000K} \right)^{-1} \left(\frac{M_*}{M_\odot} \right) AU, \qquad (1.37)$$

which is the radius at which the thermal energy is equal to the mechanical energy of a parcel of gas in keplerian rotation around the star. If some gas is outside the gravitational

radius, it is formally unbound from the star (that is, it has a positive total energy). Is this relevant in proto-planetary discs? To answer, we need to know the temperatures in the disc, a problem we did not address yet.

The bulk of the gas in a proto-planetary disc is heated by the dust. The opacity of the gas is very small in the continuum, so that a gas-only disc would be essentially transparent to the radiation from the star. Conversely, dust has a very high opacity at the optical wavelengths emitted by the star, so that the disc is highly optically thick and the radiation from the star keeps it warm. If the density is high enough (in practice, a condition always attained in the disc midplane), the collisions between gas molecules and the dust grains bring the gas at thermal equilibrium with the dust. Although a detailed calculation of the dust temperature requires a proper radiative transfer investigation, a good rule of thumb is that the temperature of the dust in the disc midplane can be expressed as:

$$T(R) = 100 \left(\frac{R}{1\text{AU}} \right)^{-1/2} K. \tag{1.38}$$

The inspection of the two formulae 1.37 and 1.38 makes it clear that with this temperature the thermal energy is much smaller than the gravitational energy. For example, a temperature of $1000K$ is attained only at $\sim 0.1AU$ from the star, whereas its gravitational radius is $\sim 100AU$. This is also consistent with the fact that proto-planetary discs are cold and thin, that is, they are characterised by $c_s \ll v_k$. A disc where the thermal energy would be a significant contribution to the total energy budget would be thick rather than thin. However, the assumption that the dust and the gas are in equilibrium does not always hold. The density structure of a disc in the vertical direction is approximately gaussian (as it was derived in section 1.3.1), so that the density at some vertical scale heights above the disc midplane is much smaller than in the midplane. These top surface layers of the disc can be reached not only by the optical photons that comprise the bulk of the stellar radiation, but also from the high energy ones. Here with high energy we mean far ultraviolet (FUV) ($6eV < h\nu < 13.7eV$), capable of dissociating the H_2 molecule, extreme ultraviolet (EUV) ($13.7eV < h\nu < 100eV$), capable of ionizing a hydrogen atom, and X-rays ($h\nu > 100eV$). Their effects on the gas cannot be neglected, and they are responsible for heating significantly the gas to temperatures in the range $100 - 10000K$.

Once this effect is taken into account, it is actually possible that some material be outside the gravitational radius corresponding to its temperature. If this happens, this gas will leave the surface of the disc, flowing in a wind with a speed comparable to the speed of sound (therefore, a relatively slow wind). This phenomenon is called "photo-evaporation". It was first conceived by Bally & Scoville (1982), although only later it was realised that it applies to proto-planetary discs.

1.6.2   EUV photoevaporation

EUV photoevaporation is, conceptually, the most simple model of photoevaporation, and from the historical point of view it was the first one formulated. Although it was not

directly used in this thesis, it is instructive to start from it before introducing X-ray photo-evaporation, which was the main photo-evaporation model used in this thesis.

The EUV heating is quite simple in that it almost uniformly heats the gas at a temperature of around $10^4 K$. The heating is mostly due to the ejection of electrons from an hydrogen atom (photoionization); the excess kinetic energy of the electron is then thermalized into the gas. The cooling is mostly due to the forbidden lines of the heavier elements, which are collisionally excited by the free electrons. As the transitions involved are typically below the critical density, the atom will de-excite emitting a photon, which carries away some of the thermal energy. Roughly speaking, both these processes scale in the same way with density, so that the balance between heating and cooling always give a constant temperature. It is useful to know also the corresponding sound speed, that is roughly 10 km s^{-1}. The mass loss rate is simply given by $\dot{\Sigma} = 2m_H n_0(r) c_s$, where m_H is the mass of an hydrogen atom and the factor 2 accounts for the two sides of the disc. The task left is only to evaluate $n_0(r)$, the density of the gas at the base of the flow. Note that no photo-evaporation can happen for radii smaller than R_g, as this gas is bound to the star. If $n_0(r)$ is known, integration of the above equation yields the total mass loss rate $\dot{M}$. Computing this quantity is the goal of a photo-evaporative model. It should be noted that in this simple case the photo-evaporation mass loss rate is set by the penetration depth of the EUV photons, that is, the height of the heated surface layer above the disc midplane. Increasing the EUV flux increases the photo-evaporation rate because it increases the penetration depth of the photons, that are now able to heat a region where the density of the gas is higher. The temperature of the flow however is not affected. More in detail, the density at the base of the flow is set by a Stromgen chriterion:

$$\alpha_B r^3 n_0^2(r) \propto \Phi, \tag{1.39}$$

where α_B is the hydrogen recombination coefficient and Φ is the flux of ionizing photons from the star (in units of photons s^{-1}). This simple formula shows that the expected scaling of the mass-loss rate is $\dot{M} \propto \Phi^{1/2}$, because of the quadratic dependence on density of the recombination rate. This has important consequences for this thesis in chapter 5. The actual calculation of an EUV photo-evaporation rate requires more work, because the ionized gas itself is very efficient in absorbing the ionizing photons. At the same time, it also re-emits ionizing photons through recombinations (roughly 1/3 of the incoming ones). Thus, the diffuse field (that is, the one re-emitted by the ionized gas) is dominant in setting the mass-loss rate, rather than the direct field (the one emitted by the star).

Analytical and numerical calculations done by Hollenbach et al. (1994) find that the density at the base of the flow is given by

$$n_0 = n_g \left(\frac{R}{R_g} \right)^{-5/2}, \tag{1.40}$$

where n_g is:

$$n_g = C \left(\frac{3\Phi}{4\pi \alpha_B R_g^3} \right)^{1/2} \tag{1.41}$$

and C is an order unity constant (which was found to be 0.14 in numerical calculations).

As stated before, we can now integrate the expression by computing the integral

$$\dot{M} = \int_{R_g}^{\infty} 2\pi R \dot{\Sigma}(R) dR. \tag{1.42}$$

For typical parameters, the result is

$$\dot{M} = 4 \times 10^{-10} \left(\frac{\Phi}{10^{41} \text{ s}^{-1}} \right)^{1/2} \left(\frac{M_*}{M_\odot} \right)^{1/2} M_\odot \text{ yr}^{-1}. \tag{1.43}$$

It can be seen that the dependence of $\dot{\Sigma}(r) \propto n_0(r)$ is very steep, so that the main contribution to the mass-loss rate comes from the region close to r_g.

It was subsequently realised that photo-evaporation can also happen for radii smaller than r_g, up to $r_{crit} \simeq r_g/5$ (Liffman, 2003; Adams et al., 2004a). The pressure gradients in this part of disc can push the material to larger radii, until it becomes unbound from the star. In addition, hydrodynamical calculation of the process were conducted by Font et al. (2004), who confirmed this behaviour and also found that the wind rate is a factor of a few smaller than the one given above, due to the fact that the wind is launched at sub-sonic speed. Finally, Alexander et al. (2006a) realised that when the disc has a hole the direct irradiation from the star cannot be neglected, and derived an expression for the mass-loss rate in this case. Their result is that the total mass-loss rate increases with the hole size, as we are removing the strongly bound material close to the star that intercepts most of the EUV photons.

1.6.3 The EUV switch

The simple model of EUV photoevaporation that we sketched in the previous paragraph can be used to study the evolution of a photoevaporating disc. The absolute value of the photo-evaporative mass loss rate might seem low compared to the typical mass accretion rates in a T Tauri star, and one might be tempted to discard photo-evaporation as an important mechanism driving the disc evolution. On the contrary, photo-evaporation has very important implications.

Let us first assume that the disc is not viscously evolving. Thus, the timescale for mass removal at each radius is given simply by $t_{depletion} = \Sigma(r)/\dot{\Sigma}(r)$, as there is no communication between the different radii. As we showed in the previous section, $\dot{\Sigma}(r)$ is a steep decreasing function of r, so that (unless Σ is even steeper) $t_{depletion}$ is an increasing function. Given that the photoevaporation rate decreases inwards than r_g, $t_{depletion}$ has a maximum at r_g. Thus, without viscous evolution we would predict that photo-evaporation would first deplete the disc at r_g; the depleted region would then expand from outside in. The disc inside r_g is relatively safe, and is expected to be long-lived. We can also estimate the time-scale for gas depletion at r_g. For a star with $M_* = 1 M_\odot$, the gravitational radius is roughly 9AU. The total mass-loss rate can be written as $\dot{M} = 4\pi\dot{\Sigma}(r_g)r_g^2$ by integrating the expression given in the previous section for $\dot{\Sigma}$; thus, $\dot{\Sigma}(r_g) \sim 5 \times 10^{-5} \text{g cm}^{-2} \text{ yr}^{-1}$. As

initial densities of the disc at this radius are typically 10^2g cm^{-2}, the timescale for complete removal of this material is of order 5 Myr, and even longer at bigger radii. However, if the surface density of the disc is already depleted, this timescale can become very short; with a depletion factor of 100 for example, the depletion timescale by photo-evaporation will become shorter than the local viscous time-scale.

Armed with this knowledge, let us introduce viscous evolution. The mass accretion flow is continuously replenishing the inner regions of the disc at the expenses of the mass supply in the outer regions. In the limit in which the replenishment rate is much bigger than the mass-loss rate, we can neglect the effect of photo-evaporation; no region of the disc will be significantly depleted. However, as was shown extensively in the previous sections, the mass accretion rate is a decreasing quantity with time. This is due to the fact that the mass supply of the disc decreases with time, and also to the fact that the time-scale for the evolution of the disc is set by the outer radius, which is expanding; the timescale for expansion is thus increasing with time. Since the typical mass accretion rates in T Tauri stars are higher than the typical photo-evaporation rate, this means that indeed the disc is initially in a state where the evolution is dominated by the viscous evolution. However, as time passes and the mass accretion rate decreases, the role of photo-evaporation can no longer be neglected; eventually, the viscous evolution will no longer be able to resupply fast enough the inner regions of the disc, and we will switch to the regime where the disc is effectively not viscously evolving described previously. Note that viscous accretion has already significantly depleted the inner region, where the depletion factor is given by the dimensionless quantity $T^{-3/2}$. For reference, after 20 viscous timescales have passed (a few Myrs for typical parameters), the surface density of the disc is depleted of a factor ~ 100. As shown in the previous paragraph, this means that on a fast timescale this location in the disc will be completely depleted. A gap will thus open in the disc; the depleted region will become bigger in time, from inside out. At the same time, in the very inner disc the viscous evolution cannot be neglected. This disc will rapidly drain onto the star on its local viscous time-scale.

To show in detail that the behaviour is indeed the one that was sketched, we need to go back to the diffusion equation (1.30), to which we add a new term on the right hand-side that represents the mass being lost through photo-evaporation:

$$\frac{\partial \Sigma}{\partial t} = \frac{3}{r} \frac{\partial}{\partial r} \left[r^{1/2} \frac{\partial}{\partial r} \left(\nu \Sigma r^{1/2} \right) \right] - \dot{\Sigma}_{photoevap}(r). \tag{1.44}$$

Clarke et al. (2001a) solved equation 1.44 numerically, and confirmed that the behaviour is the one we described. Figure 1.9 shows the surface density of the disc at various times (the evolution includes also the effects of direct irradiation, and mass-loss inside r_g). After a phase of $10^6 - 10^7$ yr where the contribution of photo-evaporation is almost negligible, a gap opens in the disc at ~ 1 AU. The inner disc drains onto the star in $\sim 10^5$ yr, while the size of the depleted region continues to grow from inside out. Therefore, a disc with a hole has been created, that closely resembles the observational class of transition discs. Ruden (2004) confirmed analytically these numerical results. It should be noted also that while the inner disc is still there, accretion is still ongoing onto the star; when the inner disc
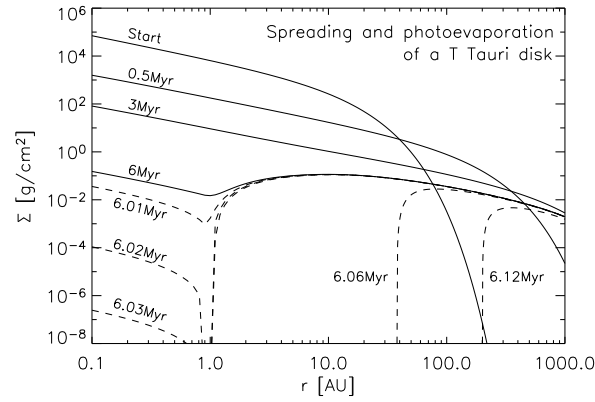
Figure 1.9: Surface density at different times for a viscously evolving photo-evaporating disc. While at the beginning the evolution is unaffected by photo-evaporation, a gap opens in the disc around 6 Myr. The inner disc then rapidly drains onto the star, while the hole increases in size with time. From Dullemond et al. (2007a).
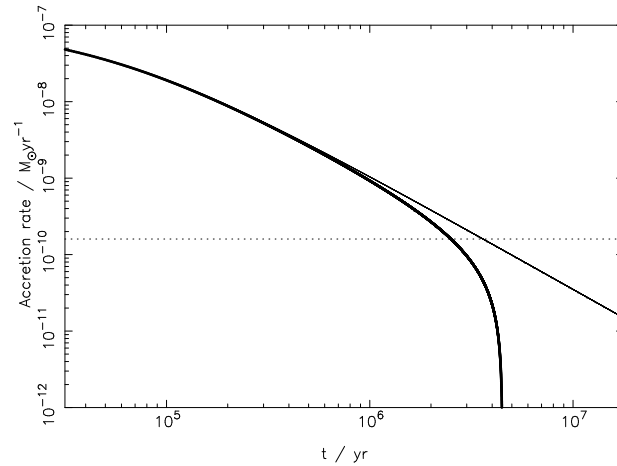
Figure 1.10: Mass accretion rate onto the star as a function of time. The thin solid line shows the evolution of the mass accretion rate in the self-similar case, while the thick one shows the evolution when also EUV photo-evaporation is included. It can be seen that at earlier times the two solutions cannot be distinguished, while after a few Myr of evolution they differ significantly. The dashed horizontal line shows the total photo-evaporative mass-loss rate. When the mass accretion rate drops below this value, accretion is rapidly shut down by the EUV switch. From Alexander (2008).

has dissipated instead, the star is no longer accreting. More in detail, figure 1.10 shows the evolution in time of the mass accretion rate for a photo-evaporating proto-planetary disc. For most of the time, the evolution is the typical power-law of a self-similar solution. When the gap opens in the disc, the mass accretion rate rapidly drops to zero, and the star stops accreting. This is the reason why this behaviour has been called "EUV switch" by Clarke et al. (2001a).

Therefore, photo-evaporation provides a convenient way to shut down mass accretion when a given threshold is reached. As we have shown, the two-timescale behaviour comes out naturally and photo-evaporation is currently thought to be the most important candidate in dispersing discs. While this picture works very well qualitatively, it is unfortunately not able to reproduce all the observed features. In particular, the outer disc is thought to be very long-lived in this simple picture (even some 10s of Myr), as the mass-loss rate drops significantly once outside R_g. Thus, one should expect to see many "relic" discs, that is, non accreting discs with large holes, significantly depleted in their mass. In addition, the mass accretion rate of the created transition disc cannot be bigger than the photo-evaporation mass-loss rate. As this is quite low, a prediction of the model is that transition discs should be accreting at low rates, contrary to many observations that find transition discs accreting at high rates. For what concerns the first problem, the inclusion of the direct field in Alexander et al. (2006a) calculations shows that the relic disc can be destroyed fast enough (a few 10^5 yr) to comply with the observational constraints. However, the problem of explaining the high accretion rates observed in transition discs remain. We will see in the next sections how improved models resolve this problem.

1.6.4   X-ray photoevaporation

The physics of heating by X-rays is quite different from the one by EUV photons. Rather than affecting the hydrogen atoms, these very energetic photons rip away the electrons in the deep shells of metals, which are tightly bound to their nuclei. The electron carries away the excess energy of the photon, which is enough to cause several other ionizations through collisions with other atoms. This energy is finally thermalised. The physics of X-ray heating is much more complicated than the one by EUV photons; it depends on all the possible energetic levels that can absorb a photon, and on the efficiency of the process (i.e., how much energy of the incoming photon is effectively going into heating of the gas). Finally, one needs of course to take into account the cooling mechanisms, of which cooling through forbidden line of metals was found to be the most dominant (Ercolano et al., 2008).

Young stars are very bright in the X-rays (in fact, their X-ray emission is one of the tools used to select them), with a median X-ray luminosity of 10^{30} erg s^{-1} (Preibisch et al., 2005). Therefore, it can be expected that the contribution to heating is significant. Ercolano et al. (2008) first modelled a disc photo-evaporated by X-rays photons, using the Montecarlo radiative transfer code MOCASSIN. Similarly to the first models of Hollenbach et al. (1994), their models assume hydrostatical equilibrium. Their findings are that X-rays are able to cause a significantly bigger mass-loss rate compared to the previous models of EUV
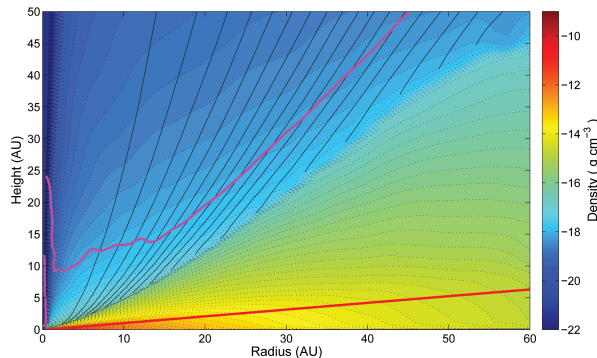
Figure 1.11: Steady state wind in a hydrodynamical calculation of Owen et al. (2010a). The magenta line shows the location of the sonic surface where the sound speed is equal to the gas velocity. The red line is the location of the optical $\tau = 1$ surface. The density jump visible in the contours happens at the penetration depth of the X-ray photons, and is at the base of the flow. The thin black solid lines are the streamlines of the flow, plotted at 5% increments of the total mass-loss rate.

photo-evaporation, up to the range of 10^{-8} $M_\odot$ yr^{-1}. The X-ray temperature, differently from the EUV case, depends significantly from the density of the gas and the distance from the star. For this reason, the atmosphere is not heated to an uniform temperature, but the temperature has a steep vertical gradient. The photo-evaporative flow does not thus have a very well defined gravitational radius, neither it is clear where the boundary separating the photo-evaporating region from the stationary one exactly is. This makes it difficult to estimate the photo-evaporative mass-loss rate from a hydrostatical calculation.

For this reason, Owen et al. (2010a) coupled the radiative transfer calculations of Er-colano et al. (2008, 2009) with a hydrodynamical simulation. To be able to run the simulation in a reasonable wall clock time, the hydrodynamical calculation does not solve the full radiative transfer problem, but uses an approximation based on the ionization parameter χ, defined as

$$\chi = \frac{L_X}{nr^2}, \tag{1.45}$$

where n is the number density of the gas. The parameter gives the number of X-ray photons available in an unit of time for an atom. Ercolano et al. (2009) showed that in the full radiative transfer problem there is a very good correlation between χ and the temperature. Therefore, one can derive a fitting function and use it to set the temperatures in the hydrodynamic simulation. Another check can be done also *a posteriori*, checking that also the temperatures obtained at the end of the dynamical evolution via the ionization parameter are compatible with the ones obtained in the full radiative transfer calculation.

Figure 1.11 shows the result of one hydrodynamical simulation, showing that a steady state wind has developed. The results of the simulations are that the wind properties are set mainly by the properties of the flow at the sonic point (where the velocity of the flow is equal to the sound speed). As at each radius the speed at the sonic point is approximately the escape speed, knowledge of the function $T(\chi)$ allows one to solve analytically for the mass loss rate, yielding a very good approximation of the results of the simulations (Owen

et al., 2012a). The photoevaporative rate is found to be

$$\dot{M}_X = 6.3 \times 10^{-9} \left(\frac{L_X}{10^{30} \text{ erg s}^{-1}} \right)^{1.14} \left(\frac{M_*}{1M_\odot} \right)^{-0.068} M_\odot \text{ yr}^{-1}, \qquad (1.46)$$

which is ~ 40 times larger than the EUV photo-evaporation rate. The main difference with the EUV profile is that the resulting mass-loss rate profile $\dot{\Sigma}$ is much shallower, yielding significant contributions to the total mass-loss rate even as out as 70 AU. The main reason for this difference is that, although the X-rays can hardly heat the gas as much as the EUV radiation, they penetrate much deeper in the disc (approximately up to columns of 10^{22} cm^2). Note also the almost linear dependence on the X-ray luminosity, which is important for chapter 5. On the other hand, if the disc has a hole the photo-evaporation rate does not change dramatically (a factor of 2 typically) since X-ray heating depends mostly on the local conditions of the gas. This differs from the EUV case, where once the disc is exposed to the direct field from the star the mass-loss rates can increase significantly.

Also for the X-ray case however the direct exposure to the photons of the star can have a big impact. Owen et al. (2012a) found that the presence of a hole in a disc combined with X-ray photo-evaporation can trigger an instability in the disc. If the surface density is low enough, the X-ray heated anulus of the disc becomes wider than its vertical scale height. Under this condition, a small expansion in the vertical direction of this region corresponds to an increased penetration of the X-ray photons, leading to a runaway effect that brings to the complete dispersal of the disc in a few dynamical timescales, that is, a few 10^4yr. This is much smaller than the evolution timescale of the disc, so that we will speak in what follows of "instantaneous" dispersal. Owen et al. (2013) conducted a parameter study, giving updated estimates for the threshold density at which thermal sweeping sets in. This is important for chapter 5.4 of this thesis.

1.6.5   Consequences of X-ray photo-evaporation

Qualitatively, the dispersal of a disc undergoing X-ray photo-evaporation is not different from the EUV switch behaviour that we described earlier. We still have two timescales, the lifetime of the disc until gap opening, of order Myr, and the timescale on which we remove the inner disc, of order 10^5 yr. However, the observative predictions of X-ray photo-evaporation are very different in the details. Since the mass-loss rates are generally higher, the disc is cleared when it is accreting at higher rates. This means that X-ray photo-evaporation can create transition discs accreting at higher rates than EUV photo-evaporation. This is shown in figure 1.12, which shows the predictions of X-ray photo-evaporation theory in the parameter space of hole size and mass accretion rate. For reference, also the observed transition discs are plotted. It is worth noting that X-ray photo-evaporation can explain discs that are accreting at $\sim 10^{-9} M_\odot$ yr or slightly higher, in contrast to EUV photo-evaporation that cannot explain discs accreting at more than a few 10^{-10}. In addition, also the hole size increases faster in the initial phases after gap opening, as the mass-loss rates are higher. This means that we can rapidly open big holes,
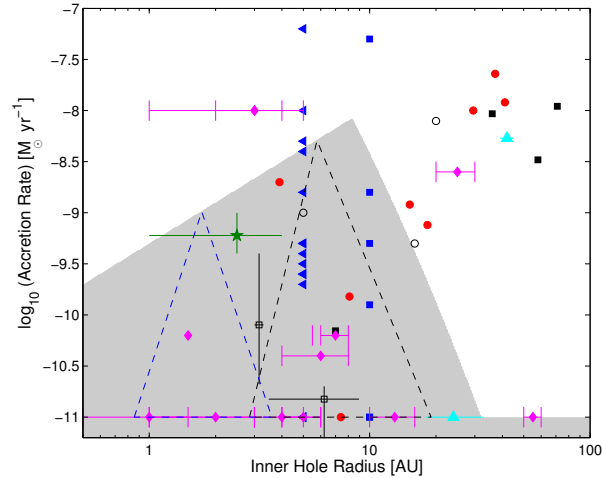
Figure 1.12: Predictions from X-ray photo-evaporation theory () in the mass accretion rate - hole size parameter space. The shaded region is where photo-evaporation can explain the existence of transition discs; the points are the observed transition discs (different shapes and colours correspond to different surveys). Photo-evaporation can explain many observed transition discs, but not the extreme cases with large holes and high accretion rates.

while we still have accretion onto the star. However, while X-ray photo-evaporation can account for $\sim 50\%$ of the observed transition discs, there are still observations that do not find an explanation - namely, discs with large holes, accreting at high rates. This class of discs will be one of the main subjects of this thesis.

The other predictions of X-ray photo-evaporation are about the population of "relic" discs. Whereas the inclusion of the direct field in EUV photo-evaporation models shows that EUV photo-evaporation is able to quickly dissipate the outer disc, we already commented that the mass-loss rate in X-ray photo-evaporation is almost insensitive to the hole size. However, we mentioned that Owen et al. (2012a) discovered an instability capable of rapidly destroying the disc on a dynamical time-scale, the thermal sweeping phenomenon. Figure 1.13 shows the prediction of thermal sweeping for the maximum size of the hole of a transition disc. It can be seen as transition discs are not expected to have a hole bigger than a few 10s of AU. In addition, the timescale over which a disc would remain non accreting before being completely dispersed is quite short (of order 10^4 yr), so that inclusion of thermal sweeping predicts that transition discs would be accreting for most of their lifetime, and no signficant population of relic discs is expected.

In synthesis, X-ray photo-evaporation can account for nearly 50% of the observed class of transition discs (contrarily to EUV photo-evaporation), it naturally explains the two time-scale behaviour, and it solves the issue of relic discs present in the first realisation of the EUV switch model. For this reason, it is one of the most important processes driving disc evolution. However, it is not capable of accounting for discs with large holes and big accretion rates. This thesis will provide other evidence that X-ray photo-evaporation is the most important process driving disc evolution in chapter 5, and explore the issue of
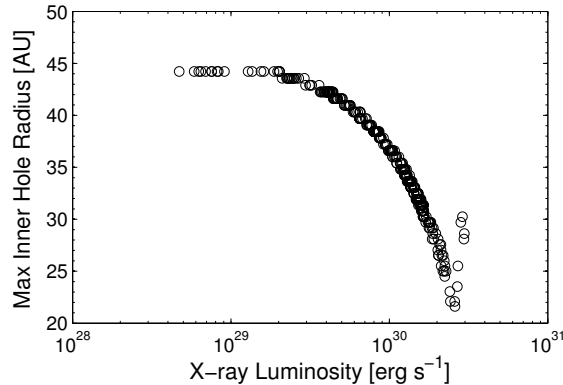
Figure 1.13: The maximum hole size that can be reached by a transition disc before being completely dispersed by thermal sweeping in the X-ray photo-evaporation model. Inclusion of thermal sweeping shows that a large population of relic discs is not expected.

discs with large holes and big accretion rates in chapters 2 and 5.4.

1.6.6   Other mechanisms: FUV and external photoevaporation

As not directly connected to this thesis, we only briefly mention in this section the existence of other models of photo-evaporation. A star also emits Far Ultra-Violet photons (FUV). Although these photons cannot cause ionizations, they can still give a significant contribution to the heating via photo-electric heating and the radiative pumping of the H_2 molecule. Models of FUV irradiation of a disc (Gorti & Hollenbach, 2009a) predict that, in sharp contrast with X-ray and EUV photo-evaporation, most of the mass-loss rate comes from large radial distances from the star, even as big as 100 AU. An important consequence is that FUV photo-evaporation, when coupled with the viscous evolution of the disc, predicts mostly an outside-in dispersal of the disc (that is, a progressive shrinkage of the disc) (Gorti et al., 2009a) rather than an inside-out dispersal as in the qualitative picture we sketched in the previous sections. The formation of a transition disc is thus not a necessary step in the evolution of a disc in this scenario, and for this reason FUV photo-evaporation predicts only a small fraction of transition discs (2%). Exploring the details of FUV photo-evaporation is outside the scope of this thesis; here we note only that currently no hydrodynamical model of a FUV photo-evaporating disc has been run, and the current calculations assume hydro-statical equilibrium. Further work thus is needed in this area.

Finally, up to now we considered only the effect of irradiation from the central star. Stars however are not isolated, and the contribution of a nearby massive star to the UV flux impinging on a disc can be significant. This motivates studies that concern with external photo-evaporation (Johnstone et al., 1998a; Adams et al., 2004a), that is, due to the effect of irradiation sources with are external to the star disc system. The effect of external photo-evaporation is particularly evident in the so-called proplyds in the ONC

(O'dell et al., 1993b; McCaughrean & O'dell, 1996), which exhibit drop-like tails oriented towards the massive stars of the Trapezium. The tail is ionized material, heated by the radiation of those stars. Although external photo-evaporation is probably important for extreme environments close to massive stars, it is unlikely to affect the bulk of the disc population, which is not formed close to a massive star (Adams, 2010a); this is the reason why we will neglect it in the rest of this thesis.

1.7 Other processes

In this section we discuss other processes that contribute to the disc evolution, namely dust growth, planet formation and encounters with other stars. The first two have also been invoked to explain the transitional disc class. On the other hand, encounters participate to the disc evolution, but are not thought to be directly responsible for transition discs. Although we showed that the two main drivers of disc evolution are viscous accretion and photo-evaporation, these are also important processes happening during the lifetime of a proto-planetary disc. In particular, this thesis will present new work on the last two processes (planet formation and dynamical encounters).

1.7.1 Dust growth

In the core accretion paradigm (Pollack et al., 1996), the dust grains grow through collisions until reaching planetesimal sizes. As the opacity of large bodies is much smaller than the opacity of small ones (since they have smaller surface area available), they become essentially invisible at NIR wavelengths. For this reason, it has been proposed that the dust in transition discs has grown up to the point of being invisible at short wavelengths (Dullemond & Dominik, 2005a). A transition disc would then be a normal disc when looked in the gas, but would possess larger, more evolved dust. Earlier attempts were successful in reproducing the SEDs of transition discs. However, the wealth of data that is being accumulated on transition discs contradicts this scenario.

In particular, the problem is with sub-mm images that clearly show huge, sharp cavities. As the dust grain growth depends smoothly on the radial location in the disc, there is no reason why it should produce such a sharp feature. Indeed, detailed models confirm that dust grain growth fails in reproducing the mm cavities seen in the images (Birnstiel et al., 2012a). This does not mean that dust grain growth is not an important process happening in proto-planetary discs; indeed, it must happen in order to form planets (unless we fail to understand the basic steps that lead to planet formation). But it is unlikely that grain growth, at least considered alone (see next section), is an explanation for transition discs.

1.7.2 Planet formation

Giant planet formation is also a process that removes gas from the disc, accelerating its dispersal. However, the simple case of the solar System reveals quite clearly that this

cannot be the main channel leading to disc dispersal. Even in the most optimistic case in which we assume that all the metals comprising the primordial solar nebula were locked in the planets, we need much more hydrogen to have a solar composition, as planets contain much more metals than the Sun, and there is no reason to think that the Sun should have a different composition from the primordial solar nebula. Following this line of reasoning, one obtains the so-called Mininum Mass Solar Nebula (MMSN) (Weidenschilling, 1977b; Hayashi, 1981a), which has a mass of roughly 15 M_{jup}. For comparison, the mass of the planets in the solar system is dominated by Jupiter (which constitutes 70% of the mass of the Solar System). Therefore, it is clear that the current mass in planets of the solar system is much smaller than the original mass of the proto-planetary disc, that is, another process must have dispersed the gas of the disc. This is not to say that planet formation cannot have interesting effects on a disc Armitage & Hansen (e.g., 1999a); relevantly for the purposes of this thesis, a giant planet can contribute to the creation of a transition disc and trigger disc dispersal.

The first type of impact is on the dust. Up to now we did not spend too much words on the dust dynamics, and we focused most on the dynamics of the gas. Generalizing what we said about the issue of radial drift of the dust particles onto the star, we can say that dust tends to migrate towards the pressure maxima of the gas. The reason is that where the pressure is decreasing with radius the gas is rotating sub-keplerian, which leads to inward drift; conversely, an increasing pressure with radius leads to outward drift.

It is well known that a giant planet, provided it is massive enough, opens a gap in a proto-planetary disc (Lin & Papaloizou, 1979). The reason is that the material that is radially close to it will exchange angular momentum with the planet, and will be pushed either inside either outside its orbit. If the effect of viscosity is not strong enough to counteract replenishing the gap, a gap opens (see Crida et al. 2006 for a more detailed discussion on the criteria for gap opening). Thus, the surface density is increasing when we move radially outwards from a giant planet, until it finally reaches a maximum and then decreases again. The pressure follows a similar shape.

Putting together this information, a planet creates a pressure maximum outside its orbit. The dust grains migrate towards this pressure maximum and are accumulated at it. If we now allow enough time for the grains in the inner disc to drift onto the star, we have a created a disc with a hole inside the concentration radius. This might seem exactly what a transition disc is, and indeed many theoretical attempts to explain transition discs have invoked the presence of a giant planet in it (Rice et al., 2006; Paardekooper & Mellema, 2006; Crida & Morbidelli, 2007; Zhu et al., 2012). Unfortunately, things are not that simple; the dust that is accumulated at the pressure maximum is only the intermediate sized one (which for typical parameters has a size of $1mm$), whereas the small one is always well coupled to the gas. This means that this mechanism can explain the cavities of transition discs observed in the sub-mm images, but fails in explaining the lack of NIR emission observed in the SEDs of transition discs (Zhu et al., 2012; Owen, 2014). There are however hints that dust coagulation can help to solve the problem; if the small dust can coagulate effectively, it will become invisible at these wavelenghts. This was investigated by Pinilla et al. (2012a). Although their model is 1d only and to the make the problem

numerically tractable they had to ignore the details of the planet disc interaction, they manage to obtain SEDs that are similar to the ones observed in transition discs. Further work is needed to confirm or disprove the hypothesis that a giant planet is able to give rise to a transition disc.

Another possible scenario that was recently proposed by Owen (2014) is that the small dust is held outside the planetary gap from the accretion luminosity of the planet, via the radiation pressure on the small dust grains. The effect depends crucially on the mass of the planet and on the accretion rate onto the planet; if these are too low, the small dust flows in the gap, creating a sub-mm cavity but not a transition disc in the SED. Indeed, such a disc has been observed. It could be that many more are present, but the selection bias has up to now hindered their discovery. Also this scenario is worth of more investigation in the future.

Note that the phenomena on the dust that we discussed up to now do not really have to do with the disc evolution and dispersal. If it is true that a transition disc is formed when a giant planet is embedded in it at several tens of AU, then it not necessarily true that all discs go through a transition phase (we do not expect all stars to have giant planets at tens of AU from what we know about exoplanets), neither that it is a short-lived phase, as the remaining lifetime can still be in the order of Myr. As already mentioned, it is possible that transition discs are actually composed by two families (Owen & Clarke, 2012a). The first one, that with small holes and low accretion rates, are the "canonical" transition discs created by photo-evaporation, a short-lived phase through which the majority of discs have to go. The second class, that with large holes and high accretion rates, could be the planet-hosting discs at large separations from the star. For this reason, It is worth to explore the impact that a giant planet has on the evolution of such a disc, and this is one of the major topics of this thesis, that will be detailed in chapters 2 and 5.4.

1.7.3   Dynamical encounters

Stars do not form in isolation, but in regions of enhanced gas and stellar densities (Lada & Lada, 2003). Therefore, it is important to assess how this environment influences the evolution of protoplanetary discs around young stars. In particular, two stars can have a close encounter between them. If one of the two stars possess a disc, this is likely to be influenced by the encounter, and possibly severely damaged (Clarke & Pringle, 1993). To get a handle on the frequency of such encounters, basic stellar dynamics theory (e.g., Binney & Tremaine, 1987) predicts that one can write the timescale for encounters approximately as

$$\tau_{\text{enc}} = 3.3 \times 10^7 \left(\frac{100 \text{ pc}^{-3}}{n} \right) \left(\frac{\sigma}{1 \text{ km s}^{-1}} \right) \left(\frac{10^3 \text{ AU}}{R_{\text{close}}} \right) \left(\frac{M_*}{M_\odot} \right) \text{ yr,} \qquad (1.47)$$

where n is the number density of stars, σ their velocity dispersion and R_{close} the maximum radius that we consider to call an encounter "close". In an extreme enviornment such as the Orion Nebula Cluster (ONC), the stellar densities can be as high as 10^4 pc^{-3} (Hillenbrand & Hartmann, 1998), bringing this timescale down to values smaller than the typical lifetime of a disc. Although this shows that for a star formed in such environment the influence of

stellar encounters cannot be neglected, these stars are probably not the significant majority of the total. This justifies the need for detailed work to establish how important are stellar encounters for disc dispersal.

Works in the literature have used either analytical arguments to explore the problem (Adams, 2010a), either pure N–body simulations in which close stellar encounters are recorded and the effect of single encounters on a putative disc is inferred a posteriori (Scally & Clarke, 2001; Olczak et al., 2006; Pfalzner et al., 2008; Olczak et al., 2012). Adams (2010a) concluded that the probability for a solar type star, when averaging over the possible birth environments, to have a close encounter in its history is only 10%, and thus stellar encounters are not likely to have a significant effect on disc dispersal. Nevertheless, there is ample evidence that the Solar System had a close encounter at around 100 AU, which truncated the disc at around 30 AU, so that the phenomenon can still have deep effects. There is a bit of controversy in the literature about the role of stellar encounters even in the ONC itself.   concluded that stellar encounters are unlikely to be a significant process contributing to disc dispersal. On the other hand, found in a few Myr of evolution that a significant fraction of discs $(10 - 15\%)$ is destroyed by the pure effect of encounters, without even considering the effect of viscous evolution or photo-evaporation, that further reduce the disc mass. Resolving this controversy is outside the scope of this thesis; we note in passing that most of what we know about proto-planetary discs comes from nearby star forming regions, where the stellar density is never as high as in the ONC. Given then that even in the ONC the exact role of stellar encounters is debated, it is safe to assume that it does not play a significant role in less extreme environments, and justifies to neglect it as we will do in most of this thesis.

The impact of stellar encounters can be nevertheless important for other properties of a proto-planetary disc, even if does not contribute significantly to deplete the disc mass. The kind of investigations that were conducted in the past were limited in this respect, as they did not have the ability of following any property other than the disc mass. From the theoretical side, the inclusion of a "live" disc in the simulation permits to investigate how the disc reacts to the stellar dynamics happening in an young stellar cluster. This thesis contains in chapter 3 a proof of concept of such a model, showing indeed that encounters, although not able to modify significantly the mass of a disc, can still change significantly its size.

1.8   The structure of this thesis

This thesis explores the problem of disc dispersal from different point of views. The main one that we explored is to define what is the interplay between photoevaporation and giant planet formation. The highly accretors observed in the population of transition discs are particularly suggestive of the presence of planets in them. As there is strong evidence that photoevaporation is one of the main drivers of disc evolution, it is natural to ask what happens in the evolution of these discs. While much work in the literature has focussed in explaining how to create a transition disc, little has been done to investigate

how a transition disc evolves in time and how long lived it is. This will be investigated in chapters 2 and 5.4.

This thesis also offers other contributions to the topic of disc dispersal. In chapter 3 we develop a model that is able to follow the evolution of "live" discs in a young stellar cluster (see section 1.7.3). In chapter 4 we propose a scenario for the issue of old accretors (see section 1.2.3.2), exploring the possibility of disc reformation. In chapter 5 we show that X-ray photo-evaporation provides a natural explanation in the observed correlations of the mass accretion rate with the stellar mass (see section 1.2.2.1), and this adds to the existing evidences that it is one of the main drivers of disc evolution.

Finally, in chapter 7 we draw our conclusions.

Chapter 2

The interplay between X-ray photo-evaporation and planet formation

Abstract

We assess the potential of planet formation instigating the early formation of a photoevaporation driven gap, up to radii larger than typical for photoevaporation alone. For our investigation we make use of hydrodynamics models of photoevaporating discs with a giant planet embedded. We find that, by reducing the mass accretion flow onto the star, discs that form giant planets will be dispersed at earlier times than discs without planets by X-ray photoevaporation. By clearing the portion of the disc inner of the planet orbital radius, planet formation induced photoevaporation (PIPE) is able to produce transition disc that for a given mass accretion rate have larger holes when compared to standard X-ray photoevaporation. This constitutes a possible route for the formation of the observed class of accreting transition discs with large holes, which are otherwise difficult to explain by planet formation or photoevaporation alone. Moreover, assuming that a planet is able to filter dust completely, PIPE produces a transition disc with a large hole and may provide a mechanism to quickly shut down accretion. This process appears to be too slow however to explain the observed desert in the population of transition disc with large holes and low mass accretion rates.

2.1 Introduction

The evolution and final dispersal of the gas and dust contained in protoplanetary discs surrounding young low-mass stars plays an important role in shaping the properties of potential planets in the system. In particular the disc dispersal time-scale sets an upper

limit for the formation of gas giants. It is therefore crucial to formulate a theory capable of describing the disc evolution and dispersal in detail, which is an important input for the planet formation theory.

For most of their lifetime, the evolution of discs is driven by viscosity. Currently, the most favoured mechanism for its origin is the magnetorotational instability (Balbus & Hawley, 1991b), although other mechanisms have been proposed, such as the transport of angular momentum by spiral waves in self-gravitating discs (Lodato & Rice, 2004). Under simplifying assumptions, the evolution in time of a disc can be described by an analytical solution (Lynden-Bell & Pringle, 1974), which was showed to be in rough agreement with the observations (Hartmann et al., 1998) of the mass accretion rates in "classical" T-Tauri discs.

However, the final evolution of protoplanetary discs appears not to be compatible with this picture. Discs have a characteristic lifetime of 3 Myr (Haisch et al., 2001; Mamajek, 2009; Fedele et al., 2010a), as can be shown looking at the fraction of disc bearing young stellar objects (YSO) in clusters of different ages, but, rather than from a homogeneous draining as predicted by pure viscosity evolution, discs seem to have a fast, final stage of clearing from the inside out (Luhman et al., 2010; Ercolano et al., 2011a; Koepferl et al., 2013a) with a typical time-scale of 10^5 years. This behaviour has been called "two-timescale" in the literature.

"Transitional discs" are objects believed to have been caught in the act of disc-dispersal and hence to be useful for shedding light on the mechanism responsible for disc clearing. First spotted by spectral energy distribution (SED) observations of YSOs more than two decades ago (Strom et al., 1989b; Skrutskie et al., 1990b), although only more recently the Spitzer space telescope gave the possibility to study them in detail (e.g. Calvet et al., 2005b; Espaillat et al., 2010b), they lack emission at the mid IR wavelengths when compared to "standard" disc. This deficit of opacity in the warm dust has been interpreted as the signature of an inner hole. SED modelling is however a rather difficult task, depending on many model parameters that are often degenerate. More recently, the advent of good quality data from sub-mm interferometers has permitted to obtain spatially resolved images of some of these objects, confirming indeed the presence of large cavities (Andrews et al., 2011), sometimes of order of tens of AU. The frequency of transitional disc (~ 10 per cent of total number of protoplanetary discs) is compatible with the interpretation that they represent a fast, final phase of disc evolution that proceeds from the inside out (Kenyon & Hartmann, 1995). It has to be remarked that, despite the images confirm large cavities both in the sub-mm and in the micron-sized dust, gas is in many cases still present. Indeed, some of these transitional discs present mass accretion rates of order 10^{-8} M$_\odot$yr^{-1}, comparable with that of classical T-Tauri stars, indicating that a substantial reservoir of gas is still present near the central object. Even more remarkably, it has to be noted that such mass accretion rates are not a general feature of all transition discs, and that there is instead a huge range of variation in the observed sample.

To explain the presence of this class of discs, many physical processes have been invoked, including grain growth (Dullemond & Dominik, 2005b), photoevaporation (Clarke et al., 2001b; Alexander et al., 2006b) and planet formation (Armitage & Hansen, 1999b; Rice

et al., 2003). However, up to now none of these processes alone have been shown to be sufficient to explain all observations.

Growing through collisions, dust particles can indeed become large enough to become essentially invisible to observations. However, while models of grain growth are able to reproduce the observed dips in their infrared SEDs of transitional discs, they predict that the dust should still be visible at millimetric wavelengths, in contrast with what is found in observations (Birnstiel et al., 2012b).

The presence of a giant planet embedded in the disc is able to open a gap, and acts like a dam, stopping the inflow of matter from the outer disc reservoir. However, the dam is porous, and while the surface density in the inner disc is lowered and the mass accretion rate reduced, the material can still flow towards its way to the star (e.g. Lubow & D'Angelo, 2006). To reconcile this with observations, it is necessary to find the right combination of parameters that makes the inner disc optically thin, while still allowing a sensible mass accretion rate. As showed by Zhu et al. (2011), theoretical calculations predict that one single planet is not able to perturb enough the surface density of the inner disc, and multiple accreting planets are required to open a gap of a size compatible with what is found in observations. This reduces however the mass accretion rates onto the star as well as the surface density. Zhu et al. (2011) conclude that even in the case of multiple planets it is not possible to interpret discs that exhibit a large hole size together with a high mass accretion rate onto the star.

Photoevaporation is the process through which high energy radiation (from the central star or from the environment) thermally drives a wind from the disc. The mass-loss rates depend on the detailed physics of the radiation field. Including the effect of EUV radiation from the central star, Clarke et al. (2001b) and Alexander et al. (2006c) showed that the coupled evolution of a viscously evolving disc with the presence of a photoevaporative wind is able to open a gap in the inner disc when the mass accretion rate through the disc becomes comparable with the mass-loss rate of the wind. Owen et al (2012) further argue that the dust in the inner disc rapidly drifts onto the star (Alexander & Armitage, 2007) – on a timescale of $\sim 10^3$ years–, the gas drains on its (much longer) viscous time-scale ($\sim 10^5$ years). The result is a disc that exhibits an inner dust cavity (hence a dip in the mid-infrared emission), and an inner gas disc that is still draining, producing a still measurable mass accretion signature. Much progress has been made in computing detailed mass-loss rates from the photoevaporative wind. This is crucial to determine the mass-accretion rate at which the wind is able to open a gap, thus determining the age of the disc and the properties of the resulting transition disc. In particular recent models have included in the calculation FUV and X-ray radiation (Gorti & Hollenbach, 2009b; Ercolano et al., 2009; Owen et al., 2011a).

In particular, Owen et al. (2011a) compared the statistics of transitional discs with evolution models including X-ray photoevaporation from the central star, showing that it is indeed possible to explain a large number of observed objects with photoevaporation alone. This model however still failed to reproduce the class of transitional discs with large holes and large mass accretion rates, due to the fact that, by the time photoevaporation has carved a large enough hole in the outer disc, the mass reservoir of the inner disc has

dropped so much that no mass accretion rate is detectable anymore.

A possible scenario, as suggested by Owen & Clarke (2012b), is that "transitional" discs are not a homogenous class, indicating that different physical processes may be at work, and there may be different paths to transitional disc formation, depending on which of these physical mechanisms is dominant. If this is the case, we expect that in some cases there may not be a single dominant process, and it may be the interplay among several of them that leads to a given transitional disc formation.

Along this route, the goal of this paper is to study if the combination of photoevaporation and planet formation, which have been up to now studied separately, can indeed help in interpreting the puzzling population of accreting transitional discs. By reducing the surface density and the mass accretion rate in the inner disc, we expect that the presence of a planet is able to trigger the opening of a gap by photoevaporation at early times. We call this process planet induced photoevaporation (PIPE). To investigate this scenario, we make use of hydrodynamics models of a photoevaporating disc with a giant planet embedded. Our purpose is to assess how the presence of a planet affects the clearing of the disc by X-ray photoevaporation.

This paper is structured as follows. In section 2 we present the numerical method we used and the results we obtained. In section 3 we discuss the results and in section 4 we draw our conclusions.

2.2   Numerical investigation

2.2.1   Methods

We study the disc-planet interaction process by means of the 2D grid-based hydrodynamics code FARGO (Masset, 2000a). The conditions at the time t_0 of the formation of the planet are provided by a 1D viscous evolution code, that takes care of evolving the disc from time $t = 0$ to t_0. This allows to save computational resources when detailed evolution of the disc is not needed.

2.2.1.1   Initial conditions (1D evolution)

As initial conditions, we use the models of Owen et al. (2011a). We include the effects of viscous evolution and X-ray photoevaporation. The evolution of the surface density of the disc is described by the following equation:

$$\frac{\partial \Sigma}{\partial t} = \frac{3}{R}\frac{\partial}{\partial R}\left[R^{1/2}\frac{\partial}{\partial R}\left(\nu\Sigma R^{1/2}\right)\right] - \dot{\Sigma}_{\rm w}(R), \tag{2.1}$$

where Σ is the surface density, $\dot{\Sigma}_{\rm w}(R)$ is the photoevaporation profile (as in the Appendix of Owen et al. 2012b) and ν is the kinematical viscosity coefficient, which sets the magnitude of viscosity. We choose the same values of the parameters as in Owen et al. (2011a), that we summarise here. We evaluate ν using the α prescription (Shakura & Sunyaev, 1973b):

$\nu = \alpha c_s H$, where c_s is the sound speed of the gas, H is the vertical scale-height and α the dimensionless Shakura-Sunyaev parameter. In our models we set $\alpha = 1.5 \times 10^{-3}$. The sound speed is a fixed function of radius, and is chosen to give a mildly-flaring disc (i.e., $H/R \propto R^{1/4}$); the normalization is chosen so that at 1 AU the aspect ratio $H/R = 0.0333$. Our computational grid covers the range $[0.0025\,\mathrm{AU}, 2500\,\mathrm{AU}]$, and it is comprised of 1000 grid points. The mesh is uniform in a scaled variable $X \propto R^{1/2}$. Our viscous code uses a flux-conserving donor-cell scheme, implicit in time. Details about the implementation can be found in Birnstiel et al. (2010).

The initial surface density profile is given by:

$$\Sigma(R, 0) = \frac{M_\mathrm{d}(0)}{2\pi R R_1} \exp(-R/R_1), \tag{2.2}$$

where $M_\mathrm{d}(0)$ is the initial mass of the disc and R_1 a scale radius describing the exponential taper of the disc's outer region. We set a value of $R_1 = 18$ AU and an initial disc mass of $0.07 \mathrm{M}_\odot$.

For what concerns the photoevaporation profile, there are two parameters, the mass of the central star M_* and the X-ray luminosity L_X. We chose $M_* = 0.7\,\mathrm{M}_\odot$, while we perform calculations with different values of the X-ray luminosity. We do runs with the median X-ray luminosity $L_X = 1.1 \times 10^{30}\,\mathrm{erg\,s^{-1}}$, that we evolve for 2 Myrs before inserting the planet, and runs with a higher X-ray luminosity of $\log L_X = 30.8$, that we evolve for 0.65 Myr. These values for the planet formation time-scale do not come from a physical model, but rather were chosen to have a similar reasonable surface density profile at the moment of the planet formation. Since in the case of the high X-ray luminosity the evolution of the disc is faster due to the increased mass-loss rate, in that case we chose a smaller value for the age of disc at the moment of planet formation. In both cases the normalization at 1 AU is approximately $500\,\mathrm{g\,cm^{-2}}$, which is a factor 3-4 lower than the Minimum Mass Solar Nebula (Hayashi, 1981b). However, it should be noted that the power-law slope is -1, rather than $-3/2$, so that in the outer region the surface density is higher. The total mass in the disc at the moment of planet formation is approximately 25 $\mathrm{M_{jup}}$ for the median X-ray luminosity, and 20 for the high X-ray luminosity (the difference due to the disc being more spread out in the first case), which is higher than the Minimum Mass Solar Nebula. We note that according to current planet formation theories it is difficult, although still plausible (Movshovitz et al., 2010), to form a gas giant in the short time-scale used in the second case; therefore the high X-ray luminosity case should be regarded as a limiting one.

2.2.1.2 fargo simulations

At time $t = t_0$, we assume that a gas giant planet forms, and we use the output of the 1D code as input for the 2D FARGO code. We assume that the formation happens on a time-scale fast enough so that we can switch from a 1D disc withouth a planet to a 2D disc with a planet. The code, which has been widely used in studies of protoplanetary discs, solves the equations of hydrodynamics through finite differences on a grid in cylindrical coordinates. FARGO uses the same algorithms as the ZEUS code (Stone & Norman, 1992)

for hydrodynamics, but employs a modified azimuthal transport technique that result in a smaller computational request for disc geometries.

The code solves the coupled system of Navier-Stokes and continuity equation. We modified the continuity equation from the publicly available version of the code to include the effects of photoevaporation on the disc. The continuity equation now reads:

$$\frac{\partial \Sigma}{\partial t} + \nabla \cdot (\Sigma \mathbf{v}) = -\dot{\Sigma}_{\mathrm{w}}(R), \qquad (2.3)$$

where $\dot{\Sigma}_{\mathrm{w}}$ is the same mass-loss profile due to photoevaporation employed in the 1D evolution. A similar implementation was also used to study planet scattering in transitional discs by Moeckel & Armitage (2012).The removal of mass is done at the beginning of the hydro time-step. To be able to follow the evolution in time of the disc, we implemented a minimum density through the disc. Whenever the density becomes smaller than a given threshold, it is reset to the minimum allowed value. We use the dimensionless value of 10^{-8} for this threshold, which is about five orders of magnitude smaller than the initial value of the density in the disc at the planet location. For safety, we modified also the timestep condition, adding another criterion that does not permit to photoevaporation to remove in a single timestep more than a given fraction f of the mass in a cell. We used for f the value of 0.1. However, we noted in our simulations that this condition is never relevant, and that the other usual conditions on the timestep are more restrictive.

We set the parameters to the same values as in the 1D evolution. We are however not able to resolve the whole disc in a 2d simulation, therefore we restrict ourselves in the range $[0.1r_p, 10r_p]$, where r_p is the planet orbital radius. We employ a resolution of $n_\phi = 256$ cells in the azimuthal direction, uniformly distributed. The radial resolution is then chosen so that each cell is approximately square, which gives $n_r = 188$ cells. While considerably higher resolution simulations can be found in the literature, we remark that here we are interested in the global evolution of the disc, rather than capturing some local property. Even if some feature is not properly resolved (such as the accretion streams onto the planet), this has little effect on the global evolution. For this reason similar studies of the disc evolution on a long timescale have employed a resolution similar to ours (e.g., Zhu et al., 2011). We have checked, running simulation M20 at double the resolution and comparing the result, that our results stay the same, with a maximum 10% difference in the mass of the inner disc up to the moment of the disc clearing.

We consider a planet embedded in the disc with a mass $M_p = 10^{-3}M_* = 0.7\ M_J$, and we let the orbital radius of the planet vary from 10 to 50 AU. The planet is not allowed to migrate, although we also performed a run in which we include this effect. In the simulation in which we included also migration, we switched it on only after 500 orbits to restrict to the case of Type II migration and exclude Type I migration. To reduce artefacts in the solutions due to a sudden insertion of the planet, we slowly increase its mass during the first 100 orbits, using the taper function provided in the publicly available version of FARGO. We use open inner boundary conditions and reflecting outer boundary (which is the default in FARGO. To test the impact of this choice, we implemented an outer boundary condition, finding no significant difference). We use planetary accretion
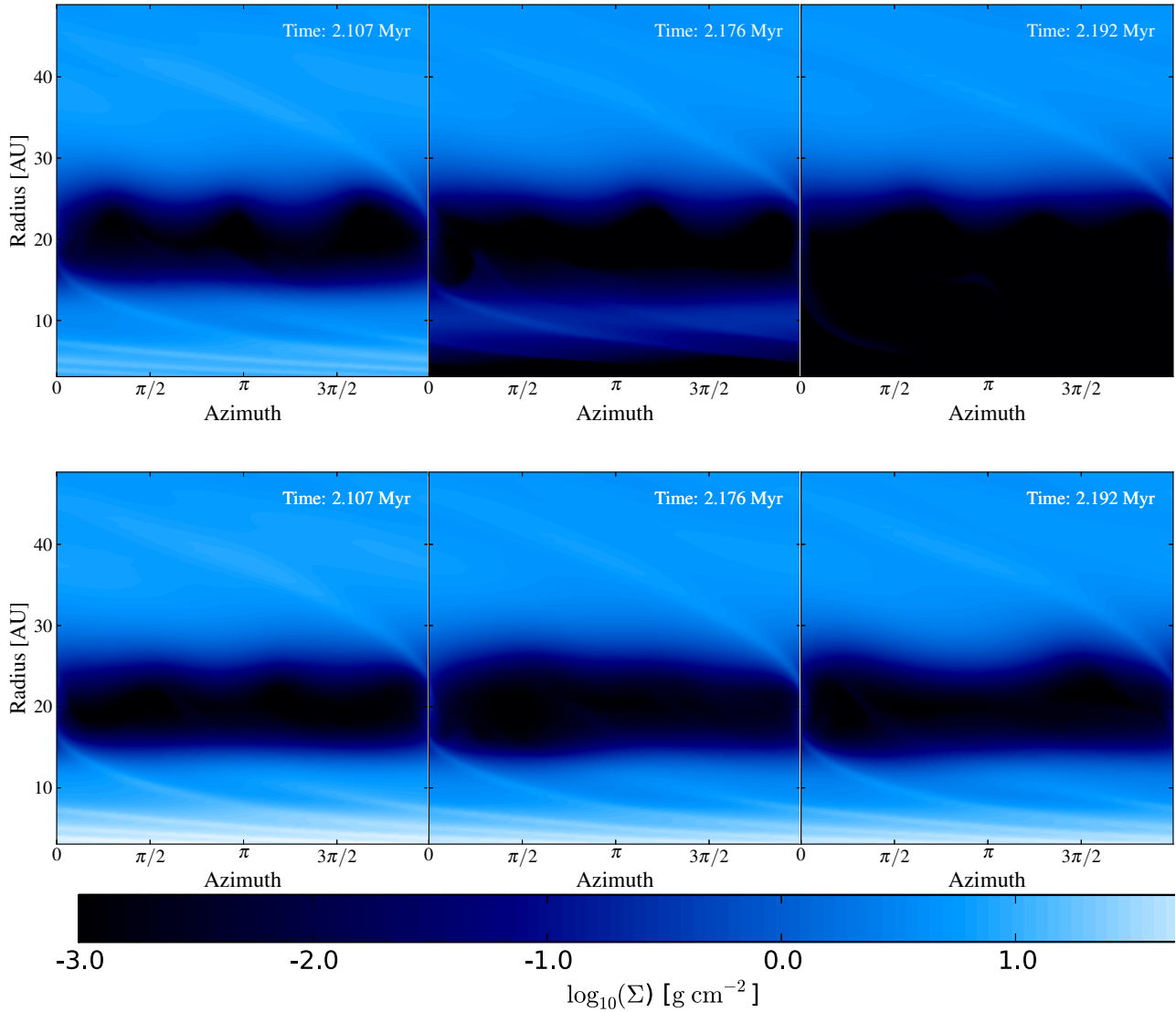
Figure 2.1: Top row: surface density in the disc at three different times from simulation M20. Bottom row: same quantities for simulation M20o, which do not include photoevaporation. While in the first snapshot the inner disc is still there also in the case including photoevaporation, it is caught in the act of clearing in the second snapshot. Finally, we are left with a disc with the outer part only in the last snapshot. In the control simulation instead the inner disc is left.

Run name	Orbital radius [AU]	$\log L_X$	t_0 [Myr]	Notes
M10	10	30.04	2	
M20	20	30.04	2	
M20m	20	30.04	2	migration
M20f	20	30.04	2	slower accretion
M20o	20	30.04	2	no photoevaporation
M30	30	30.04	2	
M40	40	30.04	2	
M50	50	30.04	2	
M20x	20	30.8	0.65	
M40x	40	30.8	0.65	

Table 2.1: The table summarises the simulations run. The number in the name of the run specifies the position of the planet in AU; the "x" denotes the runs with high X-ray luminosity. In addition to the standard runs, which let the planet position and the X-ray luminosity vary, there also tree "special runs", with names M20m, M20f and M20o, respectively including migration, with a slower planetary accretion timescale employed and without photoevaporation. The initial planet mass is in every case 0.7 M_J.

as prescribed by Kley (1999) using the publicly available implementation in FARGO. At each timestep, a fraction of the material inside the Hill radius of the planet is removed and accreted onto the planet. The fraction is controlled by a free parameter, f, that represents the inverse of the accretion timescale in dynamical units. We use $f = 1$ for our standard model, although we test also a situation with a 10 times slower accretion timescale. Table 2.1 summarises the simulations run.

Lastly, it should be noted that the inclusion of a photoevaporation profile breaks down the degeneracy of the dimensionless units used by FARGO. In the pure hydrodynamical case, we have one free mass scale and the results can then be scaled to different central star masses. This is no longer the case including photoevaporation, because $\dot{\Sigma}_w$ depends on the (physical) radius in the disc and on the mass of the star.

2.2.2   Results

2.2.2.1   Qualitative picture

The surface density in the disc at three different times from runs M20 and M20o is plotted in figure 2.1. In the left panel, at an age of approximately 2.1 Myrs, the dynamical gap cleared by the planet is evident, but photoevaporation has not yet started to clear the disc. The surface density at this stage is very similar to a control run without photoevaporation, the most notable differences are visible at the gap edges. The planet acts like a dam for the viscous flow, reducing the mass accretion rate in the inner part of the disc. This permits photoevaporation to take over, and clear the inner disc, as can be seen in the intermediate step in which photoevaporation is clearing the disc from inside out. Finally, we are left only with the outer disc, when the disc is approximately 2.2 Myrs old. It should be noted
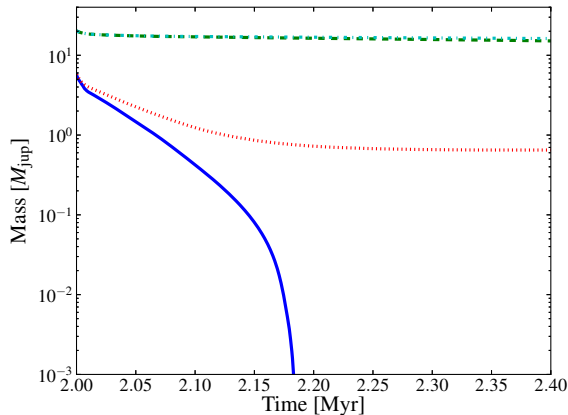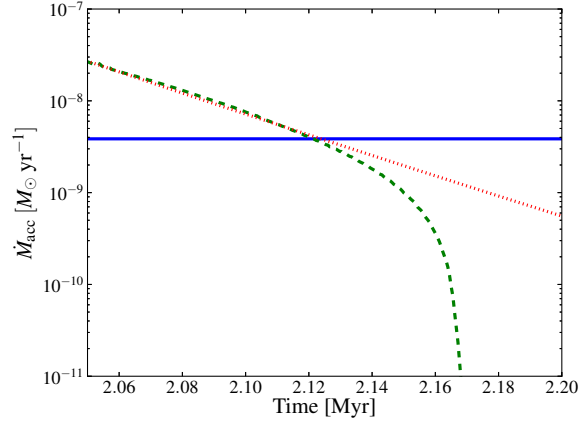
Figure 2.2: Solid blue line: mass of the inner disc (i.e., inside the planet orbital radius) with photo-evaporation (run M20). Dotted red line: mass of the inner disc without photoevaporation (run M20o). Dashed green line: mass of the outer disc (i.e., outside the planet orbital radius) with photoevaporation (run M20). Dotted-dashed cyan line: mass of the outer disc without photoevaporation (run M20o). In the run M20 with photoevaporation, the inner disc is rapidly dissipated, while in the control run M20o it reaches a sort of steady-state value.

that the clearing of the inner disc is due to the combined effect of photoevaporation and planet formation. In the control simulation M20o without photoevaporation, the mass of the inner disc is reduced, but not cleared completely, as can be seen from the bottom row of figure 2.1. On the other hand, with photoevaporation alone the disc would have cleared on a longer time-scale, after 3.3 Myrs years. It can be concluded that PIPE, i.e. the combined effects of photoevaporation and planet formation, is able to clear the inner disc at earlier times, that is, stars with giant planets will dissipate their inner discs quicker.

Figure 2.2 shows the masses of the outer and inner disc (i.e., at radii larger and smaller than the planet orbital radius) as a function of time. For reference we included also the result of the control run M20o without photoevaporation. While they start from the same initial value, the difference accumulates in time, and when photoevaporation becomes important it rapidly dissipates the inner disc. On the contrary, in the control run without photoevaporation the mass of the inner disc reaches some kind of steady state value, slightly smaller than a Jupiter mass. Due to our use of a floor density, after the clearing of the inner disc there is still a non-zero mass inside the orbit of the planet, with a value that is around 10^{-4} $M_{\rm jup}$ (out of scale in the figure). It should be noted also that there is little difference in the mass of the outer disc between the two runs, and that the final value is around 15 $M_{\rm jup}$.

In figure 2.3 we plot the mass accretion rate at the inner boundary of the grid. The change in the slope corresponds to the moment at which the inner disc starts to clear. In the figure we overplot also, as a horizontal line, the mass-loss rate due to photoevaporation (considering the inner disc only). It can be seen that only once the mass accretion rate has dropped below some factor of the mass-loss rate the clearing begins. The qualitative understanding of disc clearing is thus not really different from the evolution of a disc

Figure 2.3: Green dashed line: mass accretion rate at the inner boundary of the grid as a function of time for simulation M20. For reference, the blue solid horizontal line shows the mass-loss rate due to photoevaporation in the inner disc, while the red dotted line is a straight line added as a visual aid to distinguish the moment of the inner disc clearing. The change in the slope of the mass accretion rate corresponds to the inner disc clearing. This clearing happens when the mass accretion rate has dropped below some factor of the mass-loss rate.
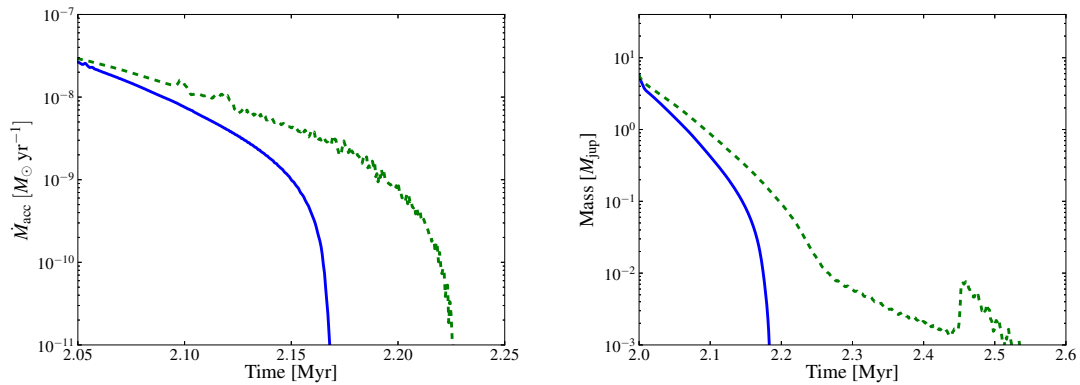
**Figure 2.4:** Left: comparison of the mass accretion rate at the inner boundary as a function of time, varying the planetary accretion timescale. The blue solid line is for the standard value ($f = 1$), run M20, and the green dashed line for the slow accretion ($f = 10$), run M20f. Right: comparison of the mass of the inner disc as a function of time. The lines have the same style as in the left panel.

without a planet, namely the two-timescale behaviour (as in the UV switch model): for most of its lifetime the evolution of the disc is driven by viscosity, and only when the mass accretion rate drops below the mass-loss rate due to photoevaporation the clearing begins. The role of the planet is that of accelerating this process, acting like a dam that reduces the mass accretion rate in the inner disc. We remark that, since the inner disc spends most of its lifetime with a mass accretion rate that is higher than the mass-loss rate, the total mass of the disc that has been lost through accretion is greater than the one carried away by photoevaporation. Thus, it is the accretion that does most of the "dirty job" of dissipating the disc, and photoevaporation only contributes in the last step of the removal. For what concerns planetary accretion, we have checked that most of the mass that ends up on the planet comes from the outer disc. This does not mean that planetary accretion does not play a role in the dispersal of the inner disc. Indeed, it controls the porosity of the planetary dam, fixing the amount of the viscous flow from the outer disc that is intercepted. This effect makes the mass of the planet increase by a factor 6 at the moment of disc dispersal. However, the direct effect, namely the mass accreted by the planet directly from the inner disc, is little compared with the mass leaving the grid from the inner boundary, apart for a small initial transient in which the planet is accreting from the region that will be dynamically cleared.

2.2.2.2   Effect of planet accretion timescale

This qualitative picture implies that a crucial parameter for estimating the impact of the presence of a planet in the disc is the porosity of the dam. We notice that in a 1D simulation the planet acts as a complete dam, and no filtering is possible. Thus, one has to insert by parametrization the porosity of the dam (e.g., Alexander & Armitage, 2009a), in a way that does not conserve angular momentum. This effect is better accounted for in 2D simulations, where the transport of angular momentum across the gap is treated in a realistic fashion, although there is still a dependence on the planet accretion time-scale. To test how robust our results are with respect to the variation of this parameter, we run a simulation with a 10 times higher value (i.e., the planet accretes 10 times slower), $f = 10$, that we call M20f. In the left panel of figure 2.4 we propose a comparison between the mass accretion rate at the inner boundary of the grid of this simulation with the standard one. The inner disc is indeed cleared at later times, since we need to wait more for the mass accretion rate to drop, due to the higher porosity of the dam. However, it should be noted that the difference is not so dramatic as one could expect by such a big variation in the timescale. This is consistent with what other authors have found, namely that the process of planetary accretion is not dramatically dependant on the value of this parameter (Kley, 1999). What cannot be seen from this plot however is that the way in which the disc clears is different. This can be seen from the mass of the inner disc versus time comparison in the right panel of figure 2.4. We can see that with a reduced planetary accretion time-scale not only the clearing happens at later times, but it is also slower. Visual inspection of the surface density distribution shows that an inner ring of material is left just inside the orbit of the planet, which is only slowly eroded. We interpret this as due to the fact that,
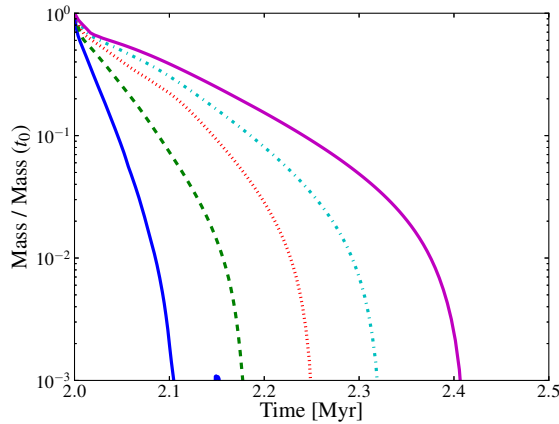
Figure 2.5: Comparison of the mass of the inner disc normalized to the initial value for simulations with different position of the planet, varying from 10 to 50 AU (runs M10-M50). The further the planet, the slower the clearing of the disc.

because of the higher mass accretion rate through the planetary gap, photoevaporation has a much more difficult job at removing this part of the disc, being continuously replenished from the outer disc. This shows the complex structures that may be formed due to the interplay between the different physical processes acting in the disc.

2.2.2.3 Varying planet position

In the simulation shown so far the planet has a semi-major axis of 20 AU. To find how the inner disc clearing depends on the planet position, we ran other simulations with different values of this physical parameter. Figure 2.5 shows a comparison in the mass of the inner disc (normalized to the initial value) as a function of time for the different simulations run, with the planet position varying from 10 to 50 AU (runs M10-M50). The further out the planet is, the slower the process of dispersal. This is expected, since more time is required for a further out planet to reduce the mass accretion rate near to the star. However, we can see that in all cases the disc dispersal is considerably faster than without the presence of a planet in the disc. A fit to the initial surface density profile with equation 6.1 gives for R_1 a value of approximately 80 AU, so that for the used values of the planet position the planet is able to cut most of the disc mass reservoir from the inner radii. From this argument we expect that a planet further out than R_1, if able to form, would not have a significant impact on the disc lifetime.

2.2.2.4 Varying X-ray luminosity

As a limiting case, we run simulations with a high value of X-ray luminosity, equal to logLx=30.8. The disc is 0.65 Myr old at the time when the giant planet is inserted. While this may sound like an unrealistically young age for planet formation, we note that the relative disc age can be obtained by the appropriate scaling of initial parameters and here
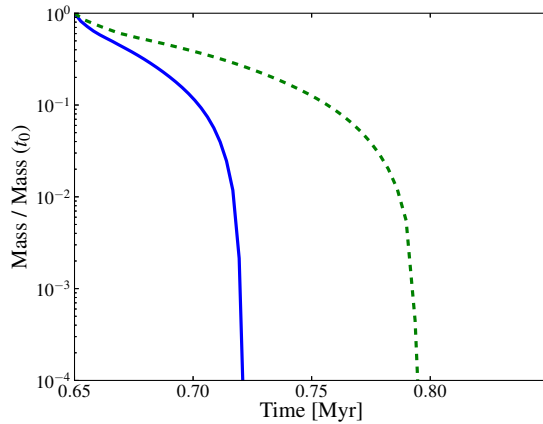
Figure 2.6: Mass of the inner disc, normalized to the initial value, as a function of time, for simulations with the high value of the X-ray luminosity with positions of the planet of 20 and 40 AU, runs M20x (solid blue line) and M40x (dashed green line).

we chose a value that gives a similar surface density normalization (although the disc is less spread, being younger) to the previous case. This shows how even quite a massive disc can be rapidly dispersed by the combined effect of X-ray photoevaporation and planet formation.

The evolution of the mass of the inner disc as a function of time, normalized to the initial value, is shown in figure 2.6 for different values of the planet initial position. Because of the higher mass-loss rates of photoevaporation, everything is happening quicker, with a dispersal that can happen so fast as less than 10^5 years after the planet formation. Also in this case the further the planet, the slower the process of disc dispersal. Visual inspection of the images confirms the same qualitative behaviour we outlined in the previous section.

2.2.2.5   Effect of migration

To test the sensitivity of our results to migration, that we neglected so far, we run a simulation with migration included, M20m. The left panel of figure 2.7 shows a comparison in the masses of the inner disc, showing that there is very little difference in the process of disc clearing. This is a consequence of the fact that the clearing proceeds from inside out, so that the beginning of the clearing is set by the properties of the disc in the inner portion, rather than in the neighbourhood of the planet that is affected by migration. The right panel of figure 2.7 shows the semi-major axis a function of time, showing that the planet has not migrated much before the disc is dispersed, approximately 2 AU. It may be argued that this is a consequence of the initial conditions, namely that we took quite an evolved disc. Inserting the planet at earlier times would have allowed more time to migrate, and therefore to be more incisive in modifying the clearing. This is what has been studied by Alexander & Armitage (2009a) and Alexander & Pascucci (2012), who coupled the disc evolution to the planet migration and studied the resulting planet distribution.
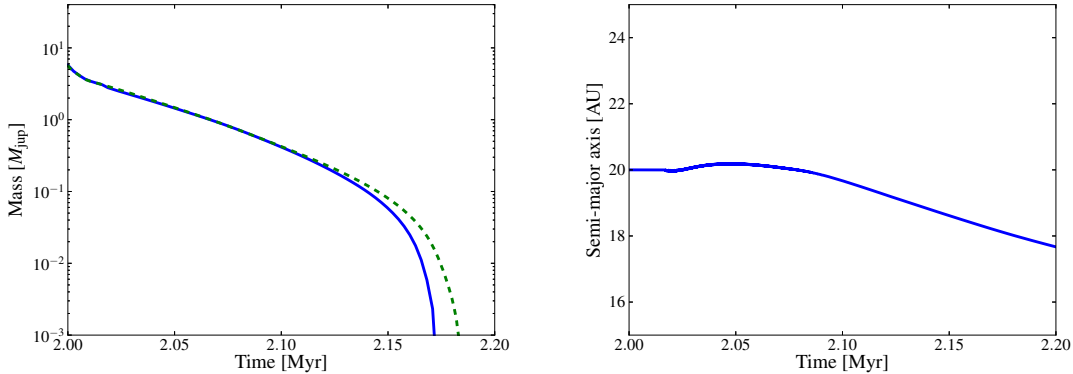
Figure 2.7: Results from the simulation M20m including migration. Left panel: the mass of the inner disc as a function of time for simulation M20m (blue solid line). For reference has been plotted also the case without migration, run M20 (green dashed line). Right panel: semi-major axis of the planet as a function of time.

The effect of more massive planets inserted in massive (self-gravitating) discs is the focus of a forthcoming study by Clarke et al. (in prep.), while in this work we focus on the study of less massive disc-planet systems.

2.3   Discussion

In the previous section we showed how PIPE is able to change the picture of disc dispersal with respect to photoevaporation or planet formation alone. The main finding is that discs with a planet are likely to be dispersed earlier than discs without. An interesting test of the PIPE scenario, is to compare its predictions with the observations of transitional disc, that are interpreted as discs caught in the act of clearing. In particular we study the $\dot{M} - R_{\text{hole}}$ parameter space. For each of our models, the aim is to compute evolutionary tracks that can be plotted in this parameter space. In contrast with Owen et al. (2011a), due to the increased computational cost, we are not able here to run a whole population synthesis; rather, we will be limited to comparing with individual datapoints. In particular, we wish to answer the question if transition discs with large holes and mass accretion rates can be accounted for by PIPE. A similar attempt has been made by Morishima (2012) through the modelling of X-ray photoevaporating discs with dead zones.

Unfortunately, our hydrodynamical modelling does not yield directly these parameters. In particular, the mass accretion rate the observations measure is the one onto the star, that we cannot resolve for numerical reasons. Therefore, we make two limiting assumptions to the modelling.

In the first, conservative assumption, we assume that the X-ray photoevaporation driven clearing of the innermost disc proceeds as it would do in the absence of a planet, opening a gap at approximately 1.5 AU. This gap is inside the region that we can resolve in the simulation. The disc will then exhibit two gaps, the dynamical one cleared by the planet
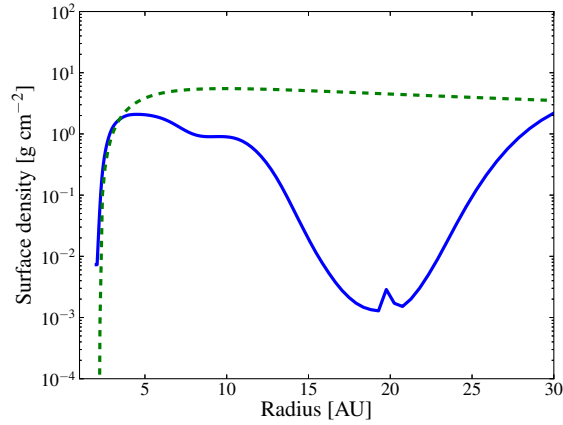
Figure 2.8: Surface density as a function of radius just before the inner disc clearing starts in run M20 (blue solid line), compared with the surface density in the 1D calculations from Owen et al. (2011a) model with the median X-ray luminosity (green solid line). The surface density are quite similar near to the inner boundary, while at greater radii in the case with a planet the surface density profile is much flatter.
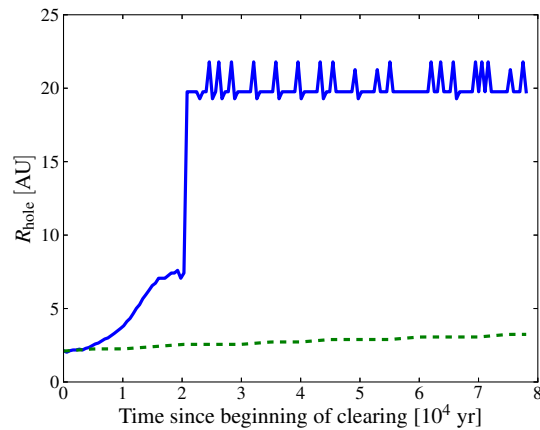
Figure 2.9: Inner hole radius a function of time (since the clearing), for the PIPE M20 calculation (blue solid line) and the 1D model with the median X-ray luminosity (green dashed line) from Owen et al. (2011a). The depletion of the surface density caused by the planet makes the opening of the hole much faster. The oscillations that can be seen in the radius of the hole in model M20 are a consequence of the oscillations at gap edges visible in figure 2.1.
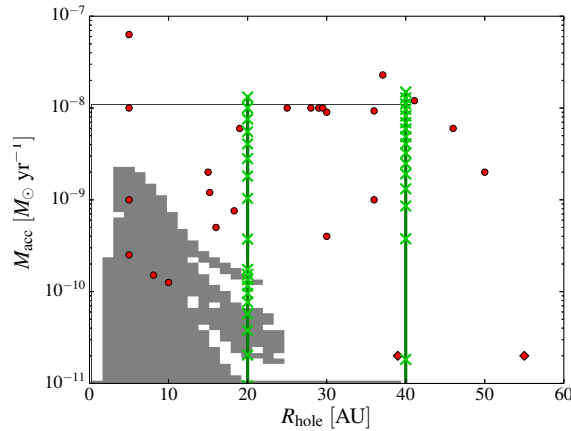
Figure 2.10: $\dot{M} - R_{\text{hole}}$ parameter space of transition discs. The grey area is the area permitted by X-ray photoevaporation alone, as in Owen et al. (2011a). Points are the observed datapoints with high millimetre flux from Owen & Clarke (2012b). Diamonds are for disc without a detected mass accretion rate. Blue dashed tracks are for the first assumption (see text) and green continuous for the second; crosses on the tracks are plotted every 10^4 years.

and the one opened by photoevaporation, that divide the disc in three distinct regions (named A,B and C in the following for clarity). As in the photoevaporation case, we assume that the dust in the innermost disc A will drain very quickly ($\sim 10^3$ yr) onto the star, so that region A will be invisible in observations. The disc will then look like a transition disc and the radius of the hole is set by the inner radius of disc B, that we can measure from the 2D simulation. While A is draining, there is still a measurable mass accretion rate. We assume that the dependence on time of the mass accretion rate onto the star is the same as in the 1D simulation, where we take as the beginning of clearing the time at which in the 1D simulation the radius of the hole is the inner boundary of our 2D grid. We note that the density structure in the region we can resolve is quite similar before the onset of clearing of the inner disc, as we show in figure 2.8. In this figure we compare the surface density from our FARGO simulation M20 just before the inner disc begins to clear with the results from the 1D run without the planet, at the time in which the radius of the hole is 2 AU (namely the inner radius of our 2D grid). The surface densities near the inner boundary are very similar, while at larger radii the density distribution is lower, due to the presence of the planet that makes this region devoid of gas. This motivates us to assume that the dependence with time of the mass accretion rate onto the star is the same as in the case without the planet, coming from the draining of the disc A onto the star, but now with a different R_{hole} dependence that is derived from the 2D simulation. In figure 2.9 we compare the R_{hole} dependence for model M20 and the corresponding model without a planet, i.e. Owen et al. (2011a) model with the median X-ray luminosity. We define the radius of the hole simply as the minimum radius where the azimuthally averaged surface density is above the imposed floor density (with an allowance factor of 10, due to the presence of numerical oscillations above the floor density). Because of the mentioned

depletion of the surface density, the clearing of the hole is much faster in the case with photoevaporation. When compared to models that include X-ray photoevaporation alone, we thus expect PIPE models to yield higher mass accretion rates for the same hole size, or conversely larger holes at the same mass accretion rate. The time $t = 0$ in the plot refers to the beginning of the clearing, and it is the one when in the 1D simulation the radius of the hole is 2 AU. We plot our results in the $\dot{M} - R_{\mathrm{hole}}$ parameter space in figure 2.10 as the blue dashed tracks. The cyan crosses are plotted every 10^4 years. Runs M20x and M40x are the ones that produce the higher mass accretion rates, while only runs M10 and M20 are visible from the runs with the median X-ray luminosity. The points in the plot are the observed datapoints that exhibit a high millimetre flux, as it is described in Owen & Clarke (2012b). The datapoints show a weak correlation between the hole radius and the mass accretion rate, which has not been explained yet. The grey area is the area permitted by X-ray photoevaporation alone, as in Owen et al. (2011a). Using this conservative assumption (blue lines), one would then conclude that the PIPE scenario is indeed able to expand the parameter space with respect to photoevaporation alone, but that the mass accretion rates obtained are still too low compared with the observations.

The other limiting assumption, that is a best case scenario for us, is the one in which the planet is able to filter the dust, so that the disc would look like in transition, even if there is still a huge quantity of gas inside the orbit of the planet. In synthesis, by modifying the surface density profile of the disc, the planet creates a pressure maximum. Dust particles, flowing inward, are unable to cross this maximum, so that the dust is filtered out from the inner portion of the disc, that becomes invisible to observations. This simple picture is complicated by the other dust processes that happen simultaneously (coagulation, fragmentation, diffusion, ...). This process has been studied in detail by Rice et al. (2006), Pinilla et al. (2012b) and Zhu et al. (2012). In this case, we take the orbital radius of the planet as the radius of the hole. Before the clearing starts, we take the mass accretion rate at the inner boundary of the grid, starting from 500 orbits since the beginning of the simulation (to exclude initial oscillations), under the assumption that the mass accretion rate in the inner portion of the grid that we do not simulate is set by the outer part that we can resolve. Once the inner disc starts to clear, we take as in the previous case the mass accretion rate as predicted by the case without the planet. The resulting tracks in this case (plotted in green continuous in figure 2.10) look like vertical lines, since there is little evolution of the radius during the simulation, and the mass accretion rate simply decreases. Using this second assumption, one would then conclude that, when the dust properties are taken into account, PIPE is able to explain discs with large holes and mass accretion rates. While up to now the theoretical effort has been to predict whether the appearance of a planet bearing disc resembles that of transitional disc, little work has been done in understanding the evolution of such systems. Photoevaporation could potentially give a reason for the shutting down of accretion, that is requested from the lack of observed datapoints in the region of the plot with large holes and low mass accretion rates. To explore this possibility, we plotted light green crosses along the tracks every 10^4 years. There is not however a clear separation between the uppermost and the lower part of the track, with only a little jump that is not enough to account for the desert

on the observed desert in the observed distribution. If this desert is real and not due to observational biases (e.g. discs with high mass accretion rates are also more massive), then a new mechanism must destroy the outer disc. Such a mechanism could be given by the "thermal sweeping" effect, an instability found in photoevaporating discs with an inner hole by Owen et al. (2012b), able to destroy the disc in the order of the dynamical timescale. The forthcoming work of Clarke et al (in prep.) presents an alternative scenario based on the carving of mm-bright accreting transition discs by massive planetary companions embedded and migrating in self-gravitating discs.

Our results suggest that the interplay between X-ray photoevaporation and planet formation is worth of further study. Our work also implies that planets are an important ingredient in the disc dispersal process, and should be included in the modelling. The ability of the upcoming ALMA facility will be hopefully be able to tell more about the gas structure in transitional discs, which is at the moment very poorly constrained.

2.3.1 Model limitations

In this paper it has been assumed that the photoevaporation profile is the same as computed by Owen et al. (2011a), who modelled the photoevaporative flow in a disc without a planet. Large scale 3D simulations that include both photoevaporation and a planet embedded are being carried out and will be presented in a forthcoming paper (Rosotti et al, in prep.).

The absolute timescales discussed in the paper should be taken with caution as they strongly depend on a number of simplifying assumptions. First of all, a source of uncertainty comes from the unknown mechanism for the angular momentum transport. In this work we have considered a simple α-disc and assumed a constant value of α. The assumption of a constant α-value is common in many theoretical studies of discs (e.g. Alexander et al., 2006c; Gorti et al., 2009b; Owen et al., 2011a), and is motivated by a lack of strong observational constraints and by simplicity, necessary to isolate the effect of the other processes that affect the evolution of the disc. However, no known theory of angular momentum transport predicts a constant value for α (Armitage, 2011a). Therefore, such an assumption should be regarded more as a matter of convenience. Studies addressing the issue of how a physical model for the viscosity, e.g. the layered accretion model proposed by Gammie (1996), changes the evolution of the disc have been conducted by, for example, Armitage et al. (2002); Morishima (2012). The layered accretion model predicts the formation of dead zones in the disc, where the viscosity is significantly lower than in the active parts of the disc. This is due to the insufficient ionization level in the cold midplane of the disc, which is not enough to couple the gas with the magnetic field and trigger the magnetorotational instability (MRI). The accretion continues in a thin layer, where the ionizing radiation (X-rays from the star and cosmic rays) are able to penetrate. The net effect, once vertically averaged, is to create a zone with a reduced viscosity. Employing a different model of photoevaporation than the one used in this paper, Armitage et al. (2002) modelled the combined evolution of a giant planet migrating in a layered disc. They find that the main effect of layered accretion is to slow down planetary migration due to the longer viscous timescale. However, as showed in section 2.2.2.5, migration is already rel-

atively unimportant for our results, so this is probably a second-order effect. Morishima (2012) found that the interplay between dead zones and photoevaporation can also be a possible route for the formation of transition discs with large holes and large mass accretion rates. Their results predict that, near the outer edge of a dead zone, the radial motion of gas is directed outwards, while it is inwards inside the dead zone region. This effect, once coupled with photoevaporation, may be able to open a gap in the disc at the outer edge of the dead zone, around 40 AU in their calculations. The dead zone in the inner disc will survive for a long time after the opening of the gap, so that $\dot{M}$ remains high even after the gap opens. Such considerations may also apply to the systems explored in this work. It is however difficult to predict the effect of a varying viscosity induced by the presence of a dead zone on the disc clearing timescales calculated here. The location and extent of the supposed dead-zone with respect to the planet will have a strong influence on how the dispersal is affected. Even the direction of the feedback from dead-zone formation is difficult to predict. On the one hand, a dead zone reduces the mass accretion rates in the region, hence reducing the mass flows through a planet gap, yielding to a faster decoupling of the inner and outer disc. However if the dead-zone contains most of the disc mass, as in the Morishima (2012) calculations, its effect could also be one of stabilisation of the mass accretion rates in the inner disc, resulting in a slower draining of the latter. Clearly a focussed exploration of the relevant parameter space would be required in order to provide educated predictions of the interaction of dead-zones (or indeed variable viscosity) with PIPE, which is beyond the scope of this work. Further uncertainties in the absolute timescales are introduced by numerical limitations, in particular the underresolution of the inner boundary that influences the resulting inner disc clearing timescales. Experiments have shown that the effect of having an inner boundary at a larger radius is to produce a higher mass accretion rate at the beginning of the simulation. This makes the disc deplete faster, thus shortening the lifetime of the disc. Therefore, while a faster disc evolution due to the combined effect of photoevaporation and planet formation is a robust prediction of PIPE (as can be seen by comparison of figure 2.1), absolute disc lifetimes may be longer than what presented here. While this effect is irrelevant for the first assumption presented here in the discussion, it could partially help in explaining the mentioned desert in the observed transitional disc population. In addition, as already said in the previous sections, this numerical limitation precluded us the possibility of following the evolution of the very inner disc, where photoevaporation is opening a gap.

Finally, another possible improvement of the models presented here is adding the modelling of the dust, in order to be able to compare directly the outcome of the model with observations. This will be particularly important to compare with ALMA observations.

2.4   Conclusions

In this paper we presented results from 2D simulations of discs with giant planets embedded undergoing X-ray photoevaporation. Our results show that planet formation influences the process of disc dispersal by photoevaporation. The main consequences of planet formation

induced photoevaporation (PIPE) can be summarized as follows:

1. by reducing the mass accretion flow onto the star, discs that form planets will be dispersed at earlier times than discs without by X-ray photoevaporation.

2. For what concerns transitional discs, PIPE is able to produce transition disc that for a given mass accretion rate have larger holes when compared to standard X-ray photoevaporation. However further modelling of the dust processes is needed to be able to fully exploit the observational consequences of this process.

3. Assuming that the planet is able to filter dust completely (Rice et al., 2006; Pinilla et al., 2012b; Zhu et al., 2012), large hole transition discs could be produced. PIPE may instigate the shutting down accretion; however, our simplified models cannot at present explain the observed desert in the population of transition disc with large holes and low mass accretion rates.

Chapter 3

Protoplanetary disc evolution affected by star-disc interactions in young stellar clusters

Abstract

Most stars form in a clustered environment. Therefore, it is important to assess how this environment influences the evolution of protoplanetary discs around young stars. In turn, this affects their ability to produce planets and ultimately life. We present here for the first time 3D SPH/N-body simulations that include both the hydrodynamical evolution of the discs around their natal stars, as well as the dynamics of the stars themselves. The discs are viscously evolving, accreting mass onto the central star and spreading. We find penetrating encounters to be very destructive for the discs as in previous studies, although the frequency of such encounters is low. We also find, however, that encounter influence the disc radii more strongly than other disc properties such as the disc mass. The disc sizes are set by the competition between viscous spreading and the disruptive effect of encounters. As discs spread, encounters become more and more important. In the regime of rapid spreading encounters simply truncate the discs, stripping the outer portions. In the opposite regime, we find that the effect of many distant encounters is able to limit the disc size. Finally, we predict from our simulations that disc sizes are limited by encounters at stellar densities exceeding $\sim 2 - 3 \times 10^3$ pc^{-2}.

3.1 Introduction

Stars form in regions of enhanced ambient gas and stellar densities compared to the Galactic field (Lada & Lada, 2003). Whether or not these density peaks are long-lived or disperse on

a dynamical time (i.e. whether they become bound stellar clusters or unbound associations) depends crucially on their initial densities and the resulting star formation efficiencies (Kruijssen et al., 2012). In Milky Way-like galaxies, about 10% of all stars are born in bound stellar clusters (Bastian, 2008), but this number increases with the gas surface density to up to $\sim 50\%$ in high-density starburst environments (Goddard et al., 2010; Adamo et al., 2011; Kruijssen, 2012; Silva-Villa et al., 2013).

The cluster environment leaves a spectacular imprint on the star formation process. Through the collective feedback of young stars such as stellar winds and photoionising radiation, natal gas is ejected and the accretion discs surrounding protostars may be destroyed by external photoevaporation (Adams et al., 2004b; Pelupessy & Portegies Zwart, 2012; Dale et al., 2013a). Combining the current observational and theoretical understanding of planet-, star-, cluster- and galaxy formation, Longmore et al. (2014) estimate that some 10% of all stars in the Universe may have the formation of planets (or lack thereof) in their habitable zones affected by their natal cluster environment. In this paper, we concentrate on the dispersal of gas from protoplanetary discs through encounters with neighbouring stars. It serves as a first step to obtaining a detailed understanding of how the cluster environment affects the evolution of protoplanetary discs.

In isolation, an effective viscosity causes the redistribution of angular momentum within the gaseous disc (Lynden-Bell & Pringle, 1974). This leads to disc spreading on the one hand and mass accretion onto the central star on the other hand. While the latter process is routinely observed (e.g., Gullbring et al., 1998; Natta et al., 2004; Herczeg & Hillenbrand, 2008b; Manara et al., 2012b), there are only a few observational reports of disc spreading (Isella et al., 2009; Guilloteau et al., 2011b), as high spatial resolution is needed to resolve the disc size. Within the current limitations, these works show how simple theoretical models are able to reproduce the observed rate of disc spreading. In practice, these works have concentrated on the nearest star-forming regions, namely Taurus-Auriga and Ophiucus, which are characterized by a lower stellar density when compared with more crowded regions, like the Orion Nebula Cluster (ONC). After several Myr of this slow and quiet evolution, it appears that another destructive process kicks in, and the disc is rapidly cleared on a $\sim 10^5$ yr timescale (Luhman et al., 2010; Ercolano et al., 2011a; Koepferl et al., 2013a). Currently, internal photoevaporation is the best candidate mechanism for such a fast disc dispersal (Clarke et al., 2001b; Alexander et al., 2006c; Gorti et al., 2009b; Owen et al., 2010b, 2011a).

Does a clustered environment impact this picture of disc evolution? de Juan Ovelar et al. (2012) found evidence of a dependence of the observed disc sizes on the environmental surface stellar density. In particular, discs in crowded environments, that is, at stellar densities above $10^{3.5}$ pc^{-2}, are systematically smaller than their counterparts in less crowded fields. Observationally, it is known that proximity to high mass stars may alter the evolution of protoplanetary discs via external photoevaporation (O'dell, 1998; Mann & Williams, 2010; Miotello et al., 2012). The high-energy radiation from massive stars can ionize and evaporate the material in the atmosphere of discs even at distances of $\simeq 1$ pc (Johnstone et al., 1998b; Adams et al., 2004b). Although there are spectacular images of this process in silhouette discs (proplyds) in the Orion Nebula Cluster (ONC), overall this

process is not expected to be the main driver of disc evolution (Adams, 2010b). Another important process occurring in a clustered environment are stellar encounters. Most of the previous work done on this problem has concentrated on modeling a given existing stellar cluster. These studies (Scally & Clarke, 2001; Olczak et al., 2006; Pfalzner et al., 2008; Olczak et al., 2012; Craig & Krumholz, 2013) involved either semi-analytic solutions or pure N–body simulations in which close stellar encounters are recorded and the effect of single encounters on a putative disc is inferred *a posteriori* (using results from simulations with pure N-body techniques, or including also hydrodynamical effects).

Scally & Clarke (2001) performed N–body simulations using 4 000 stars in virial equilibrium in an r^{-2} density distribution with a half–mass radius of ~ 1 pc to model the ONC. The ONC is a popular target, being the nearest massive star–forming region, where many protostellar discs are observed in silhouette against the bright nebula (Ricci et al., 2008; Robberto et al., 2013). The ONC contains ~ 4000 stars (i.e. $\sim 2 \times 10^3$ M$_\odot$) in a ~ 5 pc diameter volume, has a one–dimensional velocity dispersion of 2.5 km s^{-1} and a core density of 4.7×10^4 pc^{-3}. Scally & Clarke (2001) found that $\sim 8\%$ of all stars and $\sim 30\%$ of core stars suffered a sub–100 au encounter after 12.5 Myr of integration and concluded that encounters were unlikely to significantly affect the disk population. However, they cautioned that the sharp outer cutoff in their stellar distribution caused their models to expand significantly. This naturally lowers the encounter rate.

Olczak et al. (2006) used very similar initial conditions to Scally & Clarke (2001) in their N–body study of the ONC, except that they also modelled sub-virial clusters. Instead of recording the single closest encounter, as in Scally & Clarke (2001), Olczak et al. (2006) recorded the complete encounter history of objects on the following grounds: (a) the closest encounter may not be the most destructive, since a distant flyby of a massive perturber can do more damage than a near–miss with a low–mass object (Moeckel & Bally (2007) found that unequal–mass encounters are more destructive); (b) some stars will experience several encounters whose effects may be cumulative. They also concluded that the fraction of stars experiencing sub-100 auencounters in 12.5 Myr was small, at most $\sim 12\%$. They estimated disk mass–losses explicitly using a fitting formula from an extension of the parameter–space study of Pfalzner et al. (2005b) and found that serial encounters and flybys of massive perturbers were able to affect the disk population, at least in the dense core of the cluster. They concluded that, over 12.5 Myr, $\sim 4\%$ of disks in the ONC and $\sim 10\%$ of disks in the core would be destroyed outright, assuming initial disk radii of 100 au. This fraction is increased to $\sim 9\%$ and $\sim 20\%$ respectively if initial outer disc radii of 200 au are assumed instead.

Pfalzner et al. (2008), again considering the ONC, pointed out that close encounters involving disc–bearing stars in clusters can also result in bursts of accretion due to spiral arms induced in the disks. They concluded that this is a common phenomenon in dense cluster cores, driving accretion rates up by orders of magnitude for short periods (10^2–10^4 yr), during which 5–10% of the disk may be accreted. Pfalzner (2008) speculated that such events may be observed as FU Orionis outbursts.

Olczak et al. (2012) studied star–disk interactions in the Arches cluster. The Arches is more massive ($\sim 3 \times 10^4$ M$_\odot$), more compact (with a half–mass radius of ~ 0.4 pc) and

therefore much denser ($\sim 2 \times 10^5$ pc^{-3}) than the ONC. It also has a higher one–dimensional velocity dispersion (5.4 km s^{-1}). Encounter rates are therefore expected to be substantially higher in this system and, since its age is comparable to that of the ONC (a few Myr), the total number of encounters that have already occurred should also be much higher. Observations by Stolte et al. (2010) revealed that the disc fraction in the Arches cluster is an increasing function of distance from the cluster centre, rising from a few percent in the core to around ten percent at a radius of 0.3 pc. Olczak et al. (2012) again employed N–body modelling, and post–processing with techniques similar to Olczak et al. (2006) to infer disk mass–losses. They found disc destruction fractions of 10% in the entire cluster and 30% in the core over 2.5 Myr.

Malmberg et al. (2007, 2011) performed N-body simulations of clusters containing a number of stars ranging from 150 to 1000 and half-mass radii ranging from 0.38 to 7.66 pc. They quantified from the simulations the fraction of singletons, which they define as those stars that never had encounters closer than 1000 au. They found that in some cases almost $\sim 85\%$ of stars are non-singletons, with potential impact on planet-forming protoplanetary discs and already existing planetary systems. They also found frequent exchange of stars in binaries. The effect of fly-bys on already formed planetary systems is to lead to planet ejection and eccentricity excitation in planets that are left in the system, as well as increasing the probability of planet-planet scattering after the fly-by. These authors note that due to binary heating, which will lead to a significant cluster expansion, most encounters happen when the cluster is very young, and therefore the impact on proto-planetary discs can be significant.

Craig & Krumholz (2013) performed N–body simulations of a set of idealized, fractally–substructured clusters. Since the local stellar density in cluster subgroups can greatly exceed the average density, the encounter rates in a structured cluster should be considerably higher than in a smooth cluster with otherwise comparable properties. However, stellar subgroups are dynamically erased on a crossing time in bound systems, so it is not obvious that the total *number* of encounters will be higher in a structured cluster. Craig & Krumholz (2013) found that the overall enhancement in the number of encounters due to substructure is only a factor of a few, and that discs in such clusters are not likely to be significantly dynamically influenced in this way.

In this paper, we present results from hybrid N-body - smoothed particle hydrodynamics (SPH) simulations of coupled cluster and protoplanetary disc evolution. Therefore, we do not need to infer *a posteriori* the effect of encounters on discs, but we compute it self-consistently together with the stellar dynamics. This allows us to include effects that were neglected in previous studies:

- disc spreading and truncation by encounters;

- accretion onto the central star;

- the finite time for a disc to regain equilibrium after an encounter;

- the inclination of the rotation axis with respect to the inclination of the two stars'

orbital plane, which has an important effect (it is well known, for example, that a retrograde passage is much less harmful for the disc than a prograde one);

- disc-disc interactions, if both stars in an encounter have a disc;

- the mass transfer between stars, possibly leading to the formation of a new disc.

Rather than trying to accurately reproduce one particular stellar cluster, we concentrate here on an idealized model. This allows us to work in a controlled environment, identifying the new phenomena that arise due to the new computational method adopted. At this stage, we are able to make some preliminary comparison with observations. The questions we want to answer are:

- How important are stellar encounters for disc dispersal?

- What are the conditions under which disc sizes are set by stellar encounters?

- Are there observables in protoplanetary discs that can tell us if a disc or a disc population experienced significant encounters?

Our paper is organized as follows. After describing the computational method in section 3.2, we present our results in section 6.3. We discuss them in section 3.4, comparing with results from a simple semi-analytical method and with observations, and we draw our conclusions in section 3.5.

3.2   Model

3.2.1   Numerical method

We use the SPH code SEREN (Hubber et al., 2011). SEREN is capable of modelling both the hydrodynamics and stellar dynamics individually, or coupled together in the same simulation (Hubber et al., 2013a). The equations of motion are derived via the Euler-Lagrange equations, similar to the derivations of Springel & Hernquist (2002) and Price & Monaghan (2007), but including the coupled gas-star terms to maintain energy conservation. The SPH particles are integrated using a 2nd order Leapfrog kick-drift-kick integration scheme and the star particles are integrated with a 4th-order Hermite integration scheme. The equations of motion for both the SPH and star particles are integrated on hierarchical block timesteps. The smoothing lengths of SPH particles are calculated with the relation,

$$h_i = \eta \left(\frac{m_i}{\rho_i} \right)^{1/3} \tag{3.1}$$

where $\eta = 1.2$ and ρ_i is the SPH density. We use the M4 kernel (Monaghan & Lattanzio, 1985) for calculating all SPH sums.

We employ an ideal gas equation of state, assuming a mean molecular weight $\mu = 2.35$. Due to the already high computational demands of running a cluster simulation with gas dynamics, we use a simplified approach to modelling the thermal and radiation physics: the temperature of each SPH particle depends only on its position relative to the central star (we explain in detail in section 3.2.2.2 how particles temperatures are assigned). Therefore, we do not need to solve the energy equation, nor alternative forms such as the entropy equation.

In order to capture shocks and prevent interpenetration of particles, SPH needs to include an aritifical viscosity term. We use the term proposed by Monaghan (1997) of the form,

$$\left. \frac{d\mathbf{v}_i}{dt} \right|_{\text{AV}} = \sum_{j=1}^{N} \frac{m_j \, \alpha_{\text{AV}} \, v_{\text{SIG}} \, \mathbf{v}_{ij} \cdot \hat{\mathbf{r}}_{ij}}{\overline{\rho}_{ij}} \, \overline{\nabla_i W_{ij}} \,, \tag{3.2}$$

where α_{AV} is a dimensionless factor of order unity and $v_{\text{SIG}} = c_i + c_j - \beta_{\text{AV}} \, \mathbf{v}_{ij} \cdot \hat{\mathbf{r}}_{ij}$ is the signal speed between neighbouring SPH particles, with $\beta_{\text{AV}} = 2\,\alpha_{\text{AV}}$. In order to capture shocks, $\alpha_{\text{AV}} = 1$ usually suffices for adiabatic shocks for all Mach numbers (e.g. Hubber et al. 2013b). It can be shown (Artymowicz & Lubow, 1994; Murray, 1996) that the artificial viscosity term can also be used to model the physical viscosity that is responsible in accretion discs for the redistribution of angular momentum. An unwanted effect is that in this case the artificial viscosity results in both bulk viscosity, which is required to capture shocks, and shear viscosity, which is the only one required in accretion discs. In practice, this is usually not a major problem in simulations of accretion discs, as bulk viscosity acts on strongly convergent flows, which are usually not present in accretion discs.

The effective shear viscosity is resolution-dependent, and since our simulations have a relatively low resolution on the scale of individual discs, the effective shear viscosity is very high, leading to rapid viscous evolution of discs. Although a variety of viscosity switches exist in SPH that attempt to address this problem (e.g. Balsara 1995, Morris & Monaghan 1997), we simply adopt a lower value of $\alpha_{\text{AV}} = 0.1$ in all our simulations. Although this has the unwanted side effect of reducing the ability to capture strong shocks, this is a smaller problem than the high shear viscosity for our simulations. In the next section, we discuss the link between our numerical parameters and the physical values of the viscosity expected in proto-planetary discs.

To model the accretion of gas onto stars, we use sink particles similar to those described by Bate et al. (1995) and Hubber et al. (2011). The smoothing length of sink particles is simply $R_{\text{in}}/2$ for close encounters between sinks, where R_{in} is the sink accretion radius, whose value will be given in the next section. We do not allow the formation of new sinks, only the accretion of SPH particles onto existing sink/star particles. Indeed, we do not expect new sinks to form both for numerical and physical reasons. Physically, the masses contained in the discs are too low to form new stars and the discs are not gravitationally unstable. In addition, other works (Lodato et al., 2007; Forgan & Rice, 2009) have shown that encounters between stars prohibit the fragmentation of discs and stabilise them. Also, the numerical resolution is too low to follow the formation of planet-sized objects by gravitational instability (Bate & Burkert, 1997).

3.2.2 Physical set-up

3.2.2.1 Cluster set-up

Our model comprises two particle species, stars and gas. We choose to perform a controlled experiment and model the cluster dynamics as simply as possible by employing a Plummer sphere of 100 equal-mass stars. The Plummer sphere has a density profile given by:

$$\rho(r) = \frac{3M}{4\pi a^3} \left(1 + \frac{r^2}{a^2}\right)^{-5/2}, \tag{3.3}$$

where M is the cluster mass and a is a scale-radius, normally called the Plummer radius. The procedure used to generate the sphere is described in Aarseth et al. (1974), which describes also how to initialize the velocities under the assumption that the velocity distribution is isotropic. Because of their simplicity, Plummer spheres have been commonly used in previous works when dealing for the first time with a new numerical technique (Lada et al., 1984; Pelupessy & Portegies Zwart, 2012). Since the Plummer sphere density profile theoretically extends to infinity, we truncate it at 20 times the Plummer radius. We use dimensionless units in which the radius and the mass of the Plummer sphere is 1, so that our results can be rescaled to different cluster sizes and masses. However, we note that for each given simulation the ratio between the star and disc mass, and correspondingly between the cluster and the disc size, stays constant when rescaling. In the rest of the paper, we assume that each star has a mass of $1 M_\odot$ and that the Plummer radius is 0.1 pc. We then scale all other quantities accordingly.

In the spirit of performing a controlled experiment, binaries are not included. As discussed by Olczak et al. (2012), this underestimates the effect of encounters by reducing the number of stars. In addition, binaries might have also an effect on the long term evolution of the cluster, since the binding energy of a single binary can easily be larger than the binding energy of the whole cluster. On the relaxation time scale, binary heating leads to expansion of the cluster, which would instead cause a decrease in the importance of encounters. As we discuss in section 6.3, the relaxation time-scale is, however, longer than the time span we simulate. In addition, this level of sophistication would require a better dynamical model of the cluster than the Plummer sphere we employ here.

3.2.2.2 Disc set-up

The only gas initially present is in the discs; we do not include any diffuse gas. Observations of star forming regions show that, even in very young regions, a fraction of young stars show no sign of infrared excess or accretion (Fedele et al., 2010a). It could be that the discs of these stars have undergone a different, more rapid evolutionary path than the one of the discs we still observe. Recent work suggests that stars that do no longer have a disc are binary stars (Kraus et al., 2012). Another possibility is that the age spread between stars must account for this difference (although this is probably small, see Longmore et al. 2014). Therefore, we add a randomly oriented gas disc around 50 per cent of the stars.

The surface density profile of the gas is given by a power-law, with a slope of $p = 3/2$ as estimated for the Minimum Mass Solar Nebula (Hayashi, 1981b):

$$\Sigma(R) = \Sigma_0 \left(\frac{R}{R_0} \right)^{-p}, \tag{3.4}$$

where R is the distance from the star in the disc plane, R_0 is a scale radius and Σ_0 is a surface density scale. The particles are distributed so as to attain a Gaussian density profile in the vertical direction, with thickness $H = c_s/\Omega$, where c_s is the gas sound speed and Ω the Keplerian orbital frequency around the star. We choose Σ_0 as to set the initial disc mass to be 5% of the stellar mass. The disc is truncated at the initial disc radius R_{out}, and the inner disc radius is set to $R_{in} = R_{out}/5$. The true R_{in} is of the order of the star radius, but it is not possible to resolve it, because of the very short orbital time-scale there. Note that, as the disc expands, R_{in} stays constant, and the difference in the particle orbital time-scales increases. If particles move to within R_{in} of the star, they are accreted and removed from the simulation.

The temperature structure in the disc follows a power law distribution with radius:

$$T(R) = T_0 (R/R_0)^{-q}. \tag{3.5}$$

We choose the exponent q to be 1.5 for numerical convenience, although observations (e.g., Andrews & Williams, 2005) find flatter distributions, with a median value of 0.58. Our approach has the numerical advantage that it gives a constant vertical resolution and a constant α_{ss} parameter in the disc (Lodato & Pringle, 2007; Lodato & Price, 2010), where α_{ss} is the standard viscosity parameter proposed by Shakura & Sunyaev (1973b). The α_{ss} parameter is related to the kinematical viscosity ν of the gas by the prescription $\nu = \alpha_{ss} c_s H$. We fix the normalization T_0 in equation 3.5 so that the aspect ratio of the disc H/R is 0.05 at the inner radius. At each timestep, we use the distance from the nearest star to set the temperature of each SPH particle. For simplicity, we use the spherical distance rather than the distance in the disc plane, as this would require to identify at each timestep the discs and find their axis, adding extra computational cost to the simulation. In practice, the difference introduced is marginal for particles in a thin disc, and it affects only particles that get ejected by the discs. For these particles, using the distance in the disc plane would be questionable anyway. Finally, to prevent unphysically low temperatures, we impose a lower threshold corresponding to the one at a distance of $7R_{in}$, which for run R10 corresponds to 20 K.

We run simulations with $R_{out} = 10, 30, 100$ and 300 au, which will be referred to in the text as R10, R30, R100 and R300, respectively. The parameter R_{out} can be interpreted not only as the initial disc size at the beginning of the class II phase, but also as the age of the disc at the beginning of the simulation, where bigger discs are "old" discs (due to viscous spreading) and the different simulations represent different evolutionary stages. Clearly, this is not fully self-consistent as we are ignoring the effect of the encounters in the expansion that brought the discs to reach these sizes. Nevertheless, since observations (Williams & Cieza, 2011b) show that protoplanetary discs can reach these sizes, it is interesting to know what is the effect of encounters on such discs.

We initially populate the discs with SPH particles by Monte-Carlo sampling the surface density distribution given in Equation 3.4. This causes small random fluctuations which are erased on an orbital time-scale and do not affect our results. The particles are initialized in Keplerian orbit around their stars. Our resolution is 10^4 particles per disc, resulting in a total number of 5×10^5 particles for each simulation. At this resolution, using the relations in Lodato & Pringle (2007) shows that the discs are barely vertically resolved, that is, $h/H \simeq 1$, where h is the SPH smoothing length. We also check in the simulation output files that this is the actual resolution in the vertical direction. We compute the scale-height of the disc through the standard deviation of the vertical coordinate of the particles comprising the disc and by fitting a gaussian profile to the density. We find that the two methods give the same answer within a factor of ~ 1.5. In all cases, the ratio h/H is between 1 and 2.

Our choice of the resolution allows the possibility of simulating a long timespan (for run R10, we simulate 170000 orbits at the inner radius) and many discs at the same time, rather than being able to follow the detailed behaviour of the individual discs. A similar resolution has been employed in studies of star-star encounters (Heller, 1995; Pfalzner et al., 2005a). In particular, Pfalzner et al. (2005a) reported no significant difference between a simulation run with 10^4 particles and one with 10^6 particles. However, due to the accretion of particles on to the star, our spatial resolution degrades as the simulation progresses. For example, at the end of simulation R10, only ~ 10 per cent of the particles are left in the discs; when combined with the disc spreading, the analytical relations predict a degradation in the spatial resolution of a factor of 3. The actual values extracted from the simulation are however still in the same range as at the beginning of the simulation. We warn however that this does not mean that the actual resolution is higher than what we would expect; rather, it means that by definition it is not possible to resolve in the simulation features that are smaller, within a factor of order unity, than h. The interpretation of this result is thus that at the end of our simulations the discs are, for numerical reasons, thicker than what is expected from their temperatures.

It is possible to compute the resulting viscosity from the chosen density and temperature profiles. According to Lodato & Price (2010), in our simulations the Shakura-Sunyaev parameter is $\alpha_{ss} \simeq 0.004$, which is in line with the observational results (Armitage, 2011a). A possible concern is that the analytical relations do not hold at the resolutions employed in this paper. For this reason, in the next section we measure explicitly the value of the viscosity by measuring the rate of spreading of the disc. Indeed, we find the effective viscosity is higher than predicted by this estimate, yet still marginally compatible with the values found in observations.

3.2.3 A semi-analytical model for the disc size

In this section we present a semi-analytical model that we will use in section 3.4.1 to understand the results of the simulation in terms of disc sizes. A class of widely used models for a disc in isolation are the family of self-similar solutions derived by Lynden-Bell & Pringle (1974). They describe the evolution of a disc whose viscosity profile is a

power-law. The radius time evolution is given by:

$$R_{\text{disc}}(t, R_0, t_{\nu,0}) = \left(1 + \frac{t}{t_{\nu,0}}\right)^{1/(2-\gamma)} R_0, \tag{3.6}$$

where R_0 is the initial radius, $t_{\nu,0}$ the viscous time at the initial radius, and γ is the exponent of the viscosity with respect to radius. The viscous time can be related to the α_{ss} (see Section 3.2.2.2) parameter using the definition of viscous time (see equation 20 of Hartmann et al. 1998) and standard relations:

$$\alpha_{\text{ss}} = \frac{1}{6\pi} \left(\frac{t_{\nu,0}}{t_{\text{dyn}}}\right)^{-1} (H/R)^{-2} \frac{1}{(2-\gamma)^2}, \tag{3.7}$$

where t_{dyn} is the orbital time scale at R_0 and H/R is the aspect ratio. For simplicity we will use $H/R = 0.05$ when evaluating this relation numerically. We note that this is a worst-case scenario (that is, a slightly overestimate of α_{ss}), as this is the value at the inner radius and the aspect ratio is a midly growing function of radius. In addition, if the disc is vertically under-resolved, the effective H will be thicker than the one due to thermal pressure, therefore leading to a higher H/R and therefore to a lower α_{ss} than the estimate we get.

The expansion law has the nice feature that, being self-similar, one is always free to "reset" what we call initial radius, and start the evolution again from there, without changing the results (provided we also update the viscous time). In mathematical terms,

$$R_{\text{disc}}(t'', R_0, t_{\nu,0}) = R_{\text{disc}}(t'' - t', R_1, t_{\nu,1}), \tag{3.8}$$

where $R_1 = R_{\text{disc}}(t', R_0, t_{\nu,0})$ and $t_{\nu,1}$ is the viscous time at R_1.

We exploit this property in our simple semi-analytical model. We let the disc increase in size at each timestep following Equation 3.6. In order to derive the parameters, we use numerical fits to the results of the evolution of discs in isolation. At each timestep, we look in the results of the simulation for the closest star at that time to a given disc and record its distance d. We assume that the encounter would have truncated the disc at $d/3$ (Adams, 2010b). If the radius is larger than this value, we truncate the disc, otherwise we leave the disc unperturbed. We then let the viscous evolution start again. To summarise, we can compute the final disc radius assuming that:

1. the radius evolution is always given by Equation 3.6, i.e. by the Lynden-Bell & Pringle (1974) solution;

2. the encounter distances come from the results of the simulations;

3. the encounters simply truncate the discs at $d/3$.

We do not expect such a simple model to be able to capture the full results of the 3D hydro simulation, however it is useful to assess if the encounters produce a simple
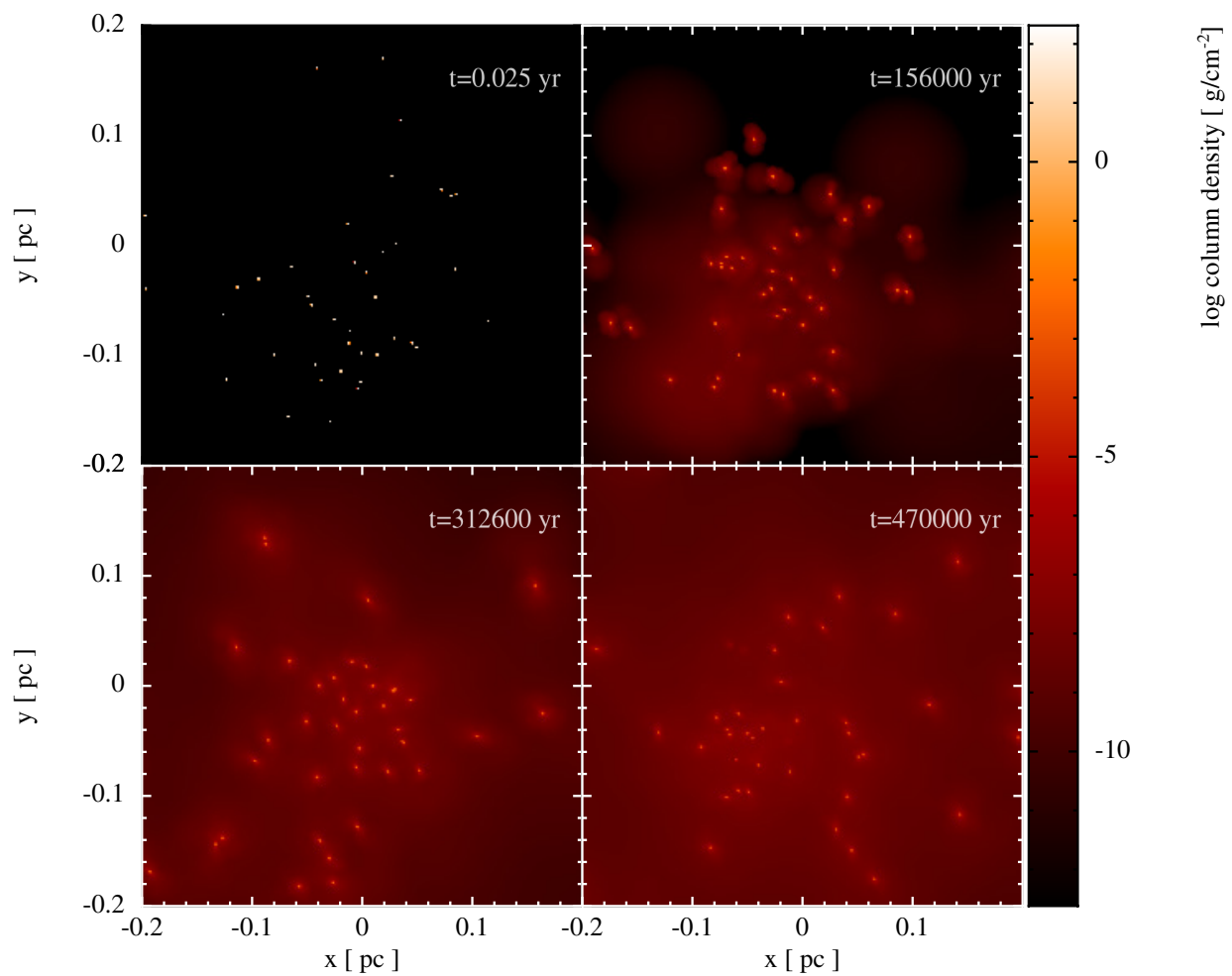
Figure 3.1: Time evolution of the gas column density in run R10. The view is restricted to the central region of the cluster to help visualizing the gas distribution. Note that stars are not plotted.

truncation or have more complicated effects. As we will show, the fact that there are cases where the model is capable of correctly reproducing some of the results shows that it is a useful tool. In particular, it highlights that in these cases the assumptions that have been used to build it are valid. On the contrary, when the model breaks down it shows that these assumption must have broken down.

3.3 Simulations

We evolve the clusters for 10 dynamical time-scales, where the dynamical time is defined as:

$$t_{\text{dyn}} = \left(\frac{r_{\text{cluster}}^3}{GM_{\text{cluster}}} \right)^{1/2}. \tag{3.9}$$

Here, G is the universal gravitational constant, M_{cluster} is the total mass of the cluster and r_{cluster} is the scale length a of the Plummer sphere (see Equation 3.3). For the scale length (0.1 pc) and mass values (100 M_*) introduced in section 3.2.2, the dynamical time-scale is $\simeq 47000$ yr. Therefore, the simulations are evolved for $t_{\text{end}} = 0.47$ Myr. For example, after this time in simulation R10, nearly 90% of the initial mass has accreted onto the stars.

Our cluster will evolve on the relaxation time, which is given by:

$$t_{\text{relax}} = \frac{N}{\ln(0.4N)} t_{\text{dyn}} \simeq 27 t_{\text{dyn}} \simeq 1.27 \text{ Myr.} \tag{3.10}$$

Given that this time is longer than the one we simulate, we do not expect a significant evolution of the cluster during the simulation due to pure N-body effects. The relaxation time is of the same order as the lifetime of protoplanetary discs (3 Myr, Fedele et al. 2010a). This means that during the life of a protoplanetary disc there will be some evolution of the cluster. This is important when interpreting discs with large outer radii as discs which have already evolved due to viscous spreading. In this case, the simulation is not fully self-consistent since we do not simulate the early dynamical evolution of the cluster but start from the same cluster initial conditions.

3.3.1 Extracting the discs from the simulation

To analyze the results of the simulations, we apply a procedure to extract the discs. Each gas particle is assigned to the star that it is most bound to. We also apply a cut off in eccentricity of 0.9, but in practice we find that very few bound particles have such high eccentricities. We define the *ambient gas* as particles that are not bound to any star. Once we have identified a disc, in order to find its plane we apply the algorithm already used in Walch et al. (2010). We compute the inertia tensor of the disc, defined as (Landau & Lifshitz, 2010):

$$I_{ij} = \sum_a m_a (x_a^2 \delta_{ij} - x_{i,a} x_{j,a}), \tag{3.11}$$
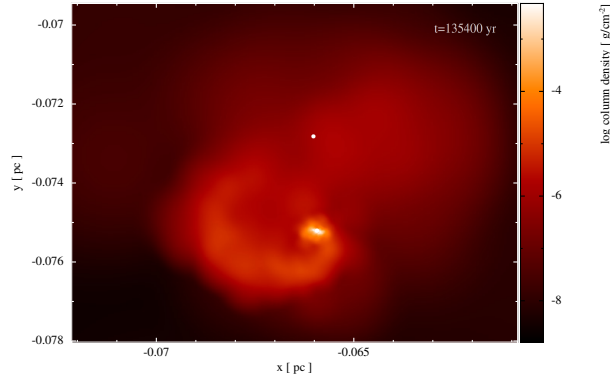
Figure 3.2: Column density distribution at time $t = 135400$ yr, showing the stripping of a disc shortly after the interaction of a star with a disc with a second star. The two stars are represented by the white dots. The tidal tail created during the interaction is clearly visible.

where $\boldsymbol{x}_a$ is the position vector of each particle in the disc with respect to the star, δ_{ik} the Kronecker delta, m_a the mass of each particle and the summation over index a is running over all the particles in the disc, while the indices $i, j = \{x, y, z\}$ are for coordinate axes. It can be shown that, in the limit of a razor thin axisymmetric disc, the eigenvalues of the tensor $I_{x'}, I_{y'}, I_{z'}$ are such that $I_{x'} = I_{y'} + I_{z'}$, where $I_{z'}$ is the eigenvalue corresponding to the eigenvector along the rotation axis z' of the disc, while the other two eigenvectors lie in the plane of the disc. Therefore, to identify the plane we diagonalize the tensor and define the direction of the eigenvector with the largest eigenvalue as the direction of the disc axis. Since the disc is a continuous structure without an abrupt end, we compute the radius of the disc as the half-mass Lagrangian radius, that is, the radius that contains half the mass of the disc. If the evolution of the disc remains purely viscous, the surface density follows one of the self-similar solutions found by Lynden-Bell & Pringle (1974) and the Lagrangian radius is proportional to the exponential tapering radius of the self-similar solution (e.g., Hartmann et al., 1998). The self-similar solution is used in sub-millimeter observations to fit the surface density profile and derive the disc size (Williams & Cieza, 2011b); therefore, it is important that our method is able to give consistent results in this case.

3.3.2 Spreading in isolation

In order to compare the model presented in section 3.2.3 with the results of the simulation, we need to know the disc expansion law. In principle, if we were to know exactly our viscosity law, we could use it to derive our expansion law. In practice, since we cannot afford a very high resolution due to computational limitations, we have to instead rely on calibrations, that are derived by fitting the evolution of a disc in isolation.

We show in table 3.1 the parameters of the fit, together with the corresponding value of the effective viscosity $\alpha_{\rm SS}$ computed using Equation 3.7. We note that these values

Run	R_{out}[au]	γ	t_ν [yr]	α_{SS}	t_{spread}[yr]	$\boldsymbol{\alpha_{\mathrm{SS,local}}}$
R10	10	1.11	18891	0.045	16800	0.1
R30	30	0.44	23218	0.062	36220	0.45
R100	100	-1.69	11762	0.133	43400	5.4
R300	300	-3.19	25432	0.161	132000	13

Table 3.1: For each simulation run, we show the parameters of the fit to the radius-time relation with the analytical solution given by equation 3.6.

are higher than those predicted from the analytical relations (by a factor of 40 in the worst case). Typical values for α_{SS} range from 10^{-2} to 10^{-4}, so that our discs are quite viscous. From the analytical relations, we would expect a constant α_{SS}, and therefore a constant viscosity, which should translate to $\gamma = 0$. Since we get a different value, this means at these resolutions the analytical formulae for SPH viscosity are not valid. On the other hand, this is an effect that we can calibrate for. Although we can not decide which viscosity law to apply, we can still derive it *a posteriori* by looking at the evolution of a disc in isolation. This also means however that care should be taken when interpreting the value of α_{SS} reported in the table. This value is to be interpreted as a *global*, effective value that describes how fast overall the disc is expanding. However, the *local*, that is, at R_{out}, level of angular momentum transport is higher than this. This is important as it is this local level that determines the ability of the disc to wash out local perturbations. For reference we report in the table also the *local* values of α_{SS}, that we compute from the formula (e.g., Armitage, 2011a):

$$\alpha_{\mathrm{SS,local}} = \frac{1}{2\pi} \left(\frac{t_{\nu,0}}{t_{\mathrm{dyn}}} \right)^{-1} (H/R)^{-2}. \tag{3.12}$$

We note that the different runs have quite different expansion laws. In particular, it is the exponent in the relation that tends to vary the most. Some of the discs show values of γ that are clearly unphysical: for example, the value -3 for R300 implies a very steep and increasing dependence of the temperature with radius, which is not present in our model. Therefore, one should regard the Lynden-Bell & Pringle (1974) similarity solution as a fitting formula for the evolution of these discs, and not as a *physical* description of their evolution. For this reason, the local estimate of α_{SS} is a more accurate description of what is going on in these simulations. Viscosity values are expected to be lower in real discs, which implies that those encounters' effects that in our simulations could not be washed out by viscosity would be even stronger in real discs. The variation of the exponent means that, despite the fact that the viscous times are similar, run R10 is the one varying the fastest (indeed, it even overtakes the other ones by the end of the simulation), while the other ones expand more slowly. For this reason, we stress that looking only at the viscous time might be misleading, since this value alone does not fully describe the evolution of the disc. As another reference, we list in the table also the value of t_{spread}, which we define
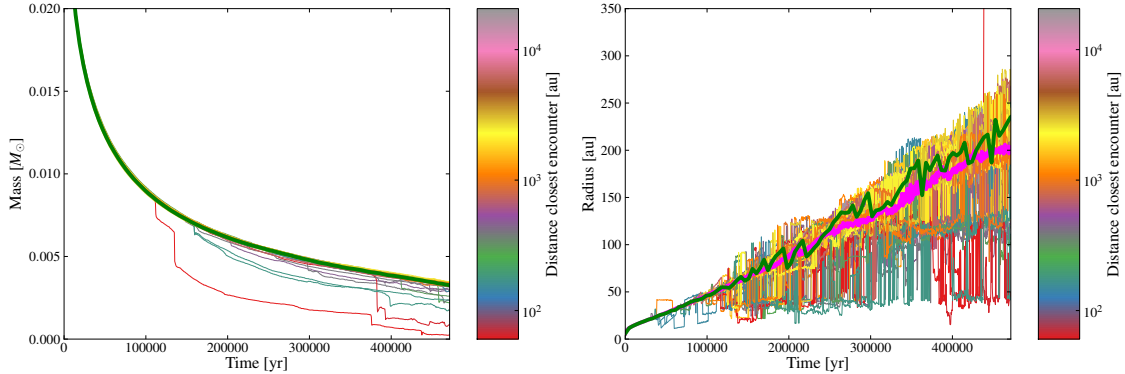
Figure 3.3: Left panel: disc masses as a function of time. Right panel: disc radii as a function of time. In both panels, lines are colored by the distance of closest encounter that the star experienced, and the color gradient shows how the closer the encounter, the more destructive the effect. The thick green line is the disc run in isolation. The thick magenta line in the right panel is the median among all the discs, and shows the truncation effect of the encounters.

as:

$$t_{\text{spread}} = \frac{R_{\text{disc}}}{dR/dt}, \tag{3.13}$$

that is, the timescale for a significant change in the disc radius. We evaluate the denominator by computing analytically the derivative of equation 3.6, and use the value of R_{disc} at $t = 0$. It can be seen that the disc R10 is the one that is varying the fastest. It is reassuring that the disc in run R300, the one with the highest value of α_{SS}, has a very long t_{spread}, so that its spreading is quite limited during the course of the simulation (see also figure 3.7).

In order to quantify the effect of the limited resolution available on the viscosity, we run resolution tests of the discs in isolation, that we report in the appendix.

The viscosity is also important after an encounter, as it allows for the particle orbits to circularize. As Clarke & Pringle (1993) pointed out, the exact form of the viscosity law probably does not matter (in fact, some of the simulations in the literature have been done only with pseudo-viscosity) for what the final surface density distribution after an encounter is. Indeed, the final surface density is given by the particle specific angular momentum, which sets the final distance from the star once all the orbits have circularized. This is true if there are no further encounters, but the exact viscosity that one assumes decides the timescale over which the disc finds a new equilibrium after an encounter. This is important in our simulation, as the outcome of a second encounter will be different depending on whether the disc had time to gain a new equilibrium or not. However, since it is not clear from the physical point of view what the viscosity after an encounter is going to be, we need to just rely on the value that comes out of the SPH algorithm.
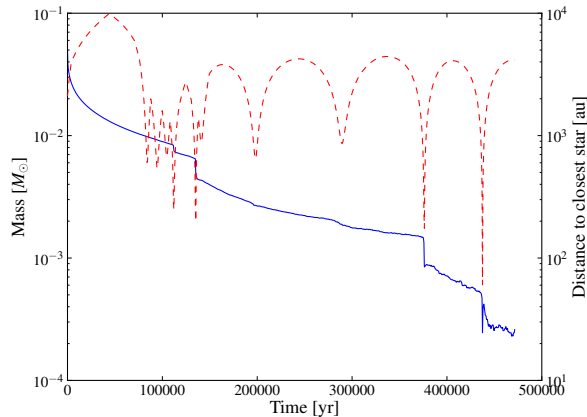
Figure 3.4: Mass versus time (blue solid line) and distance to closest star (red dashed line) for one disc from simulation R10. Sudden drops in mass are clearly caused by close encounters.

3.3.3   Simulation R10

We first comment in depth on the results from simulation R10, and use this as a reference to compare to the other simulations. Figure 3.1 shows four column density snapshots from simulation R10. While at the beginning of the simulation the discs are so small that they are barely visible on the scale of the cluster, they expand significantly due to viscous spreading. Due to this expansion, the discs become large enough to be influenced by encounters. The interactions between stars produce some unbound gas, which is visible as a non-zero background density. The amount of gas that becomes unbound is small, and at the end of the simulation, the mass of the unbound gas is one order of magnitude less than the mass in all discs at t_{end}. Figure 3.2 shows the detail of a disc during an interaction. The two stars are represented by the white dots (note that only one of them has a disc in this particular case). The tidal tail of gas that has been ejected from the disc (Toomre & Toomre, 1972; Clarke & Pringle, 1993) is clearly visible. We concentrate now on how the encounters affect the disc properties.

Figure 3.3 shows the evolution of the discs in the cluster as a function of time for simulation R10. The left panel shows the mass of the discs as a function of time, while the right panel shows the radius of the discs as a function of time. The thick green line in the plot is a control run with a single star-disc system run in isolation. It is shown here as a reference, as it allows us to distinguish the effect due to the encounters. In isolation, the radius increases due to the redistribution of angular momentum due to viscosity and the mass decreases due to accretion onto the star.

The interactions between stars are stripping mass from the disc. The lines in the plot are colored according to the distance of the closest encounter that each star had during the course of the simulation. The color gradient shows that the closer the encounter, the stronger the effect in ejecting mass from the disc. In Figure 3.4 we pick one of the discs that had a very close encounter (minimum distance smaller than 100 au), and plot against
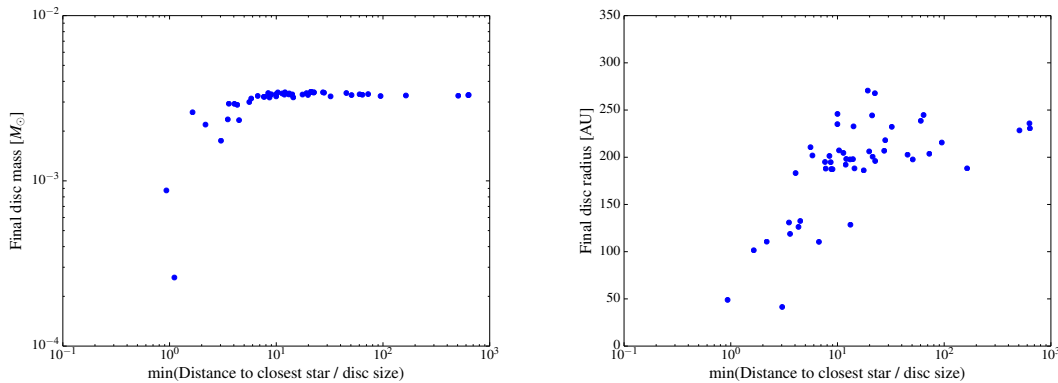
Figure 3.5: Left panel: final disc mass as a function of the distance of closest encounter, in units of the disc size at the moment of the encounter. Right panel: final disc radius a function of the distance of closest encounter, in units of the disc size at the moment of the encounter. The correlation in the disc mass is quite remarkable, and shows how the distance of the encounter is a good quantity to use to derive the mass lost in the encounter. The correlation in the disc radius has more scatter (see the text for an explanation), which shows the importance of numerical simulations to quantify the influence of encounters on the disc sizes.

time both the disc mass (blue line) and the distance to the closest star at the given time (red dashed line). This clearly shows that the drops in mass are caused by close encounters.

In the right panel of Figure 3.3, the radius evolution is not completely smooth even for the disc in isolation. Here the finite resolution certainly plays a more important role than for the mass, being an integrated quantity. Nevertheless, the effects of the encounters are much bigger than the noise for the disc in isolation. Some discs show big variations in the radius after an encounter, which is due to the fact that they are seeking a new equilibrium after they have been perturbed. It can be seen how nearly all the discs have smaller radii than the one run in isolation. To highlight this effect, we plotted also the median among all the discs, which shows the truncation effect of the encounters. The color gradient is not so clearly visible here as in the left panel. It can still be seen however that the discs that are significantly smaller than the disc in isolation experienced close encounters.

To further explore the dependency of disc parameters at t_{end} on the distance of closest encounter, we show in Figure 3.5 the final disc radii and masses as a function of the distances of the closest encounter. Since the disc size varies in time, we normalize the distance of the encounter to the disc size at the moment of the encounter. The correlation in mass (left panel) is quite strong, and confirms that the distance of the closest encounter is a good quantity to derive the mass lost in an encounter, even when disc spreading and mass accretion onto the central star are taken into account. This confirms qualitatively the validity of previous studies (e.g., Scally & Clarke, 2001; Olczak et al., 2006) that used this parameter, either recording the single closest encounter, either the history of the most destructive ones, to quantify the importance of encounters in mass removal from the disc. However, due to the presence of accretion and spreading in our work, a detailed comparison with previous work is not possible. Note that, since the discs all start from the
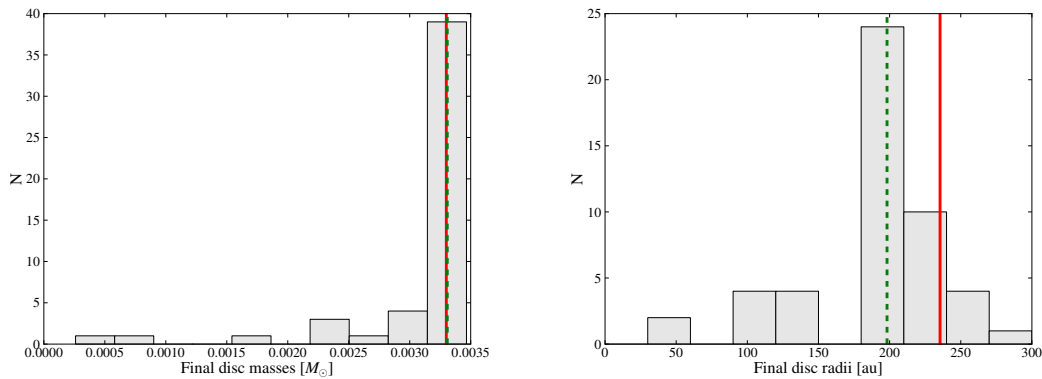
Figure 3.6: Left panel: histogram of the final disc masses. Right panel: histogram of the final disc radii. The red solid vertical line in both plots shows the value for the disc run in isolation, while the green dashed vertical line shows the median of the distribution. Although a close encounter can have a dramatic effect on the mass of the disc, few discs had such close encounters, so that the median of the mass distribution is not significantly affected. However, even distant encounters can change the disc radius, so that we see a change in the median disc radius when comparing with the disc run in isolation.

same initial conditions and follow the same evolution in absence of external perturbations, discs that experienced only distant encounters end up with the same value for the mass. We do not expect a real disc population to exhibit such behaviour, due to a spread in the initial conditions and in the evolution.

The right panel shows that also the disc size at t_{end} correlates with the distance of the closest encounter. This shows the destructive effect of encounters, which are able to truncate the discs. It is instructive to compare this correlation with the mass one. The disc size is more sensitive to distant encounters than the disc mass (Figure 3.5). In particular, distant encounters (e.g., $10 - 20$ disc radii) do not affect the disc mass, but are able to modify the disc radius. Since a star also experiences other encounters than the closest one, they can also contribute to determine the final disc size. This is one of the reasons why the radius correlation has more scatter than the mass one.

In addition, after an encounter the disc spreads again, so that, given two discs that experienced a close encounter at the same distance but at different times, we do not expect the final sizes to be the same. This also means that, while we commented before that our simulations confirm the validity of semi-analytical approximations for inferring the disc mass, the same cannot be said for the disc sizes. Numerical simulations are of primary importance here to get accurate determinations of the importance of dynamical interactions in shaping the disc size.

We show in Figure 3.6 histograms for the final disc masses and radii. The red solid vertical line in both plots shows the value for the disc run in isolation, while the green dashed vertical line shows the median of the distribution. Few discs had close encounters that modified their masses significantly (Figure 3.6, left panel), as shown in Figure 3.5, so that the median of the distribution is only marginally smaller than the value for the disc run in isolation. Therefore, although a close encounter can have a strong effect on the
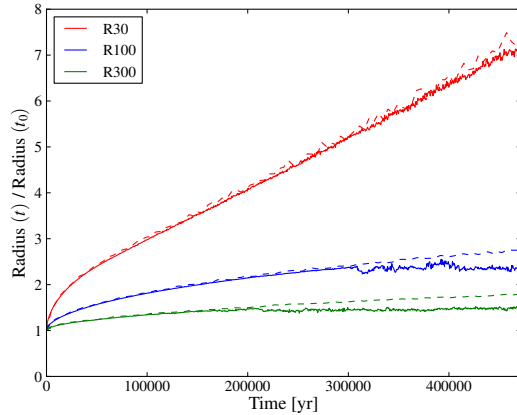
Figure 3.7: Evolution of the median disc radius for runs R30, R100 and R300 (see legend), in units of the initial disc size. The dashed line is the disc in isolation, while the solid line is the median of all the discs in the simulation. The median disc radius in run R300 no longer increases after $\sim 2 \times 10^5$ yr, showing that we have reached a regime where encounters are limiting the disc size.

specific disc, close encounters are not frequent enough to significantly alter the disc masses on average. This is highly dependent on the initial conditions for the cluster, and the absence of high-mass stars certainly plays an important role, since it removes the source of the most destructive encounters. This will be discussed in a subsequent paper.

The effect of encounters on the distribution of final disc radii (Figure 3.6, right panel) is more evident, as most of the discs experience a reduction in size due to the encounters. A number of discs are truncated at very small radii. We will show in section 3.4 that their final radii are compatible with having been truncated by the close encounters. There is also a number of discs which are not dramatically truncated, yet which are affected by more distant encounters. With respect to the disc in isolation, the final radius of these discs is reduced by $\sim 10 - 20$ %.

3.3.4 Simulations with larger initial radius

Figure 3.7 shows the evolution of the radius for runs R30, R100 and R300. For simplicity, we show only the evolution of the median radius, compared with the disc in isolation. To compute the median, we excluded discs that experienced a significant mass loss (more than 99.5 %). As they are now only represented by a handful of SPH particles, the definition of radius ceases to be meaningful for them. Note that, for different disc sizes, the viscous time and the exponent in the expansion law change (see section 3.3.2). It is clear that for run R300 we have entered a regime where the disc size is set by the encounters rather than from the size of the disc itself or from viscous spreading: the median no longer increases after $\sim 2 \times 10^5$ yr. A similar behaviour, altough only towards the end of the simulation, can be seen for run R100. The spreading of these discs happens slower, while the encounter importance increases due to the smaller ratio between the encounter distance and the disc

(a) Run R30

(b) Run R100

(c) Run R300
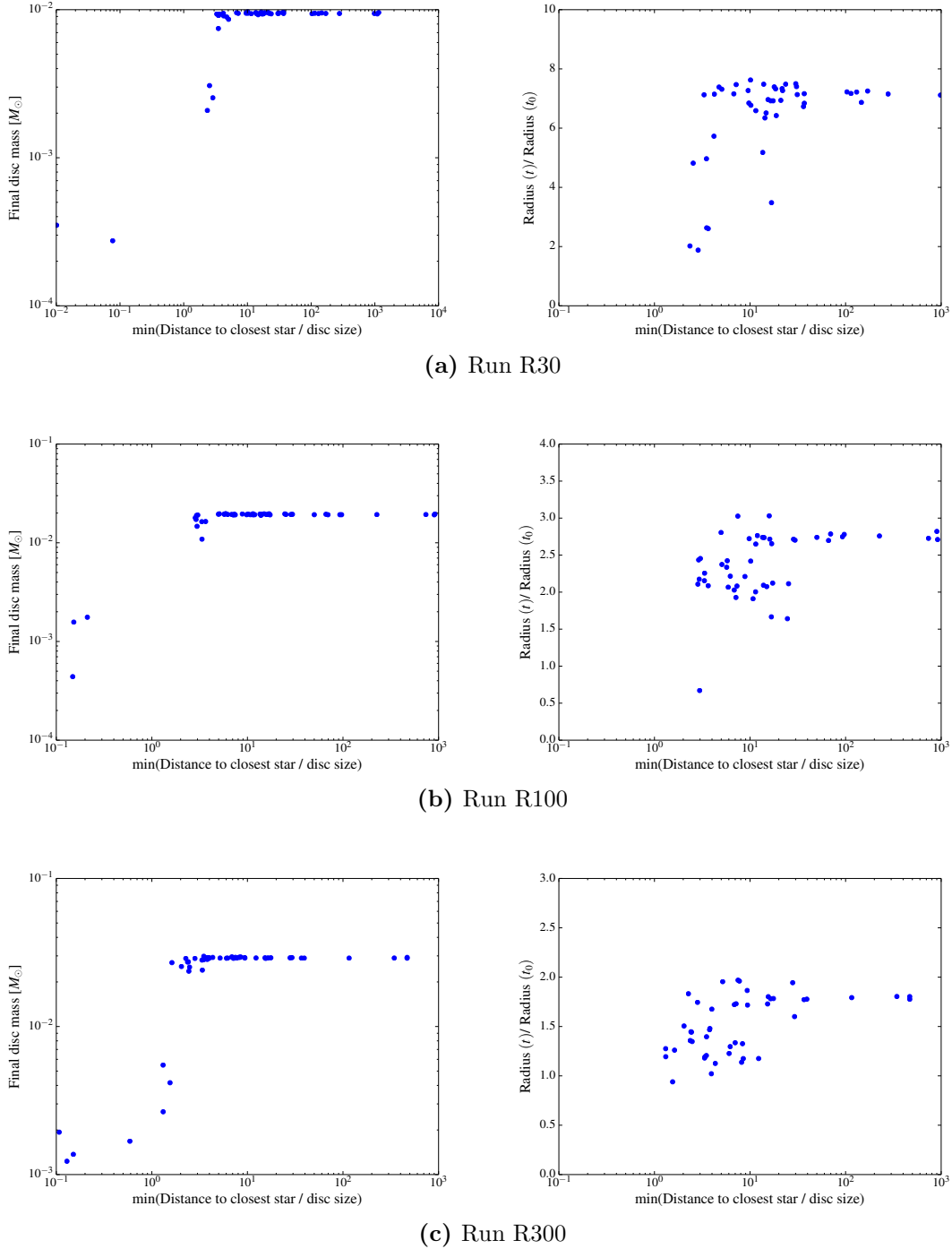
Figure 3.8: Left panels: final disc masses as a function of the distance of the closest encounter, measured in units of the disc size at that moment. Right panels: final disc radii in units of the initial size as a function of the minimum value of the ratio of the encounter distance to the instantaneous disc size.
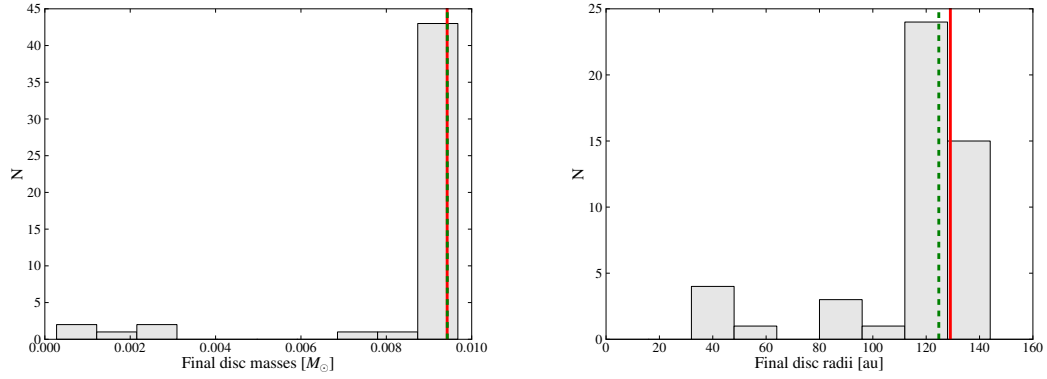
(a) Run R30
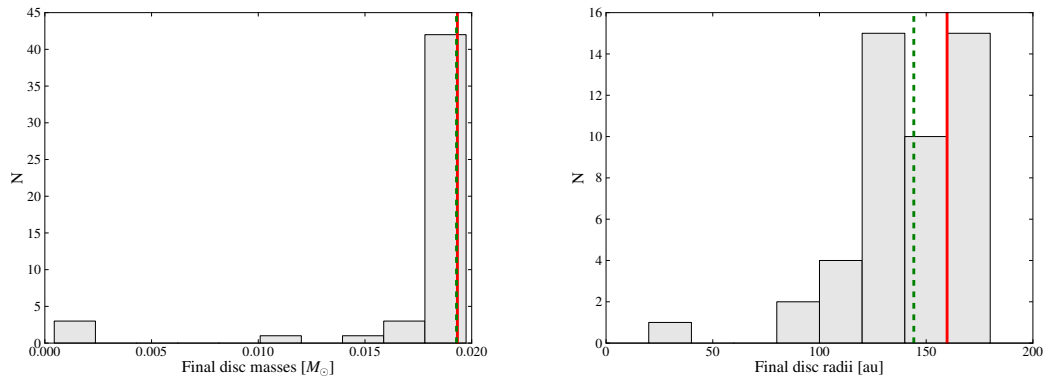
(b) Run R100
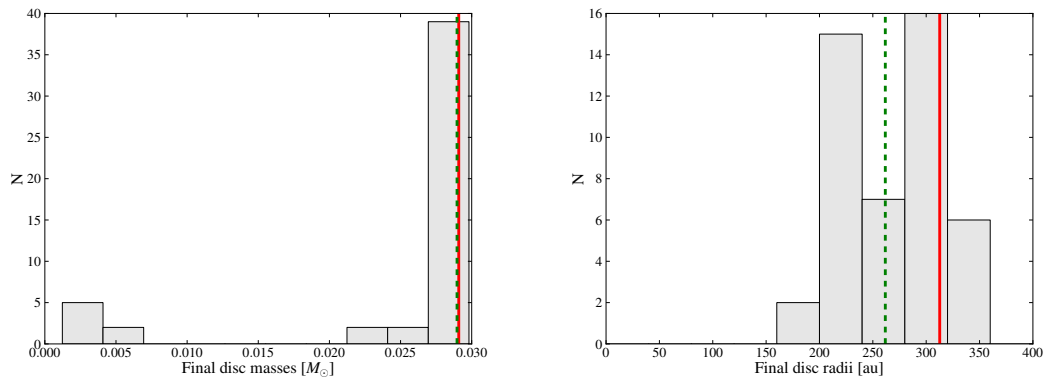
(c) Run R300

Figure 3.9: Left panels: histogram of the final disc masses. The solid red line is the value for the disc in isolation, while the green dashed line is the median of the distribution. Right panels: histogram of the final disc radii. The solid red line and the green dashed line have the same meanings as in the radii plot.

size. This behavior is not linear, however, as can be seen from the R30 and R100 runs: the radius of discs in run R30 is almost unaffected by encounters, while the effect on run R100 is visible, but smaller than in run R10. As discussed in section 3.3.2, the discs in the different runs have different spreading rates. This brings the discs in run R10 to become almost as big as the discs in run R300 within the timescale of the simulation, while the discs in run R30 and R100 are eventually overtaken by the ones in R10. This effect comes from the different viscosities that we have in the different runs, which in the SPH method we cannot control. However, it is an effect that we can calibrate for, and which shows the interplay between disc truncation and spreading.

The mass histograms (left panel of Figure 3.9) shows that the runs with bigger discs had a handful of very destructive encounters, which produced discs with very small masses compared with the unaffected ones (note that in run R10, only a couple of discs had their mass reduced by an order of magnitude compared to 8 discs in R300). This is expected, since for bigger discs the ratio between the distance of the encounter and the disc size decreases and the encounters become more penetrating. At the same time, however, the dependence of the final disc mass on the distance of the closest encounter (left panels of Figure 3.8), measured in units of the disc size, changes. While for run R10 the dependence is quite shallow, it is much steeper, almost a step function, for the other three runs. Stated in another way, the bigger discs are also more resistant to encounters, as only very close encounters are able to affect them. Therefore, while the close encounters produced a lot of damage in the discs, overall the encounters were not able to modify significantly the mass of the discs, because only a few of them were able to probe the left part of this step function. This can be seen also comparing the difference between the median mass and the disc in isolation, which is very small for all the runs. In short, the masses of small discs are not significantly affected, because the encounters are not penetrating enough; big discs are also not significantly affected, because they are more resistant to encounters.

One possible explanation for this different behaviour is that distant encounters cause a mass redistribution in the disc, "hardening" the surface density (see Hall 1997). While this is washed out easily in run R10 by the higher viscosity, through disc spreading, this effect is not strong enough in the other runs. This accounts for the steeper relation observed in the correlation between the final mass and the distance of the closest encounter, as a small difference in the encounter distance can make a big difference in the mass involved in the encounter if the surface density is steep. We discuss this idea further in section 3.4.1.

Another quantity of interest is the mass accreted onto the star. We show in Figure 3.10 the accreted mass as a function of time for the discs in the simulation, with the four panels corresponding to the four simulations. While for the small discs there is little to no effect on the accreted mass, the encounters produce strong bursts in accretion for the bigger discs. Such bursts were already found in simulations by Pfalzner et al. (2008), and they have been proposed as an explanation for FU Orionis objects. However, we caution that numerical effects may also partially contribute to this result, since bigger discs also have bigger accretion radii. Therefore, while the result is interesting, further work is needed to assess its physical relevance. Interestingly, we note also that some stars that did not possess a disc at the beginning of the simulation may accrete some mass, which they have
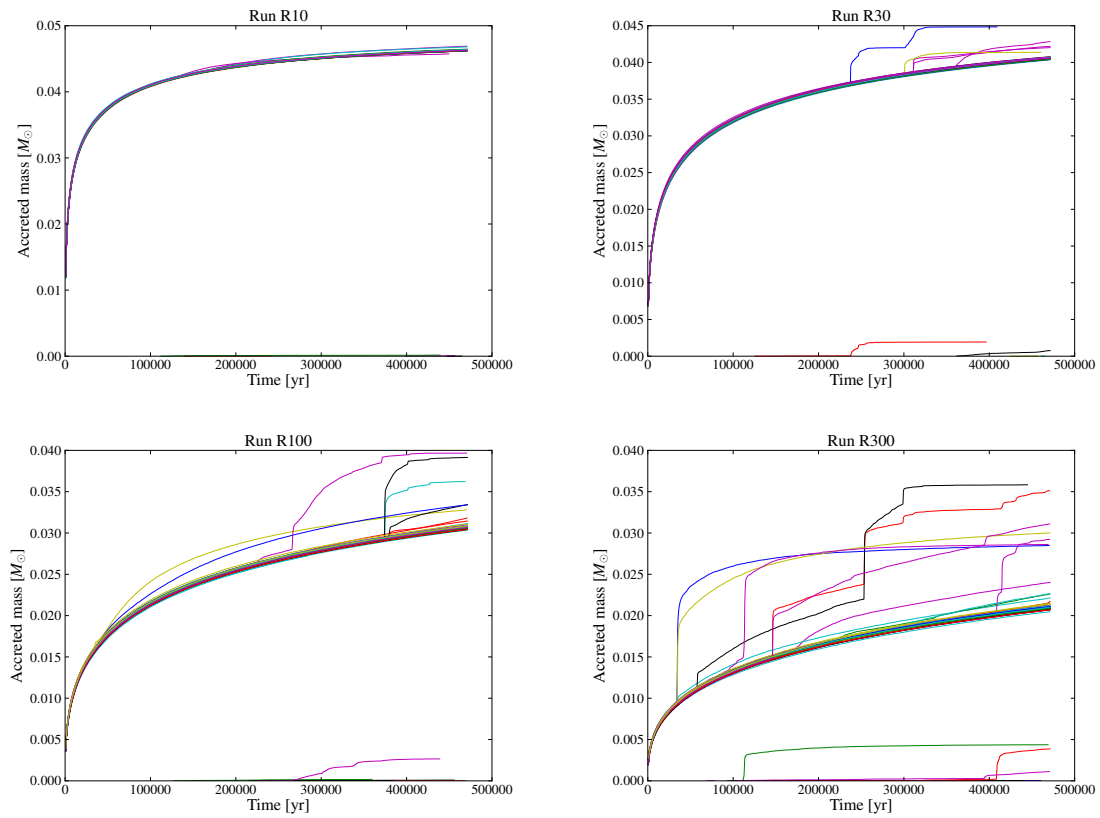
Figure 3.10: Accreted mass on the central star as a function of time for the four simulations run. Each line has a different colour to help distinguish them.
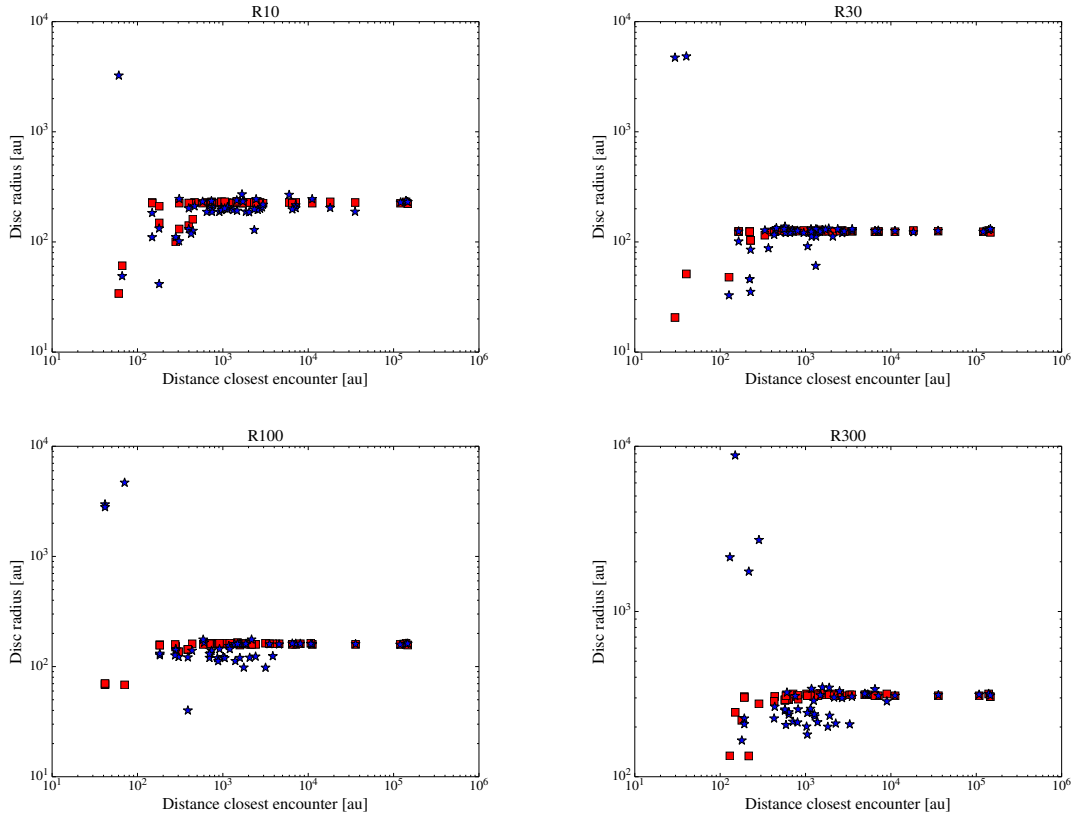
Figure 3.11: Comparison between the predicted disc sizes by the model (red squares) and the results from the simulation (blue stars). The different simulations are shown in order, from left to right and from top to bottom.

stripped in an encounter from a disc around another star. This could open the exciting possibility of reactivating accretion on a star that is already in the class III phase (i.e., has already dissipated its disc). Unfortunately it is difficult to quantify precisely how long such a burst would last and which accretion rates it could reach, due to the limited resolution available in terms of mass. We leave also this study for future work.

3.4   Discussion

3.4.1   Understanding disc sizes

We show in Figure 3.11 the results of the model presented in section 3.2.3, compared with those from the simulation. For comparison, here we plot also the discs that experienced very close encounters. It can be noticed that sometimes the sizes derived from the simulation are much bigger than the disc in isolation; this is because the very close encounter destroyed the disc, and therefore the notion of disc radius is no longer meaningful.

   We note the very good agreement for run R10, which is remarkable for such a simple

model. While it does not correctly predict the sizes of all the discs, it is still quite effective for most of them, and it correctly reproduces the correlation between the two quantities. While the agreement is not as good for the other runs, the model still correctly identifies which discs have been severely affected by the encounters and which ones are not. In particular, by combining information from these plots and the ones shown previously, we can observe three different regimes:

1. Discs that had very penetrating encounters were significantly affected in their sizes. The assumption that discs are truncated at $d/3$ made in the model correctly captures which discs are in this regime, in line with previous findings (Clarke & Pringle, 1993). Notice that in run R10 discs sizes are sometimes reproduced even in this regime, while the model clearly fails for the other runs. To interpret this result, we note that discs in run R10 are undergoing much faster spreading, and so they are in a "spreading dominated regime". Viscosity is for them the main driver of evolution, and encounters act simply to truncate the disc. In the other runs, instead, a more complicated interplay emerges;

2. Discs that had only distant encounters, but which nevertheless are smaller than the disc run in isolation. This population is present especially in runs R100 and R300. This is a feature that the simple model does not catch. We suggest that this is due to the cumulative effect of many distant encounters, which modify the mass distribution of the discs, "hardening" them (Hall, 1997) and violating the assumptions of our semi-analytical model. In run R30 the discs did not grow enough to be significantly influenced by this effect; in run R10, as previously mentioned the spreading is much faster, so that the steepening is been washed out by viscous evolution. Still, although this effect is smaller than in runs R100 and R300, also in run R10 there are discs that are a bit smaller than the prediction of the model, while still having had only distant encounters.

3. Discs that were largely unaffected by the encounters. The critical closest encounter to access this regime is of order 50 disc radii, but notice that it is different in the different runs. In particular, the number seems to decrease with the initial disc size, which would point again in the direction of the big discs been "hardened".

To check the hypothesis of modifications in the surface density distribution by the encounters, we fit the surface density at the end of the simulation with a power-law (Equation 3.4). We report in table 3.2 the results. We list the values for the disc in isolation and for the median of the discs in the hybrid simulation. In the latter case, we fit only the discs that in the course of the simulation went above the threshold value of 10^{-2} $M_\odot$, to avoid artifacts. As expected, simulation R10 shows very little difference between the isolation run and the median value, as it is the case for run R30. The steepening is instead clear in simulation R300, where the value of the median is well above the value of the disc in isolation. A hint of steepening may already be seen for run R100, with some caveats however: the surface density of the discs in this run tends to be quite steep even in isolation, another

Run	p isolation	p hybrid
R10	0.56	0.55
R30	0.85	0.87
R100	2.34	2.47
R300	1.09	2.27

Table 3.2: We report for each run the power-law index p (Equation 3.4) when fitting the surface density distribution. We list the values for the disc in isolation and for the median of the indexes obtained when fitting the discs in the hybrid simulation. The effect of steepening is evident in run R300 that has a higher value of the median with respect to the disc in isolation.
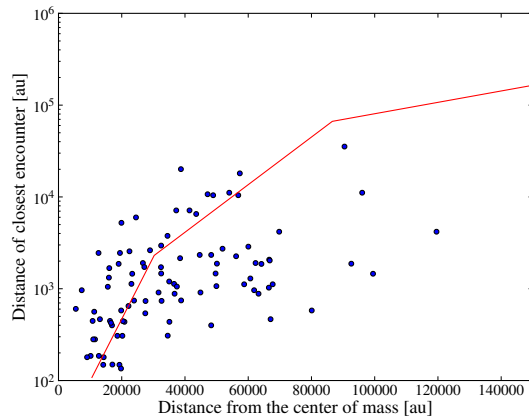
Figure 3.12: Distance of the closest encounter versus the distance from the center of mass for each star. The dots are the results of the simulation, while the solid line is the result of the Monte-Carlo experiment described in the text, which yields a prediction for the median of the distance of the closest encounter at each location.

feature that is due to the behaviour of SPH viscosity at these low resolutions. Therefore, while the analysis shows that some hardening is taking place in simulation R300, we caution that the low resolution does not allow us to measure quantitatively this effect. Future work will allow hardening to be studied more in detail. We note also that, if this effect is confirmed to be as big as measured here, it could be observationally probed by resolved observations of proto-planetary discs (Williams & Cieza, 2011b), which which would allow one to verify if discs in dense environments have steeper surface density profiles than ones in sparse environments.

3.4.2 Comparison with observations

de Juan Ovelar et al. (2012) pointed out that observational data suggests a reduced disc size in environments with high stellar surface densities (Σ_*). In particular, they looked at the measured disc size as a function of Σ_*. The population they consider is composed of 67 Class II objects in nearby star forming regions (SFR) with radii measured through re-
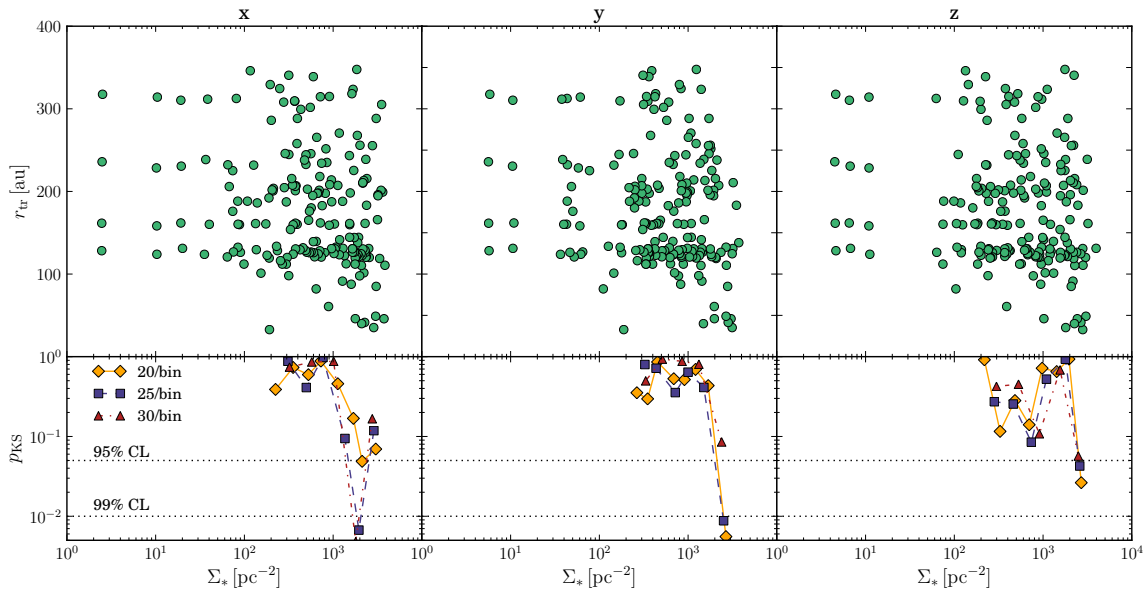
Figure 3.13: Projections along the three coordinate axes of the radii vs. environmental surface stellar density (Σ) distribution of the population of discs resulting from the combination of all discs in each of our four runs. The lower panels show the results of a Kolmogorov-Smirnov test where we bin the data and compare the distribution in each bin with the one of the discs at a lower stellar densities. The different symbols are for different number of elements in each bin. Although the stars move in the cluster, they still retain information about their original position, so that there is statistical evidence of a cut in disc sizes at high stellar densities. In particular, the probability of the last bin to be compatible with the rest is always low. Notice however that this simulation did not explore the high stellar densities that are present in some of the real clusters (compare with Figure 1 of de Juan Ovelar et al., 2012).

solved imaging. The stellar density is computed with the Casertano & Hut (1985) method. Namely, one finds the N closest stars, defines d_N as the (projected) distance of the N-th nearest neighbour and computes the surface density as $(N - 1)/\pi d_N^2$. The data shows a cut-off in disc sizes at stellar surface densities higher than $\Sigma_* > 10^{3.5} \, \mathrm{pc}^2$. To highlight this cut-off, they perform a statistical test. They bin the data from higher to lower densities and for each bin they test with the Kolmogorov-Smirnov method if the distribution of the points in the bin is compatible with the distribution at lower surface densities.

We showed in the previous sections that the disc size is correlated with the closest encounter. In turn, the distance of the closest encounter depends on the environmental stellar density, but it is also a stochastic process; after experiencing a close encounter the star might move to a lower density region inside the cluster. Therefore, numerical simulations are of primary importance to assess what kind of correlation we expect theoretically in this parameter space, which can be probed by observations. It is important to have such predictions to distinguish from other candidates for the truncation of discs in clustered environments, such as external photoevaporation by massive stars.

First of all, we want to inquire how important is the movement of the stars in the cluster. The expectation to find smaller discs at high stellar densities relies on the fact that we expect the distance of encounters to depend on the local stellar density. However, this dependence could be washed out if a star experience a close encounter in a high density region and then moves to a region with lower density. It is then important to check how important is this effect. We follow Scally & Clarke (2001) (see their Appendix A) to build a semi-analytical model of the N-body dynamics in the cluster. We make the assumption that the stars keep their distance from the cluster centre of mass fixed, and so they experience a constant stellar density throughout the simulation. We then compute with a Monte-Carlo experiment the distribution of the minimum encounter distance, and we compare it against the results of the simulation. We show in Figure 3.12 the results. We plot the distance of the closest encounter (the blue dots are the results of the simulation) versus the distance from the centre of mass of the cluster. The red solid line is the median of the distribution drawn from the Monte-Carlo experiment, which agrees with the results of the simulation. Therefore it is indeed a good assumption to assume that the stars do not move systematically in the cluster over the simulation time-scale. This means that we expect the disc sizes to retain some information about the local stellar density. In addition, while we focused here mostly on the closest encounter, we note that a higher stellar density also enhances the number of encounters closer than a given distance, which also contributes to strengthen the correlation.

To check if dynamical encounters in our simulations can produce a feature like the one observed in the de Juan Ovelar et al. (2012) study, we go through the same exercise they carry out. We chose $N = 20$ to compute the stellar surface density. Since our data is three dimensional, we show the results of projecting along three different axes (we chose the coordinate axes for simplicity). However, our simulations are carried out for different values of initial disc radius separately. Our radii vs. ambient stellar density distribution is strongly influenced by this initial condition. To generate a more realistic population, and therefore more similar to that of the de Juan Ovelar et al. (2012) study, we combine the

discs in all four simulations into a single population conserving the separated projections onto the x, y and z axes. We then perform the KS-test over this composite distribution for each axis separately. Figure 3.13 shows the radii vs. ambient surface stellar density distribution and the results of the test for each axis in the same format as in Figure 1 of de Juan Ovelar et al. (2012). To show the effect of the bin size, we compute the KS-test for $[20, 25, 30]$ elements per bin and our composite population has 192 discs. To avoid edge effects we perform the test only over bins where the population at lower densities is larger than a sixth of the complete population.

The result is that, despite the fact that stars move in the cluster, there is still statistical evidence of a reduction in disc sizes at high stellar densities, namely above $\sim 2 - 3 \times 10^3$ stars/pc^2. In particular, the data in the last bins systematically show a low probability of being compatible with the rest of the distribution. Notice that these simulations did not explore the high stellar densities that are present in some of the real clusters (compare with Figure 1 of de Juan Ovelar et al., 2012), which can go up to the 10^4 stars/pc^2 in the ONC, and we are thus just beginning to sample the cut-off. It is however very promising that the density at which this cut-off happens is consistent with the one found by de Juan Ovelar et al. (2012). We leave future work to assess this regime, where the inclusion of massive stars is also important. Future work will also explore higher resolutions than what is currently possible, and measure with more accuracy the exact threshold at which the cut-off takes place.

We also note that in the literature there are indications of other influences of the environment on protoplanetary discs. For example, Sicilia-Aguilar et al. (2011, 2013) consider the Coronet cluster, which having ~ 50 stars inside 0.15 pc is not very dissimilar from our simulations. These authors find that discs in the Coronet cluster are more evolved than in the Tr 37 cluster. This is quite surprising, given that the Coronet cluster is 1-2 Myr old, while Tr 37 has an estimated age of 4 Myr. Their interpretation is that the difference is due to the much higher stellar density in the Coronet cluster. While our simulations do not yet allow for a detailed comparison with their results, this is an interesting path to be explored in future works.

Finally, in the present work we have ignored the effect of external photo-evaporation, with the goal to isolate the effect of the encounters. External photo-evaporation is also a process that limits the disc size. Using a time-scale argument, Adams et al. (2004b) estimated that a proto-planetary disc around a solar mass star would have its size reduced by external photo-evaporation down to $30 - 60$ au (depending on the assumptions on the disc viscosity) in a time scale of several Myr. Clarke (2007) confirmed these results through the modelling of the viscous evolution of a protoplanetary disc undergoing external photo-evaporation, and found a significant shrinking of discs around solar-mass stars down to ~ 100 au after approximately 1 Myr.

These radii are much smaller than the final radii of the discs in our simulation. However, we remark that these authors simulate conditions ($G_0 = 3000$, where G_0 is the value of the far ultra-violet field in the inter-stellar medium) which are more relevant for a massive cluster such as the ONC than for the cluster we simulate here. Indeed, the ONC is a spectacular example of the potential impact of external photo-evaporation on proto-

planetary discs. However, a cluster with only 100 stars is unlikely to have massive stars due to the limited sampling of the IMF, and therefore we do not expect any significant external photo-evaporation to happen in it.

More massive clusters have instead a higher probability of hosting massive stars, increasing the importance of external photo-evaporation. In addition, the importance of both external photoevaporation and encounters depend on the number density of stars, so that it is not trivial to understand which process would dominate. The picture is complicated even more by mass segregation that acts on different time scales, making massive stars sink to the central dense regions more rapidly in low mass clusters. Nevertheless, if it is confirmed that external photo-evaporation is more important than encounters in limiting disc sizes in massive clusters, then there must exist a threshold mass of the cluster where one switches from an encounter dominated regime to an external photo-evaporation dominated regime. Further work is needed to include the effects of external photo-evaporation in simulations like the one we conducted here and investigate these effects. While only a minority of all stars form in bound clusters (Lada & Lada, 2003; Kruijssen, 2012), up to 50% of all stars forming in bound clusters do so in clusters of $M < 10^3$ M$_\odot$. Hence, both high and low-mass clusters are worth exploring, which we plan to do in future work.

3.5   Conclusions

We have presented results from the first hybrid N-body - SPH simulations of coupled cluster and protoplanetary disc evolution. The discs in our simulation are expanding and accreting material onto the star due to viscous evolution, but they are also affected by close encounters between stars. Our simulations allow us to study whether a clustered environment, through the effect of encounters, modifies the protoplanetary disc evolution. We find that encounters can be very destructive for some of the discs, leading to almost complete dispersal for some of them. However, overall the median mass of the discs is not severely affected by the encounters.

We find that disc size is much more affected by encounters than disc mass. In the case in which disc spreading is fast, due to a high viscosity, only close encounters matter, as any mass redistribution in the disc caused by more distant encounters is quickly washed out. In this case, the close encounters simply truncate the disc at a given radius. If instead the spreading is not fast enough, we find a regime where distant encounters can have a significant impact on the discs, hardening their surface densities, and thus shrinking their radii. This also makes the discs more resistant to mass stripping by subsequent encounters. Therefore, we stress the importance of hydrodynamical numerical simulations of this kind to yield accurate predictions of the impact of stellar encounters on disc sizes.

Finally, we confirm that theoretically we expect to see a cut-off at stellar densities higher than $10^{3.5}\,\mathrm{pc}^{-2}$ in the disc sizes due to the effect of encounters. Further work is needed to probe the high stellar densities present in real stellar clusters.

Chapter 4

Old pre-main-sequence stars. Disc reformation by Bondi-Hoyle accretion

Abstract

Young stars show evidence of accretion discs which evolve quickly and disperse with an e-folding time of $\sim$ 3Myr. This is in striking contrast with recent observations that suggest evidence for numerous > 30 Myr old stars with an accretion disc in large star-forming complexes. We consider whether these observations of apparently old accretors could be explained by invoking Bondi-Hoyle accretion to rebuild a new disc around these stars during passage through a clumpy molecular cloud. We combine a simple Monte Carlo model to explore the capture of mass by such systems with a viscous evolution model to infer the levels of accretion that would be observed. We find that a significant fraction of stars may capture enough material via the Bondi-Hoyle mechanism to rebuild a disc of mass $\gtrsim$ 1 minimum-mass solar nebula, and $\lesssim$ 10% accrete at observable levels at any given time. A significant fraction of the observed old accretors may be explained with our proposed mechanism. Such accretion may provide a chance for a second epoch of planet formation, and have unpredictable consequences for planetary evolution.

4.1 Introduction

Circumstellar discs form around protostars as a result of angular momentum conservation during gravitational collapse (e.g. Shu et al., 1987). In the early phases of star formation, disc material loses angular momentum and is accreted onto the central star. The most direct observational signature of the presence of a protoplanetary disc is the excess emission, on top of the expected naked stellar photosphere, at infrared and millimetre wavelengths,

in the ultraviolet and in optical/infrared emission lines. The long wavelength emission is produced by a dusty disc, heated by internal dissipation processes or reprocessing of stellar radiation (e.g. Dullemond et al., 2007b). The short wavelength excess and the optical/infrared emission lines are thought to be produced by the disc-star interaction as matter accretes onto the star or is ejected in a wind/jet (Hartmann, 2009). Strong observational evidence shows that both the inner dusty disc and accretion onto the central star quickly disappear during the early stages of pre-main-sequence evolution; the fractions of stars with near infrared excess and with accretion signatures decay with an e-folding time of 2-3 Myr (Fedele et al., 2010b; Hernández et al., 2007). This disc dissipation timescale, even considering the possible revision by Bell et al. (2013), sets a stringent constraint on the timescales for planet formation.

Recent work has challenged this paradigm. Sensitive, wide field Hα surveys of large star-forming complexes in the Magellanic Clouds and our own Galaxy have revealed a population of pre-main-sequence stars that appear to be older than 10 Myr but still show prominent Hα emission and/or infrared excess (Beccari et al., 2010b; De Marchi et al., 2013a, 2011b,f, 2013c). Although some of these "old" accretor candidates in nearby star-forming regions have been shown to be misclassified young stellar objects (Manara et al., 2013), it is difficult to believe that this is the case for all the candidates; these populations of old accretors are not as centrally condensed as the young stellar clusters in the same fields (e.g. De Marchi et al., 2011d). If the line emission is interpreted as due to accretion as in young pre-main-sequence stars, the implied accretion rates are similar to those derived at early ages, and typically higher than nearby transitional discs[1]. These findings are hard to understand in a framework in which the primordial disc is still the reservoir of accreting material at such old ages; even one disc of age > 30Myr implies an initial population $> 10^5$ (assuming exponential decay with an e-folding timescale of 3Myr).

In this paper we explore the possibility that the old accretors do not have a primordial disc, but a disc that they re-accreted after the primordial disc had dissipated. Previous studies (Moeckel & Throop, 2009; Padoan et al., 2005; Throop & Bally, 2008) have investigated the influence of Bondi-Hoyle accretion on pre-main-sequence mass-accretion rates and the protoplanetary disc at earlier phases, during the initial evolution of the disc-star system within the progenitor cloud. Here we investigate the possibility that a star older than 5-10Myr happens to travel through a clumpy molecular cloud, typically unrelated to that in which the star formed, and is able to accrete enough material to form a new accretion disc.

4.2 Modelling

4.2.1 Bondi-Hoyle accretion

Hoyle & Lyttleton (1939), Bondi & Hoyle (1944) and Bondi (1952) proposed a mechanism by which objects can capture matter from the interstellar medium. A massive object

---

[1]although these are systematically lower mass objects

Parameter	Values	Parameter	Values
f_V	$10^{-2}, 10^{-3}, 10^{-4}, 10^{-5}$	c_s	0.3 km s^{-1}
N_{stars}	$10^5, 10^5, 10^6, 10^7$	σ_v	1 km s^{-1}
R_{cl}	0.1 pc	α	2.35
n_{cl}	10^4 cm^{-3}		

Table 4.1: Parameters for Monte Carlo models

moving through the ISM causes a perturbation, pulling material toward the object. As the capture of material is roughly symmetrical with respect to the direction of motion of the star, much of the angular momentum of the material cancels out, and hence it is captured by the star to eventually be accreted (Davies & Pringle, 1980).

The rate at which material is captured is given by

$$\dot{M}_{\text{BH}} = \mu n v \pi R_{\text{BH}}^2, \tag{4.1}$$

where v is the relative velocity between the star and the ISM, n is the number density of the ISM, and μ is the mean molecular weight (usually taken as $2.3 m_{\text{H}}$). The gravitational cross-section is given by πR_{BH}^2, where R_{BH} is the Bondi-Hoyle radius

$$R_{\text{BH}} = \frac{2 G M_*}{\text{v}^2 + c_s^2}; \tag{4.2}$$

c_s is the sound-speed of the ISM, typically 0.3 km s^{-1}. For a $1 M_\odot$ star moving at 1km s^{-1}, $R_{\text{BH}} \sim 1500$ au.

To explore the effect of this process in reconstituting discs around young stars, we build a simple Monte Carlo model to treat interactions between stars and clumps with densities typical for molecular clouds. We assume a stationary clumpy molecular cloud, which we model as a collection of identical spherical clumps with radius R_{cl} and density n_{cl}. We parametrise the density of clumps through a volume filling factor of dense gas f_V. We assume a population of "old" young stars that has lost their primordial disc enters the cloud and moves through the clumpy medium. By randomly generating stars with masses between $0.7 M_\odot$ and $3.2 M_\odot$[2] from a Salpeter IMF ($M \propto M^{-\alpha}$ Salpeter, 1955) and velocities generated assuming a velocity dispersion of $\sigma_v = 1$ km s^{-1}, we sample the parameters required in Eq. 4.2 from the values given in Table 4.1. The model simulates 10Myr treated as a series of quasi-static time steps of length $t_{\text{st}} = 2 R_{\text{cl}}/\text{v}_*$, assuming that each star is independent. For each star, we calculate R_{BH}, the volume swept out per time-step $V_{\text{st}} = \text{v}_* t_{\text{st}} \times \pi \left(R_{\text{cl}} + R_{\text{BH}} \right)^2$, and hence the probability of encountering a dense clump

$$p = \frac{V_{\text{st}} \times f_V}{(4/3) \pi R_{\text{cl}}^3}. \tag{4.3}$$

---

[2]Stars above $\sim 3 M_\odot$ have strong winds which make a simple model inappropriate, while observations of old accretors are incomplete for stars below 0.7-1$M_\odot$ depending on the distance to the observed region.

In each time-step a uniform random number ζ is drawn, and the star encounters a clump when $\zeta \leq p$; the impact parameter b of the encounter is given by drawing a second random number ζ_2 from the same generator such that $b = (R_{\mathrm{cl}} + R_{\mathrm{BH}})\,\zeta_2^{1/2}$. We then determine the accretion rate (Eq. 4.1) and resolve the stellar accretion and the clump-mass depletion on a finer time-grid of 1000 sub-steps to accurately determine the accreted mass. Interactions where $R_{\mathrm{BH}} > R_{\mathrm{cl}}$ and grazing encounters are treated correctly by taking the projected area of intersection. By repeating this process for $> 10^5$ stars we build up meaningful statistics about the range of possible BH accretion histories and their probabilities. Note that each star is modelled independently, and mass accreted by a star does not influence the mass-budget available to later stars.

The accretion histories determined by this model are then passed to a viscous evolution model (Sect. 4.2.2) to estimate the rate at which material is accreted by the star.

Our choice of f_{V} is based on a reanalysis of SPH simulations of star-forming regions including feedback mechanisms presented in Dale et al. (2012, 2013b) to determine the filling factor of gas at densities higher than 10^4 cm^{-3}. We find that for bound clouds of similar stellar mass to the regions observed by Beccari et al. (2010b); De Marchi et al. (2013c), $10^{-6} < f_{\mathrm{V}} \lesssim 10^{-3}$ irrespective of whether feedback from massive stars is included.

While this provides a useful estimate of the amount of mass captured in this way, it somewhat overestimates the total as we neglect a number of physical processes. First, we neglect the motion of the clumps and assume that $\mathrm{v} = \mathrm{v}_*$ in Eq. 4.2. Correct treatment of the relative motions would in general reduce R_{BH} and hence the accretion rates. Second, stars above $2\mathrm{M}_\odot$ have significant wind and radiation pressure that will depress the accretion rate (Edgar & Clarke, 2004). Similarly, we do not include the possible influence of the X-ray photoevaporation on the accretion, which may have an analagous effect for lower mass stars. We also ignore the possible influence of magnetic fields, which recent studies (e.g. Lee et al., 2014) have shown may reduce accretion rates by a factor of a few. Likewise, we neglect structure on scales smaller than a single clump; such structure is required for a disc to form, and would reduce accretion rates relative to the homogeneous clump case treated here. Finally, we do not include binaries. However, the only influence of binarity in the context of Bondi-Hoyle accretion is to increase R_{BH}, since binaries behave as a single object of mass $M = M_1 + M_2$.

4.2.2   Viscous evolution modelling

Due to the angular momentum of the material accreted from the clump, which may be due to a density gradient within the clump or the rotation of the clump itself, accretion cannot proceed directly onto the star (Ruffert, 1997). Therefore, the formation of a thin accretion disc is expected as the result of the viscous spreading of a thin ring. Throop & Bally (2008) described the "buffer" effect of an accretion disc, but did not directly model it. We assume that the material accreted from the medium circularises at a radius $r_0 = 0.1R_{\mathrm{BH}}$. After a single impulse of accretion onto the disc, the surface density is described by $\Sigma(r) = M_0/(2\pi)\delta(r - r_0)$, where M_0 is the deposited mass. Under the influence of an effective viscosity ν that redistributes the angular momentum in the disc,

the spreading ring solution (Lynden-Bell & Pringle, 1974) describes the evolution in time of this initial surface density,

$$\Sigma(r,t) = \frac{GM_*(rr_0)^{1/4}}{3\pi r^2 \nu \Omega} \exp\left[-\left(\frac{(r_0^{1/2} - r^{1/2})^2 r}{3t\nu}\right)\right] \exp(-\lambda)I_{1/2}(\lambda), \qquad (4.4)$$

where ν is the kinematic viscosity of the gas, Ω the keplerian angular speed, $I_{1/2}$ the modified Bessel function of order $1/2$, $\lambda = 2r^{3/2}/(3(GM_*)^{3/2}\nu t r_0)$, and we have specialized the expression for the $\nu \propto r$ case. From this analytical solution, it is possible to compute the mass accretion rate onto the star $\dot{M}_{\mathrm{kernel}}$. To derive the mass accretion rate history onto the star, we convolve this function with the mass accretion rate history onto the disc:

$$\dot{M}_*(t) = \int \dot{M}_{\mathrm{BH}}(t')\dot{M}_{\mathrm{kernel}}(t-t')\mathrm{d}t'. \qquad (4.5)$$

Given a stellar mass, the loading radius, and a law for viscosity, the evolution in time is now completely determined. We fix the viscosity by using the well-known Shakura & Sunyaev (1973b) prescription, $\nu = \alpha(h/r)^2 r^2 \Omega$, where α is the Shakura-Sunyaev parameter and h/r the aspect ratio of the disc. We choose typical values of $\alpha = 0.01$ and $h/r = 0.05(r/1\mathrm{AU})^{1/4}$ (Armitage, 2011b). Operationally, we sample Eq. 4.4 numerically on a space and time grid. We integrate over space to get the mass of the disc and we numerically differentiate the result to get the mass accretion rate kernel, which can be convolved with the Bondi-Hoyle history (Sect. 4.2.1).

4.3   Results

Our model indicates that a fraction of the population $\sim 40 - 50 \times f_{\mathrm{V}}$ encounter dense regions and accrete more than $0.001\mathrm{M}_\odot$ material by the end of the simulation (Fig. 4.1). The median accreted mass is typically $\sim 0.01\mathrm{M}_\odot$, similar to the mass of discs around young pre-main-sequence stars, with strong dependence on the stellar mass. In extreme cases, however, more massive stars ($>2\mathrm{M}_\odot$) with low v_* that encounter several clumps can capture $\geq\mathrm{M}_\odot$. Our treatment of the disc formation and evolution is probably inadequate for these extreme cases.

Converting the Bondi-Hoyle accretion into stellar accretion rates, we find $\dot{M}_* \lesssim 10^{-6}$ $\mathrm{M}_\odot$ yr^{-1} after the formation of the disc. Owing to the assumptions inherent in our model, this rate declines from the peak as a power law as in primordial discs.

By calculating the time each star spends accreting above a certain threshold accretion rate, one can derive a mean time per star as a function of the threshold and hence an estimate of the fraction of the population which one expects to observe accreting at a given time. As shown in Fig. 4.2, for a threshold rate of 10^{-8} $\mathrm{M}_\odot$yr^{-1} we typically find that the cumulative probability is $\sim 20f_{\mathrm{V}}$, i.e. the fraction of a stellar population that one expects to observe as "old" accretors at a given time is an order of magnitude larger than the volume filling-factor of dense clumps.
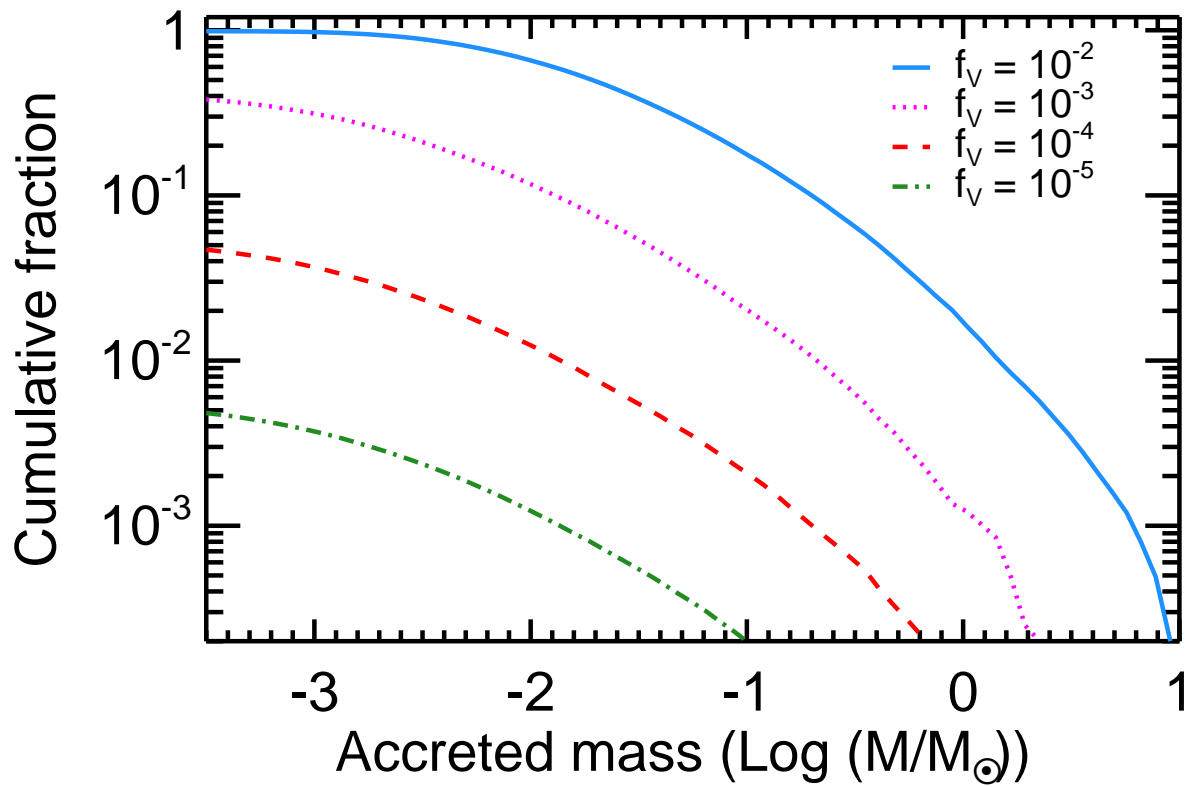
Figure 4.1: Cumulative fraction of the stellar population that has accreted mass as a function of total accreted mass. The solid blue line indicates a filling-factor of 10^{-2}, the dotted magenta line 10^{-3}, the dashed red line 10^{-4}, and the dot-dashed green line 10^{-5}.
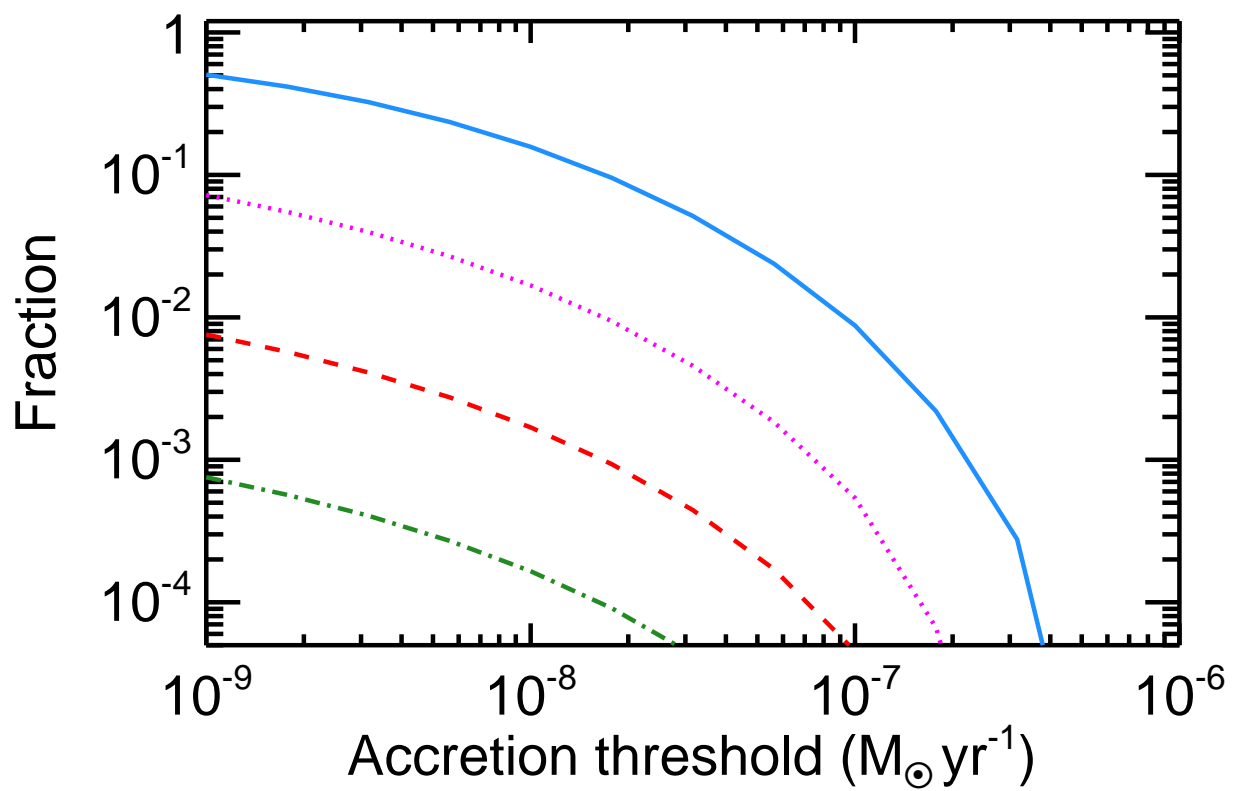
Figure 4.2: Fraction of the population that would be detected as an old accretor at a given time, plotted as a function of the instantaneous accretion rate. The models are indicated using the same colours and line-styles as Fig. 4.1.

4.4   Discussion

Our primary goal is to assess whether the Bondi-Hoyle mechanism can contribute significantly to observations of old accretors in regions with ongoing star formation, under a number of simple assumptions. This involves stars from a previous star-formation episode, after their primordial discs have dispersed, interacting with a clumpy molecular cloud. Our model indicates that up to several percent of the population passing through a region containing dense clumps may accrete more than $0.001 M_\odot$ of material. Because of the factors indicated above (Sect. 4.2.1), the model is likely to overestimate the total accreted mass. However, since the Bondi-Hoyle accretion is a well-understood process, the largest sources of uncertainty derive from the parameters assumed as input to the model, and in particular the clump geometry and filling factor, as well as the assumption that the accreted material will form a thin disc.

Our initial choice of filling factor was based on a reanalysis of the simulations of Dale et al. (2012, 2013b) for clouds similar to those observed to host old accretors. A further estimate can be obtained from the high-resolution sub-mm maps of the 30 Dor region from Indebetouw et al. (2013). These reveal a wealth of clumpy structures, similar in scale and density to the clumps in the Monte Carlo model used here. Assuming that the clumps are uniform spheres with an average radius $R_{cl} = 0.15$ pc and distributed in a cube whose depth is equal to the projected size of the observed region ($10 \times 10 \times 10$ pc^3) yields a filling factor of $f_V = 1.5 \times 10^{-3}$, at the upper end of our parameter range.

The behaviour of the accretion disc depends strongly on the viscous timescale τ_ν, as parametrised in terms of r_0 and α. An order of magnitude change in τ_ν has little effect on the observable old-accretor fractions at low thresholds, but the fractions at high thresholds decline approximately in proportion to $1/\tau_\nu$. For larger changes in viscosity, this also affects the lowest thresholds explored in Sect. 4.3

Since we do not include stars down to the peak of IMF ($\sim 0.3 M_\odot$) and Bondi-Hoyle accretion rates are $\propto M^2$, we may overestimate the total fraction of old accretors by a factor ~ 3 for the Salpeter IMF assumed here. However, Eq. 4.3 is dominated by R_{cl} for low-mass stars, so one would expect a similar fraction of old accretors when $\dot{M}$ is a factor of 4 lower.

Comparisons between our model and the observations of old accretors are difficult, as there are no firm constraints on the size of the old population (including non-accretors). Nevertheless, from Fig. 4.2 one can see that without an unrealistically large filling factor ($\gg 10^{-3}$) of dense clumps, the small, nearby star-forming regions are unlikely to produce more than one old accretor, as their typical mass is a few hundred $M_\odot$. As no old accretors have been identified in these regions, this is consistent with our model. From the recent identification of a large ($\sim 3 \times 10^3 M_\odot$) diffuse population with ages $\gtrsim 10$ Myr toward Orion (Bouy et al., 2014) one expects a few tens of reformed discs, although it is unclear whether there is any overlap between this population and the Orion molecular clouds.

Observations of old accretors in large star-forming complexes typically detect up to several hundred such sources in each observed region. Given the formation efficiency we have computed and our assumed filling factors, this requires a total population at least

of the order of 10^4 stars in the mass range of the observed old accretors, or $\sim 3 \times 10^4$ stars correcting for the IMF, which must have passed through the regions in which the clumps are distributed. In the case of NGC3603, which is inferred to have a population $\sim 10^{4.2} M_\odot$ (Rahman et al., 2013) and ~ 100 old accretors, this implies either that the old population was significantly richer, or that f_V is or was very high. The 30 Doradus region, on the other hand, shows a similar total of old accretors, although the total population is likely ~ 100 times larger than NGC3603. Only a small fraction (1%) of the stars in 30Dor need to pass through regions containing dense clumps to produce the observed numbers. In reality, f_V will evolve with time, and it is possible that the difference we observe between these regions may be due to 30Dor being more evolved, or having evolved more rapidly, than NGC3603.

In our model, a significant fraction (up to several tens of percent) of stars capture enough material to form a circumstellar disc of mass similar to primordial protoplanetary discs. This raises a number of interesting questions, such as whether a second epoch of planet formation is possible, and how the interaction between inflowing material and an existing planetary system might alter the accretion or the planetary evolution.

The answers to these queries depend strongly on how the inflowing material interacts with the existing system, which we have not treated. Nevertheless, Bondi-Hoyle accretion presents a mechanism by which a new reservoir of potentially planet-forming material may be built by up to a few percent of stars. This gives them a second chance to form planets, from material that is potentially of different composition from the material that formed the star. Another possibility is that these stars are already surrounded by a planetary system formed out of the primordial disc. If they accrete new material, typically with an angular momentum different from that of the original planetary system, the interaction of the new material and the existing planets may have a range of outcomes. Understanding the range of possible outcomes will require detailed simulations of the accretion process and of the dynamical interactions with the planetary systems which are beyond the scope of the present paper.

4.5 Conclusions

We have presented a model in which Bondi-Hoyle accretion by stars passing through dense clumps in the outer regions of their natal molecular cloud leads to the re-formation of a circumstellar disc. As a result, these stars may masquerade as pre-main-sequence objects due to ongoing accretion and the presence of infrared excess emission. A significant part of the observed populations of old accretors in large star-forming regions may be explained by this mechanism. As it may have wide-ranging consequences for the early evolution of planetary systems in rich stellar environments, we believe that further investigation of this mechanism is warranted.

Chapter 5

The $\dot{M} - M_*$ relation of pre-main-sequence stars: a consequence of X-ray driven disc evolution

Abstract

We analyse current measurements of accretion rates onto pre-main sequence stars as a function of stellar mass, and conclude that the steep dependance of accretion rates on stellar mass is real and not driven by selection/detection threshold, as has been previously feared.

These conclusions are reached by means of statistical tests including a survival analysis which can account for upper limits. The power-law slope of the $\dot{M} - M_*$ relation is found to be in the range of 1.6-1.9 for young stars with masses lower than 1 $M_\odot$.

The measured slopes and distributions can be easily reproduced by means of a simple disc model which includes viscous accretion and X-ray photoevaporation. We conclude that the $\dot{M} - M_*$ relation in pre-main sequence stars bears the signature of disc dispersal by X-ray photoevaporation, suggesting that the relation is a straightforward consequence of disc physics rather than an imprint of initial conditions.

5.1   Introduction

The scaling of the accretion rate, $\dot{M}$, with stellar mass, M_* for low-mass stars has been the focus of much debate over the last few years. Measurements in the first half of the naughties, indicated that $\dot{M}$ correlates with the square of the stellar mass (Muzerolle et al 2003; Natta et al 2004; Calvet et al 2004; Muzerolle et al 2005; Mohanty et al 2005; Natta

et al 2006). This deviation from a simple linear scaling encouraged the development of a number of theoretical models to interpret this results, including Bondi-Hoyle accretion (Padoan et al 2005, see also Throop & Bally 2008) and dependance on the initial conditions of the parent cloud from which the protoplanetary disc formed (Dullemond, Natta & Testi, 2006, Alexander & Armitage 2006). Clarke & Pringle (2006, CP06), and later Tilling et al. (2008), questioned the quantitative value of the power-law exponent, α, in the $\dot{M}$-M_* relation, suggesting that incompleteness of the data at both high and low accretion rates may have conspired to yield a higher than expected value of α. By considering disc dispersal by EUV photoevaporation CP06 derive a theoretical value of $\alpha = 1.35$. A similar slope was also obtained by an independent model of Gregory et al (2006) based on a steady state accretion which considered both dipolar and complex magnetic fields.

Recent observational data, however, lend credence to higher values of the α exponent. Using different observational methods and samples in different regions, the typical derived values of α are around 1.5-1.8 (e.g., Herczeg & Hillenbrand 2008; Rigliaco et al. 2011a; Antoniucci et al. 2011; Biazzo et al. 2012). In particular, Manara et al. (2012) used the Hubble Space Telescope to investigate the $\dot{M}$-M_* relation in the Orion Nebula Cluster, finding a value of $\alpha = 1.68 \pm 0.02$ (compatible with the results of Natta et al. 2006). Selecting sources according to the method used for the determination of the accretion rates in the same sample returns values varying from $\alpha = 1.59 \pm 0.04$ to $\alpha = 1.73 \pm 0.02$.

In this paper we show that values of $\alpha \sim$ 1.45-1.70 are expected for stars with solar mass or lower, in the context of a protoplanetary disc dispersal mechanism based on X-ray photoevaporation. The work is organised as follows. In section 2 we describe the available observational data and perform some simple survival statistics to account for upper limit measurements. In Section 3 we describe the theoretical prediction of the $\dot{M}$-M_* relation for a population of discs dispersed by X-ray photoevaporation, showing that this agrees with the observational values and perform additional statistical tests. In Section 4 we briefly summarise our findings.

5.2   Observational Samples

We have collected mass accretion rates versus stellar mass data from the literature in order to investigate the correlation between $\dot{M}$ and M_* implied by recent observational data. Our dataset is described in Table 2. In order to address the concern raised by CP06, that the steepness of the $\dot{M}$-M_* relation may be driven by selection effects in the data, we have collected, where available, all upper limits and included them in the calculation of α by means of survival statistics techniques. The total number of data-points we have collected is 3764 of which 15.4% are upper limits. Necessarily a number of measurements are duplicated in various sources, namely 84.1% are duplicates. In such cases we have taken the geometrical average of the measurements. In cases where both measurements and upper limits are available for an individual source we neglect the upper limits and only use the measurements. Binaries are a further source of contamination, around 7% of the objects in the total sample are in known systems, but it is unclear how many unknown

binaries may still be left. In total we are left with 1623 measurements for individual objects of which 294 are upper limits. A plot of the full dataset is shown in Figure 1.

The largest from the recent surveys is the HST/WFPC2 of Manara et al (2012, M12), which includes measurements of $\dot{M}$ based on U-band excess and H-α luminosity for approximately 700 sources in the ONC. The large and homogeneously determined set of $\dot{M}$ obtained by M12 allowed them to draw some important conclusions on the behaviour of $\dot{M}$ as a function of stellar mass and stellar age. Based on the whole survey they found α = 1.68, or α = 1.73/1.59 if only the sources with $\dot{M}$ measured from U-band excess/Hα method are selected. Values of $\alpha \sim 1.6 - 1.8$ are often found when analyzing different regions and using various methodologies. This is inconsistent with the results by Fang et al. (2009) , who derive an α=3 in their sample of sub-solar mass targets in the Lynds 1630N and 1641 clouds in Orion. This inconsistency is perhaps related to the different methodologies used, in particular in the different relations between the accretion luminosity and the line luminosity and in the different evolutionary models used with respect to any other work. When converting the values of $L_{\rm acc}$ reported by Fang et al. (2009, 2013) in $\dot{M}$ using classical evolutionary models we derive values of the slope ~ 2, compatible with the values reported in other works, even if still slightly higher.

	α				β			
	total sample	#	Manara	#	COUP	#	Güdel	#
all data	1.66 ± 0.07	1320	1.65 ± 0.14	698	1.28 ± 0.07	544	1.38 ± 0.13	116
" EM method	1.93 ± 0.07	1608	2.06 ± 0.14	783				
" BJ method	1.61 ± 0.07	1608	1.38 ± 0.14	783				
$0.032\ M_\odot < \mathrm{M} < 10\ M_\odot$	1.62 ± 0.07	1311	1.65 ± 0.14	698	1.44 ± 0.08	537	1.38 ± 0.13	116
" EM method	1.89 ± 0.08	1592	2.06 ± 0.14	783				
" BJ method	1.61 ± 0.07	1592	1.38 ± 0.14	783				
$1.0\ M_\odot < \mathrm{M} < 10\ M_\odot$	3.00 ± 0.43	111	2.24 ± 1.42	24	1.46 ± 0.42	83	1.04 ± 1.20	18
" EM method	3.25 ± 0.48	127	no upper limits					
" BJ method	3.20 ± 0.42	127	no upper limits					
$0.032\ M_\odot < \mathrm{M} < 1.0\ M_\odot$	1.57 ± 0.10	1200	1.63 ± 0.18	674	1.71 ± 0.12	454	1.44 ± 0.17	98
" EM method	1.99 ± 0.10	1465	2.19 ± 0.18	759				
" BJ method	1.61 ± 0.10	1465	1.29 ± 0.18	759				

Table 5.1: Slopes of the $\dot{M}$ versus M_* relation (α) and of the L_X versus M_* relation (β).
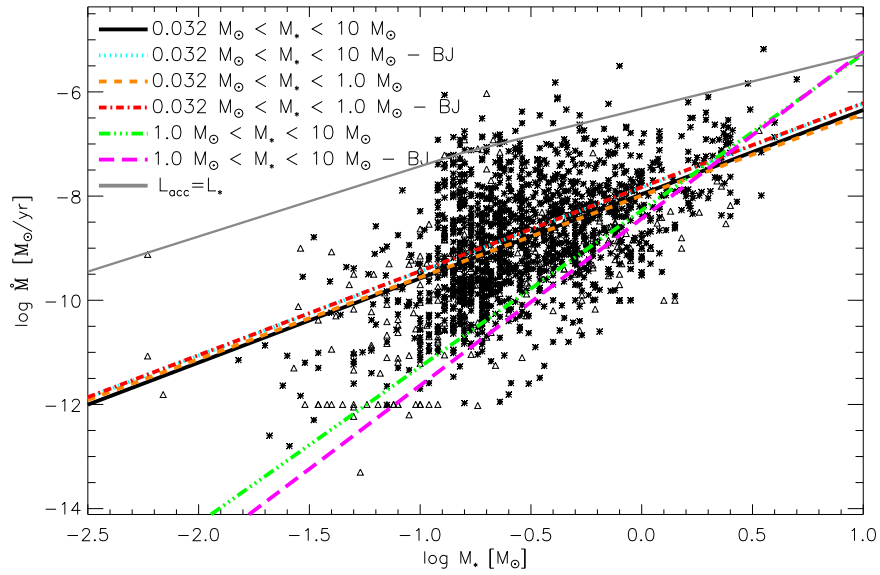
Figure 5.1: Accretion rates as a function of stellar mass for the whole collected sample. Crosses represent measurements and triangles upper limits. The slopes of the distributions are listed in Table 1. The grey solid lines shows the locus where the accretion and bolometric luminosity are equal.

One of the main drawbacks of previous analyses and one of the main arguments of CP06 and Tilling et al. (2008) against over interpreting any possible correlation is the fact that the lowest possible accretion rate measurement in nearby star forming regions correlates strongly with stellar mass, something that is particularly evident in Figure 1. Manara et al. (2013a) analyzed a sample of 24 non-accreting (Class III) YSOs to derive the threshold on the estimates of accretion luminosities, L_{acc}, in accreting YSOs determined with line luminosity. They found that this threshold, when converted in $\dot{M}$, depends on the mass of the targets. More interestingly, this threshold happens to be right below the typical values of $\dot{M}$ derived in other works, and seems to follow the trend of the $\dot{M}$-M_* relation. Given that this threshold is determined only for estimates of L_{acc} derived from line luminosity the data obtained with U-band excess determination should not be affected. Still, the detection of U-band excess for hotter targets is more challenging because the typical photospheric temperature is similar to that of the accretion shock (e.g., Calvet et al. 2004, M12). Nevertheless, upper limit determinations should take this effect into account.

In order to test the null-hypothesis that the observed correlation is purely driven by upper-limit selection effects we perform a Cox regression test (e.g. Feigelson et al. 1985) which account for the upper limits. Given the now large number of available measurements, we are able to reject the null-hypothesis at the $>10\sigma$ level. This confirms that the observed correlation between $\dot{M}$ and M_* is infact real, and not driven by upper limit selection affects. This is obviously not surprising when one inspects Figure 1 given the amount of data now available; however, it casts away any doubt from previous analyses when the data samples
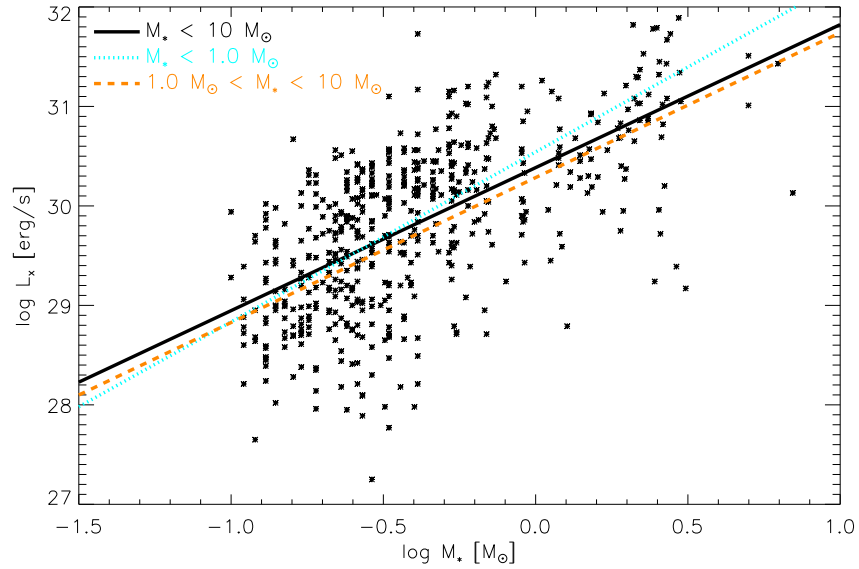
Figure 5.2: X-ray luminosities as a function of stellar mass in the Orion Nebular Cluster obtained with the Chandra X-ray Telescope as part of the COUP project (Preibisch et al 2005).
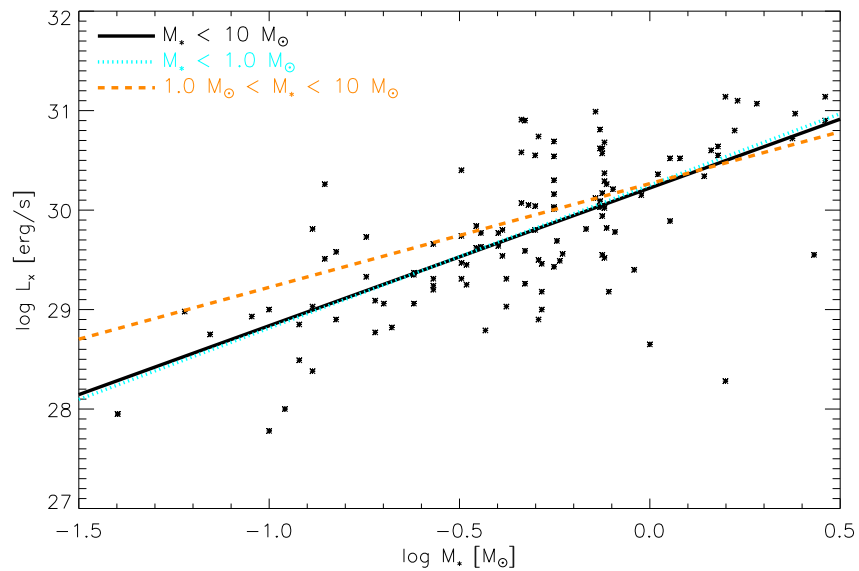
Figure 5.3: X-ray luminosities as a function of stellar mass in the Taurus Molecular Cloud obtained with the XMM Newton X-ray Telescope (Güdel et al 2007).

were smaller and such a concern was legitimate as pointed out by CP06.

We have recalculated slopes for the $\dot{M}$-M_* relation using the full collected sample and the sample of Manara et al (2012), and summarise the results in Table 1. We also include the slopes obtained using two different survival statistics algorithms for linear regression: the one assuming normal residuals (EM algorithm) and the other assuming Kepler-Meyer residuals (The Buckley-James algorithm, BJ). More information about the statistical methods and the ASURV package which was employed for the analysis is given in Lavalley, Isobe & Feigelson (1992). The slope, α, of the $\dot{M}$ -M_* changes significantly for different mass ranges, as already noted by several authors (e.g. Rigliaco et al 2012). Indeed α is smaller in the lower stellar mass range ($M_* < 1 M_\odot$, $\alpha = 1.5 - 1.9$) compared to the higher stellar mass range ($1 M_\odot < M_* < 10 M_\odot$, $\alpha = 3. - 3.2$). The dramatic change in the slope suggests that different physical processes may be at play in the two mass regimes. Qualitatively similar conclusions are reached by examination of the slopes yielded by the sample of M12 alone. Typical slopes obtained for the two mass ranges and for the full sample are shown in Figure 1 and summarised in Table 1.

The data used to calculate the slopes cited in Table 1 are the mass accretion rates and stellar masses given by the various authors. This constitutes an inhomogeneous sample as different authors adopted different evolutionary models. We have also recalculated the entire dataset using consistent evolutionary tracks for all objects when possible, and note here that the slopes are sensitive to the choice of evolutionary track. In all cases however the slopes for the low-mass range are between 1.3 and 1.9 when upper limits are excluded and between 1.4 and 2.4 using the Buckley-James algorithm. The tracks used include D'Antona & Mazzitelli (1997), Baraffe et al. 1998, Palla & Stahler (1999), Siess et al. (2000, with and without overshoot).

Another possible selection effect discussed by CP06 is that the upper bound of the distribution is limited by those cases where the accretion luminosity, L_{acc}, becomes larger than the bolometric luminosity of the star, L_{bol}. Indeed this is a legitimate concern when one analyses the data that were available in 2006. In Figure 4 of CP06 one sees indeed that the data seem to uniformly fill the space up to $k = 1$, where $k = L_{acc}/L_{bol}$. However, the larger collection of data that is available today clearly shows that the majority of datapoints, which drive the $\dot{M}$-M_* relation, lie well below the $k = 1$ limit. To show this we overplot the $L_{acc} = L_{bol}$ line (i.e. $k = 1$) to the data in Figure 1.

For completeness we have also checked the possibility of a straight proportionality between accretion rates and stellar mass. A likelihood ratio test allows the rejection of the null hypothesis $\dot{M} \propto M_*$ to more than six σ.

5.3 $\dot{M}$-M_* as predicted by X-ray photoevaporation

In the previous section we briefly summarised the available observations to date and showed that they never yield values of α below 1.55 in the solar mass range. This is difficult to reconcile with the value of 1.35 predicted by Clarke & Pringle (2006), for a population of discs dispersed by EUV photoevaporation in the UV switch model (Clarke et al. 2001,

Alexander, Clarke & Pringle, 2006ab). Following CP06's argument, the lowest accretion rate measured at a given mass should be set by the lowest possible photoevaporation rate for the same mass. Before the onset of photoevaporation the evolution of the mass accretion rate follows the usual viscous laws, which predict an power-law decay with time of $\dot{M}$. Hence young stars spend most of their time at low accretion rates where one has a higher chance of observing them. If the lowest allowed accretion rate is determined by photoevaporation, then this is equivalent to saying that the most probable observed accretion rate for a given star is $\dot{M} = \dot{M}_{wind}$, where $\dot{M}_{wind}$ ist the mass loss rate due to photoevaporation. For solar mass stars in the UV-switch model this rate is $\sim 10^{10} M_{\odot}/yr$ and scales as the square root of the product of stellar mass and ionising flux:

$$\dot{M}_{wind} \propto (M_* \phi)^{1/2} \tag{5.1}$$

giving $\dot{M} \propto M_*^{1.35}$ if the ionising flux simply scales with stellar luminosity. If however the UV flux is mainly chromospheric in origin and thus has the same scaling with stellar mass as the X-ray luminosity, then

$$\dot{M} \propto M_*^{(1+\beta)/2}, \tag{5.2}$$

where β is the exponent of the X-ray luminosity function. As will be shown below β is roughly 1.7 (Preibisch et al 2005) for low mass stars, giving again $\dot{M} \propto M_*^{1.35}$, like in the case where the ionising flux scales with stellar luminosity .

In recent years several works have shown that X-ray photoevaporation dominates over EUV photoevaporation for stars with masses of one or below one solar mass (Ercolano et al. 2009, Owen et al. 2010, 2011, 2012). In the case of X-ray photoevaporation the mass loss rate, $\dot{M}_{wind}$, scales linearly with the X-ray luminosity, implying that the $\dot{M}$-M_* relation for a population of discs dispersing via X-ray photoevaporation is completely determined by the shape of the X-ray luminosity function. As opposed to Dullemond, Natta & Testi, (2006) and Alexander & Armitage (2006), this requires no spread in initial conditions other than the dependance on stellar mass. Indeed we argue here that the relation is primarily driven by the observed accretion rate at late times (just before dispersal) where the disc spends most of its time. Therefore the initial conditions are completely irrelevant as they are washed out after one viscous time. Our model would return the same result regardless of whether a spread in intial conditions is assumed.

In Figure 2 we show L_X as function of stellar mass for various mass ranges in the COUP sample (Preibisch et al. 2005), obtained with the Chandra X-ray Telescope in the Orion Nebular Cloud (ONC). This plot also shows roughly two regimes for the $L_X - M_*$ distribution, where the lower mass stars have a steeper dependence on stellar mass compared to the higher mass stars. It is indeed well known that the slope of the distribution flattens out for the higher stellar masses, where X-ray production becomes less efficient. The black solid line shows the power-law slope, β, for the entire sample ($\beta = 1.28$), the cyan dotted line shows the slope obtained when only stars with masses lower than 1. $M_{\odot}$ are considered ($\beta = 1.71$), and the orange dashed line shows the slope for objects in the higher mass range between 1 and 10 $M_{\odot}$ ($\beta \sim 1.46$).

It is worth noticing at this point that the slopes quoted include the entire sample of accretors and non-accretors in the Preibisch et al (2005) data set. According to Preibisch et al (2005), however, there are differences in the X-ray luminosities between accretors and non-accretors, where non-accretors show marginally higher X-ray luminosities that are roughly consistent with those of rapidly rotating main sequence stars and they also show a clearer correlation with stellar mass, compared to the accretors. The accretors, on the other hand, have somewhat suppressed X-ray luminosities and the correlation with stellar mass is also not so clear; this is probably due to whatever effect is suppressing the X-ray luminosity, which may have to do with the presence of a disc or with whatever is damping the X-ray activity (although see Drake et al. 2009 for the opposite interpretation). One has to be careful however not to over-interpret this discrepancy and it is indeed difficult to estimate any uncertainty on the X-ray luminosity function. The main problem is that the definition of accretors and non-acccretors used by Preibisch et al. (2005) was based on emission lines and it is well known that these can show strong time-variability, leading to large uncertainties in the classification. In view of this, and also considering the differences between this data-set and the Taurus data-set which will be discussed below, we conclude that the uncertainties on the quoted value of the slope in the X-ray luminosity function are probably larger than those stated here.

Figure 3 shows the same for the sample of Güdel et al. (2007) obtained with the XMM Newton X-ray telescope in the Taurus molecular cloud. The number of sources in this survey is however much lower and hence it is more difficult to draw significant statistics, particularly in the higher mass bin. However qualitatively similar results are obtained, where $\beta = 1.38, 1.44$ and 1.04 for the whole sample, the lower and the higher mass ranges defined above, respectively.

The values of β obtained for the lower mass objects in the Preibisch et al (2005) sample compare well with the values of α obtained for the same mass range, which is what one would expect if disc dispersal in this stellar mass range is dominated by X-ray photoevaporation. The same process is not expected to be the dominant disc dispersal mechanism for discs around high mass stars, where X-ray production is expected to be lower and the corresponding photoevaporation rates then too weak to compete with the higher accretion rates. In this context the lack of agreement between α and β in the higher mass range is not surprising.

It is difficult to speculate what the dominant dispersal mechanism at higher masses may be. The drop in the X-ray luminosities for these higher mass stars, implies that if photoevaporation is still the main driver of dispersal, the main heating source must be EUV or FUV photons. Detailed hydrodynamical wind solutions for these objects have yet to be calculated, although some estimates using a simpler approach were provided by Gorti, Dullemond & Hollenbach (2009), which show that photoevaporation by FUV radiation may be a viable solution for the fast dispersal of discs around higher mass stars.

If X-ray photoevaporation is indeed controlling disc dispersal around low mass stars, hence determining the slope of the $\dot{M}$-M_* relation, one other issue to be considered is the lowest possible accretion rate mesurable at a given mass in a sample of discs that are dispersed by X-ray photoevaporation. Owen et al (2010) show that the final phase

of rapid disc dispersal begins roughly when the accretion rates become about a factor ten lower than the photoevaporation rates. For the ONC sources shown in Figure 1, the lowest X-ray luminosities for solar mass stars are of the order of approximately 10^{29} ergs/s. This corresponds roughly to X-ray photoevaporation rates of $10^{-9} M_\odot$/yr, implying that the lowest accretion rates that should be measurable are of order $10^{-10} M_\odot$/yr, which is consistent with observational data in this mass bin (Manara et al 2012).

A final, perhaps more stringent test of this model is a comparison of the L_X-M_* distribution against the $\dot{M}$-M_* distribution. The one-to-one mapping of the wind mass loss rate with the X-ray luminosity would indeed suggest that their normalised distribution in the low mass bin, where X-ray photoevaporation dominates, should be indistinguishable. Unfortunately a direct comparison of the data-sets is impossible since the distributions of stellar masses in the two samples (even in bins around solar-type stars) is formally different to very high significance. The likely cause of this is that our $\dot{M}$-M_* sample contains a large number of objects from Taurus, which is known to have an unusual IMF (Luhman 2004). Therefore, in order to perform a meaningful statistical test we need to resample both distributions onto the same underlying mass-function.

Thus we construct a statistical test to see if we can rule out the null-hypothesis that the observed $\dot{M}$ distribution is purely driven by disc accretion terminated by X-ray photoevaporation. We choose the mass range (0.2-1.2M$\odot$) where X-ray photoevaporation is likely to be dominant (e.g. Owen et al. 2012). In this mass-range we then randomly sample both our $\dot{M}$-M_* and $\dot{M}$-L_X distributions onto a Chabrier IMF (Chabrier 2003) where the new resampled distributions consist of 100 data points (roughly the maximum number possible before random noise is the dominant source of variation). We then convert our $\dot{M}$-L_X distribution into a $\dot{M}$-M_* distribution by assuming that the accretion rate follows a simple viscous disc model of a $t^{-3/2}$ decline in accretion rate until the accretion rate equals the mass-loss rate, where we use the Owen et al. (2012) fitting function:

$$\dot{M}_w = 6.25 \times 10^{-9} \left(\frac{L_X}{10^{30} \text{ ergs}^{-1}} \right)^{1.14} \tag{5.3}$$

but ignore the very weak ($\sim M_*^{-0.068}$) stellar mass dependance. At this point the accretion rate follows an exponential cut-off with a time-scale approximately 10% of the disc's lifetime. Formally the expression we use is given by:

$$\dot{M}_* \propto t^{-3/2} \exp\left[-\left(\frac{t}{\tau_{\text{disc}}} \right)^7 \right] \tag{5.4}$$

where τ_{disc} is a scale time which modifies the disc's life-time so the exponential cut-off begins when the viscous disc's accretion rate drops below the wind rate. Such an evolution does not contain information about the wind profile, as it is just matching together two different phases of disc evolution (primordial disc evolution & inner disc draining, see Owen et al. 2010 for a discussion)[1]. Formally this exercise is completed in a scale-free

---

[1]Note the form of the accretion rate evolution looks very similar to the semi-analytic solutions presented by Ruden (2004) using a Green's function approach for the EUV wind
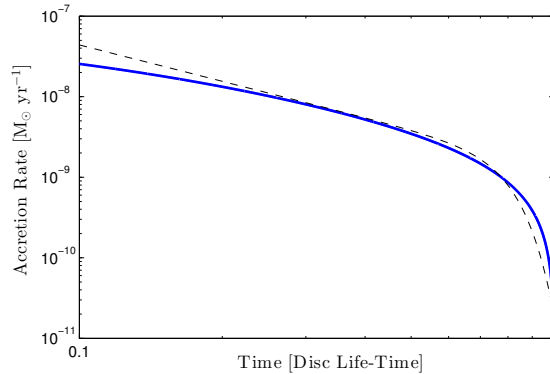
Figure 5.4: Comparison between a full viscous calculation (solid) and the simple formula (dashed)

manner (allowing us to ignore unconstrained disc parameters e.g. α), with no explicit choice of what τ_{disc} is. In order to find the lifetime τ_{disc}, we find the time τ_{disc} so that $\dot{M}(t) = \dot{M}_w(L_X)$. For simplicity, we approximate the dependence of $\dot{M}$ with $t^{-3/2}$, so that the equation can be solved analytically. We note that this construction is consistent with providing the observed spread in disc lifetimes from the spread in X-ray luminosity alone, as demonstrated in Owen et al. (2011). A comparison between this formula and an actual viscous calculation from Owen et al. (2011) is shown in Figure 5.4.

Such a formula provides an approximate description of the disc's accretion rate evolution. The $\dot{M}$-L_X distribution is thus convolved with this expression in order to produce an $\dot{M}$-M_* relation which can then be compared with the observed $\dot{M}$-M_* relation. Thus with our two re-sampled $\dot{M}$-M_* relations (one observed, one calculated from the M_*-L_X) we calculated the Kaplan-Meier distributions and perform a null-hypothesis test to determine whether we can reject the null-hypothesis that these two distributions are different. Since we are re-sampling our two distributions onto the same underlying mass distribution we perform 500 realisations of this random samplings to get a sense of the re-sampling error. In Figure 5, we show the Kaplan-Meier distributions resulting from 10 re-sampling realisations for the observed M_*-$\dot{M}$ (solid) and the M_*-$\dot{M}$ distributions calculated from the observed M_*-L_X distribution (dashed). Furthermore, in Figure 5.6 we show a histogram of the P-values resulting from our hypothesis tests (both using the log-rank and Gehan methods - see Feigelson & Nelson 1985) for each of our random realisations, where the P value is an estimate of the probability that the two distributions are drawn from the same underlying sample. Therefore, they are unlikely to come from the same underlying distribution if P is small ($<0.05 \sim 2\sigma$). Given that in our case P is clearly generally not small one cannot rule out the null hypothesis. This is striking given that the two distributions should be independent unless they are connected by the photoevaporation model. In summary, both figures show extremely good agreement between the two distributions and we are unable to reject the null hypothesis, suggesting that the two populations are indeed connected by the X-ray photoevaporation model.

We note, further, that the disagreement is very small, and mostly evident at high
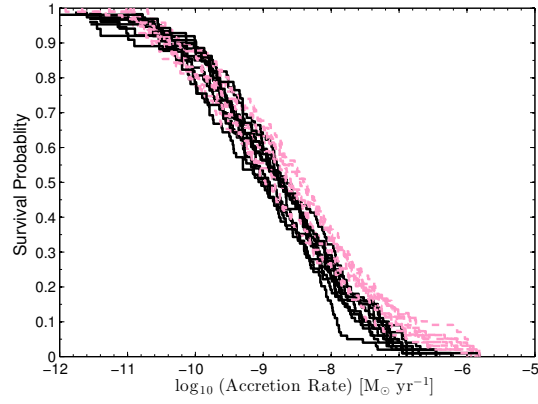
Figure 5.5: KM distributions for the re-sampled $\dot{M}$-M$_*$ (solid) and calculate $\dot{M}$-M$_*$ (dashed) relations.
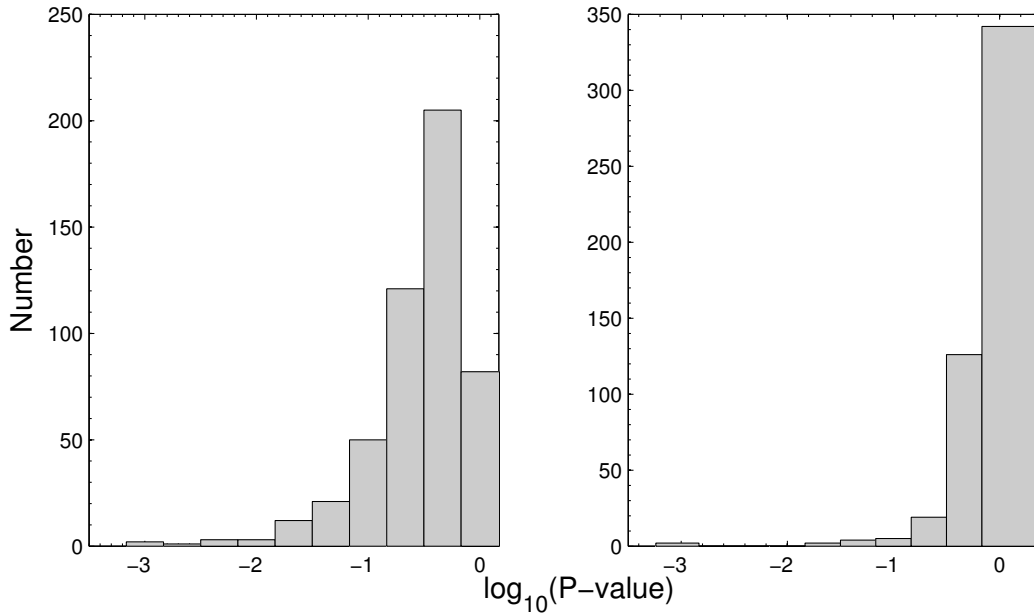
Figure 5.6: P-values from the hypothesis test: log-rank (left), Gehan (right)

accretion rates which are likely dominated by accretion rates calculated from flaring X-ray values. Furthermore the simple viscous model is likely to break down at early times due to variability.

The X-ray luminosity data then shows, in summary, that the observed $\dot{M}$-M_* relation in pre-main-sequence stars is consistent with being a simple consequence of disc dispersal by X-ray photoevaporation.

5.4   Summary

We have presented a statistical analysis of accretion rates of pre-main sequence stars as a function of stellar mass in order to establish whether the steep relation between accretion rates and mass may be a consequence of selection or detection thresholds, as feared in past (e.g. Clarke & Pringle, 2006; Tilling et al 2008). With the large amount of data available we show (using survival statistics) that selections/detection biases are *not* driving the $\dot{M} - M_*$ relation.

We find the slope of the power law relation to be between ∼1.6 and 1.9 for stars with masses lower that 1 $M_\odot$. Such slopes are similar to the slopes observed in the X-ray luminosity function of young stars in near-by clusters (e.g. Preibisch et al, 2005; Güdel et al 2007). We show that X-ray photoevaporation predicts indeed that the observed $\dot{M} - M_*$ relation should be completely determined by the X-ray luminosity of the stars, which thus imprints a signature on the observed accretion rates distribution in a given cluster.

Furthermore we demonstrate that a synthetic $\dot{M} - M_*$ dataset constructed from the X-ray luminosity function of young stars in the Orion Nebular Cluster (Preibisch et al. 2005) is statistically indistinguishable from the observed $\dot{M} - M_*$ dataset, hence lending further support that discs around young stars disperse predominantly by X-ray photoevaporation.

Chapter 6

The evolution of transition discs

6.1   Introduction

Disc dispersal is a crucial problem in understanding planetary formation. In particular, the time for the survival of gas in protoplanetary discs sets important constraints on the time available for the formation of gas giants. This is particularly relevant for what concerns the core accretion scenario, for which the timescale of giant planet formation (Pollack et al., 1996) is predicted to be of the same order of the lifetime of discs.

Discs have a typical lifetime of a few Myrs (Haisch et al., 2001; Mamajek, 2009; Fedele et al., 2010a; Ribas et al., 2014). For most of their time, the redistribution of angular momentum operated by viscosity dominates their evolution and a simple analytical relation (Lynden-Bell & Pringle, 1974) can be used to describe the observed decline of the mass accretion rate with the age of the system (e.g. Hartmann et al. 1998). The exact nature of this viscosity is still matter of debate, although the magnetic rotational instability is the most ideal candidate (Turner et al., 2014). Observations of star forming regions also reveal a particular class of discs, called "transition discs" (Strom et al., 1989a; Skrutskie et al., 1990a; Espaillat et al., 2014). These discs show a dip in the spectral energy distribution (SED) at near-infrared (NIR) wavelengths, which is usually interpreted as a deficit of warm dust in their innermost regions (i.e., a few AUs) (Calvet et al., 2005a; Currie & Kenyon, 2009; Muzerolle et al., 2010; Lada et al., 2006; Cieza et al., 2010; Espaillat et al., 2010a). This is not expected in the viscous evolution framework, and it shows that, while viscosity is certainly a main ingredient of disc evolution, another process must also be at play. Observations currently show that approximately 10 percent of all observed discs are in this "transition" phase. If all discs go through the transition disc phase, this implies that this phase must be short-lived (of order of 10^5 years), implying that disc evolution observes a "two-time scale behaviour". Transition discs have also been imaged by sub-mm interferometers (Piétu et al., 2006; Brown et al., 2009; Andrews et al., 2011; Isella et al., 2012), confirming the presence of huge (tens of AU) cavities in the mm-dust.

Photoevaporation (Hollenbach et al., 1994; Font et al., 2004; Alexander et al., 2006a) is an ideal candidate as another process, together with viscosity, regulating disc evolution.

Clarke et al. (2001a) showed that when the mass accretion rate becomes comparable with the mass loss by photoevaporation, the outer disc can no longer resupply the inner disc fast enough, and a gap opens at around a few AUs, rapidly shutting down accretion (the so-called UV switch) and naturally producing a transition disc. The outer disc left is quickly eroded from the inside out by photoevaporation, which agrees with observational findings (Ercolano et al., 2011b; Koepferl et al., 2013b). However, these models predict that discs with large holes should not be accreting, since by the time photo-evaporation has managed to open a big hole, the mass accretion rate onto the star has become negligible. This is in contrast with observations. Indeed, the fact that some transition discs accrete at very high rates is a challenge for all the models that have been proposed so far. Recent observational work has remeasured accurately the accretion rates of a sample of highly accreting transition discs (Manara et al., 2014), confirming their values and finding that, from the point of view of accretion, these discs show the same properties of normal discs.

In recent years, photo-evaporation rates have been revised upwards due to the previous neglect of important energy sources (Ercolano et al., 2008; Gorti & Hollenbach, 2009a; Owen et al., 2010a). It has also been recognised that, after hole opening, when the disc is directly exposed to the X-ray radiation from the star, a "thermal sweeping" instability can develop, that rapidly destroys the leftovers of the disc (Owen et al., 2012a, 2013). This has helped explaining why non-accreting transition discs with large holes are not observed, as they are destroyed before reaching this state. The revised rates provide a way of explaining the observed correlation between mass accretion rates and star masses (Ercolano et al., 2014), confirming that photoevaporation is a fundamental ingredient of disc evolution. Roughly 50% of transition discs can be explained by photoevaporation (Owen et al., 2011b, 2013), but despite all efforts there is still a class of objects that remains in a region of the parameter space that cannot be explained by any photoevaporation model.

This has led to the hypothesis that transition discs might actually consist of two different families (Owen & Clarke, 2012a), created by different physical processes. Photoevaporation can explain the class of low accretors, that also happen to have a lower mm flux, while another process would be needed to explain the other ones. Note that in this picture discs belonging to this second class need not necessarily represent the final phases of proto-planetary disc evolution and they do not need to be necessarily short-lived; it is perfectly plausible that only some of the discs are subject to this phase. The theoretical difficulty in explaining them resides in having to simultaneously explain objects with large holes, almost perfectly clear in the mm resolved images, which sustain a very high mass accretion rate, meaning that they contain high quantities of gas (although see Rosenfeld et al. 2014 for an alternative explanation).

Grain growth has been proposed as a possible explanation. In this picture, the lack of the near IR excess is not interpreted as the presence of a physical hole in the disc, but rather as a lack of opacity (Dullemond & Dominik, 2005a). If grains grow efficiently enough to became mm sized or more, they effectively become invisible in the IR. While models of grain growth can indeed explain transition discs SEDs, it is difficult to reconcile their findings with the sub-mm interferometric images (Birnstiel et al., 2012a). The images show quite sharp holes, which are not expected by this scenario.

An alternative scenario that has much success at the moment in the community is the presence of a planet in the disc. If this were true, large hole, highly accreting transition discs would represent indirect evidence for the youngest planets ever found. The main idea, first envisaged by Paardekooper & Mellema (2006) and Rice et al. (2006), is that a planet, if massive enough to open a gap in the disc, produces a pressure maximum outside its orbital radius. The dust grains with a stokes number ~ 1, which for normal parameters correspond to $\sim 1mm$, are trapped at this radius by the gas drag forces. Recent observations support this idea; for example van der Marel et al. (2013) recently imaged a dust trap in Iras 48 with ALMA. Images in the polarized light of transition discs (Garufi et al., 2013; Avenhaus et al., 2014) show much sub-structure in some of these transition discs, which can be speculatively connected with the presence of a planet. While this basic idea seems very effective, it is not without problems. Specifically, this argument ignores what happens to the small dust. Being strongly coupled to the gas, small grains will always manage to flow through the gap and replenish the inner disc. For example Zhu et al. (2012) needed to invoke grain growth in the inner disc to remove these small grains which produce too much (unobserved) emission in the MIR. Indeed, Pinilla et al. (2012c) and de Juan Ovelar et al. (2013) presented models including also the effect of grain coagulation, that in some cases can successfully clear the inner disc of the small dust. Recently, another scenario was proposed by Owen (2014), who investigated the effect of radiation pressure from the accretion luminosity on the planet on the dust grains. They find that, provided there is gas accretion onto the planet, the radiation pressure acts to keep the small dust outside of the gap. The process depends sensitively on the mass of the planet; if this is too small, this effect is not strong enough, and the small dust will flow in the gap. This is consistent with several existing observations, which show a hole at mm wavelength, but have the SED of a primordial disc (Andrews et al., 2011).

The goal of this study is to investigate what is the type of evolution leading to the creation of this class of transition discs. While considerable theoretical effort has been invested in understanding what process may be responsible for the creation of a transition disc, relatively little has been done to understand their time evolution (but see for example Alexander & Armitage 2009b, although the holes there are much smaller, and Clarke & Owen 2013). In this work we will just assume that a planet is a sufficient condition to produce a transition disc, and we explore what happens when such a system is allowed to evolve. As viscous evolution and photo-evaporation are thought to be the main drivers of disc evolution, these are the ingredients that we consider to follow the evolution in time of the disc. Specifically, we want to address the issue that very few (if any) transition discs with low mass accretion rates and large holes are observed. Naively, one would expect to see the mass accretion rate of these discs going down with time as they age. If this decay happens in a power-law fashion, as it is the case for viscously evolving discs non in transition, then we should see more and more discs at low rates, contrary to the observations.

Thermal sweeping, which is included in pur modelling, may provide a reason for this discrepancy. This is an instability proposed by Owen et al. (2012a), potentially triggered when the outer disc of a transition disc is directly exposed to the X-ray radiation from

the star. Owen et al. (2012a) found that when the width of the layer directly heated by the X-ray radiation is comparable with its vertical scale-height an instability is triggered, that rapidly destroys the disc on an orbital timescale (10^4 yr). The purpose of this work is therefore to investigate whether this mechanism is effective enough in destroying the leftovers of transition discs. In a previous paper (Rosotti et al., 2013) we investigated what happens to the inner disc, finding that the presence of a planet can trigger its dispersal at times significant earlier than what would have happened otherwise. After the dispersal of the inner disc, the outer disc is directly exposed to the X-ray radiation, and can be prone to the thermal sweeping instability. As this phase is short lived, it is then unlikely to observe it, and we would expect to observe only transition discs that are accreting at higher rates. The goal of this study is to quantify how effective this process may be.

This chapter is structured as follows. In section 6.2 we explain our numerical procedure. In section 6.3 we presents our results, and finally we present our conclusions in section 6.4.

6.2   Numerical model

We refer the reader to Rosotti et al. (2013), where the details of our model are reported. We summarise in what follows the most important points, and describe the addition of thermal sweeping.

Our model consists of a proto-planetary disc undergoing viscous evolution and X-ray photoevaporation. We follow the evolution in time of the disc using the publicly available hydrodynamical code FARGO (Masset, 2000b), which we modified to include the effect of mass removal by photoevaporation. At a time t_{creation} we assume that a planet forms in the disc with an initial mass of $M_p = 0.7 M_j$. Similar to many other works found in the literature, we do not model the formation of the planet itself. Computational time is saved by modelling the evolution of the disc until the moment of planet insertion in 1d, since the disc is azimuthally symmetric up to that point. We assume that the planet accretes material from the surrounding circumplanetary disc, as prescribed by Kley (1999). We use the publicly available implementation in FARGO, controlled by a free parameter, f, that represents the inverse of the accretion timescale in dynamical units. We set $f = 1$ in all of our models.

We assume a fixed profile for viscosity and temperature. The sound speed is a fixed function of radius, and is chosen to give a mildly-flaring disc (i.e., $H/R \propto R^{\mathbf{1/4}}$); the normalization is chosen so that at 1 AU the aspect ratio $H/R = 0.0333$. We evaluate the viscosity using the well-known relation $\nu = \alpha c_s H$ (Shakura & Sunyaev, 1973a). We set $\alpha = 1.5 \times 10^{-3}$. All the discs have the same initial conditions, that are taken from Owen et al. (2011b), who showed that the scatter in the X-ray luminosity alone can account for the scatter in the properties of observed discs. The surface density is assumed to be a self-similar solution:

$$\Sigma(R, 0) = \frac{M_{\mathrm{d}}(0)}{2\pi R R_1} \exp(-R/R_1), \tag{6.1}$$

where $M_{\mathrm{d}}(0)$ is the initial mass of the disc and R_1 a scale radius describing the exponential

taper of the disc's outer region. We set a value of $R_1 = 18$ AU and an initial disc mass of 10% the mass of the star, which is fixed to be $0.7 M_*$.

The details of the photoevaporation profile assumed can be found in the appendix of Owen et al. (2012a). In our simulations we do not allow the planet to migrate,as Rosotti et al. (2013) found migration to have little impact. It should be noted that the extension done here to a considerably wider parameter space could change this conclusion, although verifying this is outside the scope of this thesis.

6.2.1 Thermal sweeping

Owen et al. (2012a) discovered in 2d hydrodynamical simulations of photoevaporating discs an instability that can rapidly destroy the disc. In particular, the instability is triggered when the width of the X-ray heated layer becomes comparable with the vertical scale height of the layer. If this condition is satisfied, a slight readjustment in the vertical direction causes the X-rays to penetrate slightly more, heating a wider layer. This causes a runaway effect that was found to effectively destroy the disc. By means of 1.5d hydrodynamical simulations and analytical arguments, Owen et al. (2013) found a relation for the surface density threshold at the inner edge of the disc that describes if the disc is prone to the thermal sweeping instability. If the surface density is below the threshold, the instability will be triggered; conversely, the disc is safe. Their result is that thermal sweeping sets in at a surface density of

$$
\begin{aligned}
\Sigma_{TS} = \quad & 0.14 \, \text{g cm}^{-2} \left(\frac{L_X}{10^{30} \, \text{erg s}^{-1}} \right) \left(\frac{T_{1\text{AU}}}{100 \, \text{K}} \right)^{-1/2} \\
& \times \left(\frac{M_*}{0.7 \, \text{M}_\odot} \right)^{-1/2} \left(\frac{R_{\text{hole}}}{10 \, \text{AU}} \right)^{-1/4} \\
& \times \exp \left[\left(\frac{R_{\text{hole}}}{10 \, \text{AU}} \right)^{1/2} \left(\frac{T_{1\text{AU}}}{100 \, \text{K}} \right)^{-1/2} \right]
\end{aligned}
\tag{6.2}
$$

where L_X is the X-ray luminosity of the star, $T_{1\text{AU}}$ is the temperature at $1AU$ and R_{hole} is the size of the hole. We use equation (6.2) to determine if the outer disc of our simulations is stable or not. At each snapshot, we monitor if the inner disc is still present or if it has already dispersed. We experimented with using a criterion based on the total column of material in the midplane, ensuring that it is less than $10^{22} cm^{-2}$, which is the penetration depth of ~ 1 keV X-rays, and checking that the mass in the inner disc is a factor of a few (we tipically use 5) above the value it had if the disc had the floor surface density everywhere. Apart for some corner cases where manual intervention was required, we find the two criteria to yield little difference in practice. When the inner disc is no longer present, we inspect the maximum of the azimuthally averaged surface density outside the planet orbital radius. If this is smaller than the threshold at that radius, then we assume that the disc is going to be rapidly destroyed by thermal sweeping and we stop the simulation.
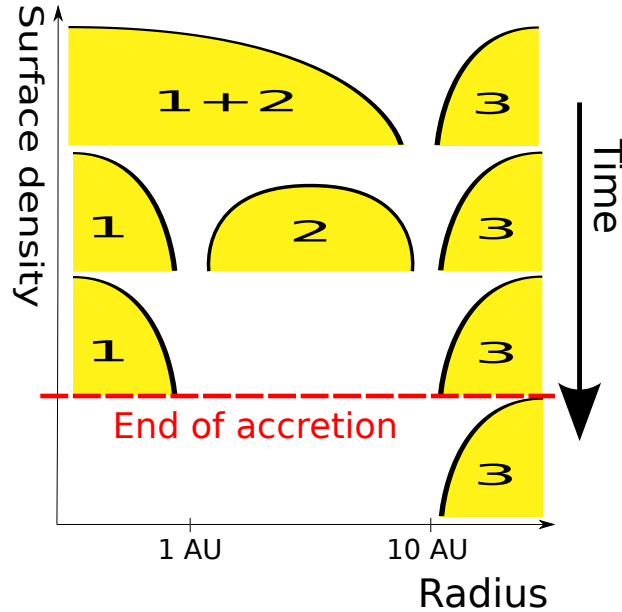
Figure 6.1: Classification scheme used to separate the lifetime of a transition disc in different phases.

6.2.2   Parameters varied

We let the disc mass (which corresponds to the age of the disc at the moment of planet creation), the X-ray luminosity and the planet location vary. Unfortunately we cannot perform a true population synthesis model, as not all the distributions of the parameters are known. In particular, neither the formation time of planets is known, neither the distribution of planet orbital radii. Recent surveys (Chauvin et al., 2014; Brandt et al., 2014) are starting to put constraints on the fraction and distribution of planets in wide orbits. However, it is difficult to relate the properties of these planets around main sequence stars to the putative ones present in transition discs, as significant migration might have happened (Clarke & Owen, 2013). Rather, the purpose of this investigation is to get an handle on the possible outcomes in different regions of the parameter space.

We explore values of $4 \times 10^{29}, 10^{30}, 4 \times 10^{30}$ $ergs^{-1}$ for the X-ray luminosity, which are roughly the median and the values found at $\pm 2\sigma$ (that is, at values of the cumulative distribution function of 16 and 84 %) of the Taurus X-ray luminosity function (Güdel et al., 2007). These values bracket most of the possible outcomes, depending on the level of X-ray luminosity. We experiment with planet locations of 20 and 40 AU. For what concerns the mass, we used values of $15, 30, 45, 60$ M_{jup}.

6.3 Results

6.3.1 Classification scheme for comparison with observations

As already stated, we assume that the presence of a planet is a sufficient condition to produce a transition disc and we do not include any modelling of the dust component in our simulations. Therefore, we cannot directly relate the outcomes of our simulations to continuum images or SEDs. Rather, the observational proxies that we would like to compare with are the following:

- the presence of cold gas in the cavity of transition discs;

- the presence of a detectable mass accretion rate.

While some unsuccessful attempt to detect cold gas in the cavity was done with the previous generation of interferometers (Dutrey et al., 2008; Lyo et al., 2011), ALMA has now the sensitivity and the spatial resolution necessary to accomplish this goal (Rosenfeld et al., 2012; Bruderer et al., 2014; Casassus et al., 2013; Zhang et al., 2014). As measurements of this kind are becoming routinely available, we believe that is of primary importance for models of transition discs to come up with predictions for the gas content. This quantity is much "cleaner" from the hydrodynamical side, in contrast to the dust that can be observed in the continuum. The dust has a much more complicated dynamics, as it interacts differently with the gas depending on its size. In addition, dust grains have a distributions of sizes, and processes of coagulation and fragmentation happening in the disc introduce other uncertainties and make difficult the predictions for the dust distribution. In fairness, observations of the gas are also not straightforward, as H_2, the most abundant molecule, is essentially invisible. Nevertheless, observations of other molecules (particularly CO) and modelling of their chemistry has now advanced to a point where it is possible to compute the expected emission in the gas lines from a given gas surface density. It is straightforward to know in our models if CO emission would be observed from a cavity of a transition disc, as the region sampled by ALMA is in our computational grid. Bruderer (2013) showed that ALMA has the sensitivity to detect through observations of the CO 3-2 transition in Band 7 up to a few Earth masses of gas in the cavity. Measuring how much mass is present involves more complicated modelling using different isotopologues of the molecule. For the sake of simplicity, we restrict ourselves here to explore only if there is going to be a detection, rather than focussing on the strength of the expected emission. Note that we are more concerned with the detection of the rotational transitions of the CO molecule rather than the observations of the fundamental rovibrational transition at $4.7\mu m$. The reason is that this transition does not trace the bulk of the gas mass inside the cavity, but rather the warm gas (roughly between 100 and 1000 K) up to distances of several AUs.

Unfortunately, the mass accretion rate is not so straightforward to get from our simulations. Here we must use an assumption, as the inner boundary of our grid is much bigger than the true inner boundary of the disc, the radius at which the disc is truncated by the star magnetic field. We assume that for the first part of the evolution the inner disc just

readjusts its structure in order to supply the star with the same mass accretion rate that we have at the inner boundary of our grid. This assumption is justified by the fact that the viscous time in the inner region that we do not simulate is smaller than the one in the region that we simulate. When photo-evaporation mass-loss rates are coupled with viscous evolution (Clarke et al., 2001a; Ruden, 2004), it is found that when the mass accretion rate goes below the photoevaporation rate, a gap opens in the disc, at a radius around $1AU$. We assume that the clearing of this inner region (that is, disc 1 in figure 6.1) is independent of what happens in the outer region of the disc. We thus use 1d models of the whole disc to complement our 2d simulations. We monitor the mass accretion rate at which a gap opens in the disc in our 1d models, and we assume that the same happens in the disc we do not resolve when the mass accretion rate at the inner boundary of the grid reaches this threshold. Subsequently, we take the evolution in time of the mass accretion rate of the 1d model as the mass accretion rate onto the star. Note that this is not the same as what was done by Rosotti et al. (2013), who matched the 1d and 2d models monitoring the radius of the inner hole in the 2d grid. However, this assumes that the disc resolved in the 2d simulations always clears from inside out. We decided to switch to this criterion because in some of our simulations, which cover a larger region of the parameter space than what was done by Rosotti et al. (2013), the central disc clears from the outside in, and therefore the criterion used by Rosotti et al. (2013) would trigger the opening of a photoevaporation gap at slightly later times.

The qualitative behaviour that we have described can be summarised in 4 phases, which are shown in figure 6.1. Initially, only the dynamical gap created by the planet is present (phase A), and the disc is otherwise continuous. As the disc ages and mass accretes onto the star, the mass accretion rate will decrease up to the point where photoevaporation is able to open a gap in the innermost region of the disc. We note that, as Rosotti et al. (2013) reported, this will happen at earlier times than if the planet was not present, as the planet partially cuts out the inner from the outer disc, where most of the mass is. Thus, we assume that the disc will have two gaps (phase B), dividing the disc in three regions. Disc 2 is cleared on a relatively short phase (tipically less than 10^5 years) by photoevaporation, leaving only disc 1 and 3 (phase C). This disc will not show emission in the CO rotational lines, which trace the bulk of the cold mass, but will still have a measurable accretion onto the star due to the presence of disc A. Finally, disc 1 can not last longer than 10^5 years (its viscous time scale), and in the last phase (phase D) only the outer disc will be present. Observationally, this is a non-accreting transition disc without gas in the cavity. Non accreting transition discs are rarely seen in observations, and the main goal of this paper is exactly to quantify how long lived is this phase before the set in of thermal sweeping.

As in every classification scheme, we do not expect it to hold necessarily for all discs; rather, we are interested that it catches the majority of the behaviour. We inspected visually the results of our simulations and confirm that this is the case. Differences are found in the way disc 2 clears, which happens sometimes from inside in and sometimes from inside out. Since, as said before, the clearing of this disc is quite fast, this different behaviour is unlikely to have an observational impact.

In 2 simulations out of the 24 we have run, disc 2 is eroded briefly from inside out, but then the erosion by photoevaporation reaches an equilibrium with the material filtering through the gap. In one case, the disc 2 is very long lived (almost $1Myr$), creating a transition disc without accretion (as disc 1 cannot be so long lived, being cut out from the mass resupply) but with cold gas in the cavity (although the mass is very small: just a few Earth masses, at the limit of detectability with ALMA). We remove this disc from what follows, as it might falsify the results.

6.3.2   Lifetimes

Simulation	accretion	non accretion	phase A	phase B	phase C	phase D
1.1e+30X_45Mj_20.0AU	2.03	7.58	1.73	0.20	0.90	6.78
1.1e+30X_45Mj_40.0AU	3.65	0.80	3.36	0.23	0.87	0.00
1.1e+30X_60Mj_20.0AU	2.33	0.80	2.03	0.08	1.02	0.00
1.1e+30X_60Mj_40.0AU	4.18	0.80	3.89	0.22	0.87	0.00
1.1e+30X_30Mj_20.0AU	1.88	8.83	1.58	0.24	0.86	8.02
1.1e+30X_30Mj_40.0AU	3.26	0.80	2.97	0.24	0.86	0.00
1.1e+30X_15Mj_20.0AU	1.22	5.18	0.93	0.33	0.77	4.38
1.1e+30X_15Mj_40.0AU	2.38	0.80	2.07	0.42	0.68	0.00
4e+29X_60Mj_40.0AU	5.26	0.87	5.25	0.36	0.52	0.00
4e+29X_30Mj_20.0AU	12.70	17.30	15.69	8.57	-7.68	13.42
4e+29X_30Mj_40.0AU	4.25	5.35	4.24	0.34	0.54	4.48
4e+29X_15Mj_20.0AU	1.32	15.85	1.33	1.38	-0.49	14.96
4e+29X_15Mj_40.0AU	2.95	2.14	2.94	0.75	0.13	1.28
4e+29X_45Mj_20.0AU	19.99	10.01	25.49	0.63	0.25	3.63
4e+29X_45Mj_40.0AU	5.28	0.88	5.28	0.34	0.54	0.00
4e+30X_15Mj_20.0AU	1.29	0.63	0.57	0.19	1.17	0.00
4e+30X_15Mj_40.0AU	1.86	0.63	1.13	0.35	1.01	0.00
4e+30X_60Mj_20.0AU	2.14	0.63	1.42	0.09	1.26	0.00
4e+30X_60Mj_40.0AU	3.31	0.63	2.59	0.24	1.11	0.00
4e+30X_45Mj_20.0AU	2.05	0.63	1.33	0.10	1.25	0.00
4e+30X_45Mj_40.0AU	3.12	0.63	2.39	0.24	1.11	0.00
4e+30X_30Mj_20.0AU	1.79	0.63	1.06	0.09	1.26	0.00
4e+30X_30Mj_40.0AU	2.71	0.63	1.98	0.26	1.09	0.00

Table 6.1: Lifetimes of discs in our simulations in units of 10^5 years. The name of the simulation si given by the X-ray luminosity, the initial mass of the disc and the location of the planet. A negative phase C means that disc 1 clears before disc 2. In this case, the absolute value of phase C is the time of the phase where the disc is non accreting, but still has cold gas in the cavity (although the mass of this disc is only a few Earth masses).
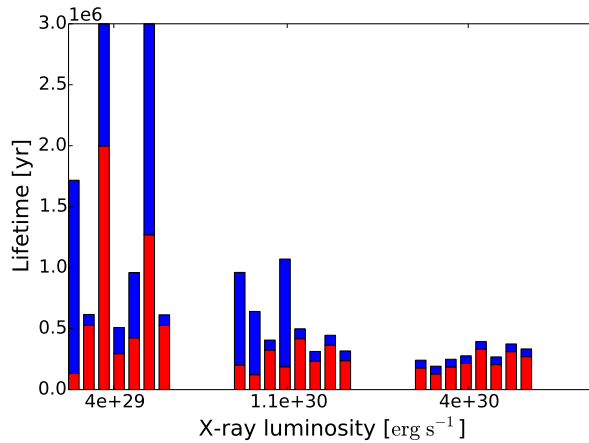
Figure 6.2: Total lifetime of each simulation, decomposed in accreting and non accreting phase.

The main result that we extract from each simulation consists in the length of each phase that was introduced in section 6.3.1. Results for all the simulations, except for the oddity we mentioned in the previous section, are presented in table 6.1.

In figure 6.2 we show a bar chart that decompose the life of each disc in the accreting and non accreting phase. The discs are grouped together based on their X-ray luminosity. The figure clearly shows the importance of X-ray luminosity on the total lifetime of the discs. The lifetime of the disc can range from a few 10^5 to several Myrs, and there is a significant trend for higher X-ray luminosities to yield shorter lifetimes. The average values are respectively 1.5 Myrs, $5 \times 10^5 yr$ and $2 \times 10^5 yr$, from lowest to highest X-ray luminosity. This result is expected, since the photo-evaporation rates are higher for higher X-ray luminosities.

When looking at the relative length of the accreting and non accreting phases, it can be seen that some discs almost never go through the non accreting phase. As soon as their outer disc is directly exposed to the X-ray radiation from the star, it is prone to the thermal sweeping instability. This depends very sensitively from the X-ray luminosity; we note that indeed all the discs we run at high X-ray luminosity go through this behaviour, as well as some of the ones at the median luminosity. In contrast, all the discs at low X-ray luminosity experienced a significant non accreting phase before being dispersed. This has important consequences on the expected population of transition discs found by observations. We can take, inside each X-ray luminosity bin, the fraction of discs that would be expected to be accreting. This is done by computing

$$f_{\mathrm{acc}} = \frac{\sum t_{\mathrm{acc}}}{\sum t_{\mathrm{total}}}, \tag{6.3}$$

that is, the mean duration of accretion divided by the mean lifetime. This calculation assumes that, save for the X-ray luminosity, the other two parameters have a uniform distribution. Although this is probably not true, their true distribution is not known; the purpose of the calculation is to get a handle on the result, and not to get an accurate
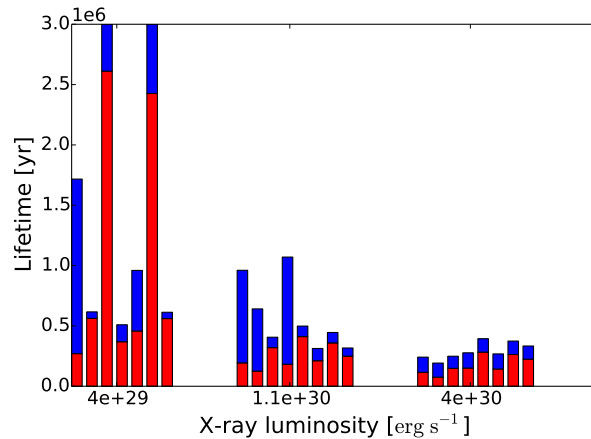
Figure 6.3: Total lifetime of each simulation, decomposed in phase with and without cold gas in the cavity.

statistical prediction. The fraction of accretors is found to be roughly 50 percent for the low and median X-ray luminosity case, and nearly 80 percent for the high X-ray luminosity case. It is interesting that in the high X-ray luminosity case the fraction of accretors is quite high. Since only a handful of transition discs with large holes have been observed up to now (roughly 20 in the compilations of Owen & Clarke 2012a and Manara et al. 2014), such a high fraction would explain why only few non accreting discs (for example, 2 in the compilation of Manara et al. 2014) have been observed. However, already in the median X-ray luminosity case the fraction goes down to one half, which is not compatible with observations.

Figure 6.3 shows again the lifetime of each simulations, but this time decomposed in the two phases with and without cold gas in the cavity. There is little difference with the accretion for the median X-ray luminosity case; the fraction of discs expected to have cold gas in this case is 45 percent, which should be compared with the 50 percent of discs expected to be accreting. As explained in section 6.3.1, the cold gas in the cavity and the presence of accretion have almost the same lifetime; a little difference is due only to phase C, where the disc is still accreting but disc 2 has been already dispersed. However, phase C is short enough that in practice this causes little difference, and it would be unlikely to observe such a disc. More interesting is the case of high X-ray luminosity; here the fraction of discs with cold gas in the cavity is 60 percent. This is due to the fact that all the other phases are faster with a high X-ray luminosity, so that the relative importance of phase C increases and the difference is bigger. Although still unlikely given the number of observed transition discs, this predicts that one could in principle observe a disc that is still accreting but no longer has cold gas in the cavity. Future observations with ALMA will be able to tell if such discs exist. Finally, also the low X-ray luminosity case is interesting. Here, the fraction of discs with cold gas rises to almost 70 percent, which is puzzling to explain in the framework we presented up to now. The reason is that in this case there is a long phase where the disc is technically accreting, but the accretion rate is under the

current observational limits (we used 10^{-11} $M_\odot$ yr^{-1} as threshold), whereas ALMA will have the capability of detecting cold gas in the cavity down to very low masses. As in the previous case, future observations will be able to tell if such discs exist.

6.4 Conclusions

In this chapter we investigated, by including the effect of thermal sweeping, the lifetime of the outer disc that is left after the inner disc has been cleared by the combined effect of photo-evaporation and the formation of a giant planet. We find that, provided the X-ray luminosity is high enough, this outer disc is very short lived. This could explain why very few non accreting transition discs with large holes have been observed; since this phase is extremely short, it is unlikely to be observed. However, already for the median X-ray luminosity case the mechanism stops to be so effective, yielding a fraction of accreting transition discs of roughly one half. Although this shows that this is an interesting avenue to be explored further, it is unclear if this mechanism is effective enough to reconcile the theoretical predictions with observations. Inclusion of other energy sources, such as the FUV that is important at large separations from the star, might enhance the efficiency of thermal sweeping and produce a higher fraction of accretors.

Chapter 7

Conclusions

The main topic of this thesis is protoplanetary disc evolution and dispersal. In the current paradigm for planet formation, protoplanetary discs are the natal environment of planets, allowing dust to grow from a few nanometers (as it is found in the interstellar medium) up to kilometers in size, finally becoming self-gravitating and (possibly) attracting a gas atmosphere. The timescale for planet formation is set by the disc lifetime, implying that disc dispersal should play an important role in establishing the properties of a newly formed planetary system. Although we are still far to understand all the possible implications, this simple fact motivates the study of disc dispersal.

There are several processes that can drive disc evolution, which are discussed in the introductory chapter. In summary, the two most important drivers of disc evolution are viscous accretion and photo-evaporation. Under the effect of the former, a disc steadily looses mass which is accreted onto the star, while it spreads in order to conserve angular momentum, which is redistributed through the disc by an effective viscosity. The origin of this viscosity is still debated, although the magneto rotational instability (MRI) is currently the best candidate. For most of the evolution of a disc, photo-evaporation is almost negligible, as the rate of mass-loss is much smaller than the rate of mass accretion. Eventually, however, the mass accretion rate decreases to low enough values such that the two rates become comparable; at this point, photo-evaporation takes over and quickly ($\sim 10^5$ years) clears the disc. The disc clears from inside out, producing a disc with an inner cavity. This explains naturally the many observations of discs with holes, the so-called "transition discs". In this framework, transition discs are interpreted as discs caught in the act of clearing. Since the clearing is quick, this produces a "two-timescale" evolutionary behaviour (that is, the transition disc phase is short-lived compared to the full disc one), which explains why transition discs are only a small fraction (~ 10 percent) of the total disc population.

However, this picture is challenged by observations that find transition discs with large holes (several tens of AU) accreting at high rates. According to photo-evaporation models, this should not be possible; by the time the hole has grown to the sizes observed, accretion onto the star should have stopped. A solution to this problem has been proposed by considering giant planet formation within a disc. A planet influences the dust dynamics

creating a pressure maximum in the disc, which traps the dust outside its orbit, thus creating a hole in the dust. Observations are more sensitive to the dust rather than to the gas component of a disc, hence it is possible that large quantities of gas are present inside a transition disc cavity and remain undetected. This would explain simultaneously the high accretion rates and the large holes observed (provided planets may exist at such large separations from the star).

While the dust trap mechanism works very effectively on mm-sized dust, explaining what happens to the small dust is more complicated. Being strongly coupled to the gas, small grains will always manage to flow through the gap and replenish the inner disc. Inclusion of grain coagulation, or radiation pressure due to the accretion onto the planet, may help in explaining why also the small dust is not observed in a transition disc cavity. It should be noted however that just invoking the presence of a giant planet ignores what is the possible time evolution of a transition discs. The works in the literature have just focussed in producing a disc that *at a given time* looks in transition. In addition, up to now the interplay between photo-evaporation and the presence of a giant planet in a disc has not been considered. There is ample evidence that photo-evaporation is one of the main agents driving disc evolution, and therefore it is essential to consider this interplay. The work presented in this thesis aims to fill this gap. We run hydrodynamical simulations of a proto-planetary disc undergoing X-ray photo-evaporation with a giant planet embedded. We find that there is a deep mutual influence between photo-evaporation and the presence of a giant planet. The planet divides the disc in two separate regions, the inner and the outer disc. The planet tends to reduce the mass accretion flow from the outer to the inner disc, cutting out in this way the inner disc from the bigger mass reservoir of the outer disc. The effect is that the inner disc is cleared by photo-evaporation at much earlier times than what would be possible without the planet. This constitutes a possible route for the formation of the observed class of accreting transition discs with large holes. The process can quickly shut down accretion onto the star, so that we expect only few discs to be moderately accreting. The transition is however not fast enough to reconcile theoretical predictions with observations. Inclusion in the model of the so-called "thermal sweeping", a violent instability that can destroy completely the disc in as little as 10^4 years, allows to study the survival of the outer disc after the dispersal of the inner one. We find that, provided the X-ray luminosity of the star is high enough, the outer disc can be completely destroyed as soon as the inner disc is dispersed. This would explain why transition discs are always observed to be accreting: the non accreting phase is too short to be observed. However, since for low X-ray luminosities the mechanism is not effective enough, we would still expect a big fraction of non accreting transition discs (up to one half), which are not observed. A full answer requires a statistical study that is outside the scope of this thesis, neverthless we conclude that this an interesting route that needs to be explored.

In this thesis we present also another piece of independent evidence that X-ray photo-evaporation is the main driver, combined with viscous accretion, of disc evolution. It has been known observationally for almost a decade that the mass accretion rate of young stellar objects correlates with roughly the square of the mass of the star. Because of the power-law decay with time of the mass accretion rate due to viscous evolution, we show

that in the X-ray photo-evaporation framework one is more likely to observe a disc when its accretion rate is comparable to the mass loss rate. In turn, this depends on the X-ray luminosity of the star, which correlates with the stellar mass. Therefore, a correlation between the mass accretion rate and the mass is expected. We show that this statement can also be brought forward quantitatively and that we are able to reproduce the observed slope of the correlation of $1.6 - 1.9$.

Despite not being the main driver of disc evolution for the majority of objects, a close encounter with a nearby star can have a significant impact on a proto-planetary disc. In this thesis we develop a model that for the first time follows the dynamics of a young stellar cluster together with the evolution of the proto-planetary discs. Previous studies were restricted to infer a posteriori the effect of encounters on the putative discs around the stars. Our findings are that, in line with previous studies, an encounter can have a significant impact on a disc, removing a significant portion of its mass. However, only few discs in a cluster undergo such destructive events, so that statistically star encounters are not a significant driver of disc evolution. We also find that the effect of encounters is more important on the disc size than on its mass. Provided that the ambient stellar density is high enough, the encounters strip the outer portions of the disc, limiting the maximum disc size. Although this is still pioneeristic, there is a good agreement between the stellar densities at which this effect starts to be relevant and what is found in observations.

Finally, in this thesis we investigate if it is possible to reform discs after their dispersal. This would have very important consequences on planet formation, as it would give a system a second chance to form planets. We study what happens to stars that, after having dispersed their natal discs, happen to be in a region that is currently forming stars. If the star passes through a region of high density, it can accrete material from it, possibly reforming a disc. Quantitatively, we expect up to a few percent of stars in each star forming region that are able to reform a disc, despite being significantly older than a common young stellar object. This is a possible explanation of observations of so called "old accretors", that find some stars still accreting (evidence for the presence of a disc) in massive star forming regions (where the number of stars is high enough to have sufficient statistics) despite being several tens of $Myrs$ old.

Bibliography

Aarseth S. J., Henon M., Wielen R., 1974, A&A, 37, 183

Adamo A., Östlin G., Zackrisson E., 2011, MNRAS, 417, 1904

Adams F. C., 2010a, ARA&A, 48, 47

Adams F. C., 2010b, ARA&A, 48, 47

Adams F. C., Hollenbach D., Laughlin G., Gorti U., 2004a, ApJ, 611, 360

Adams F. C., Hollenbach D., Laughlin G., Gorti U., 2004b, ApJ, 611, 360

Alexander R., 2008, New A Rev., 52, 60

Alexander R. D., Armitage P. J., 2007, MNRAS, 375, 500

Alexander R. D., Armitage P. J., 2009a, ApJ, 704, 989

Alexander R. D., Armitage P. J., 2009b, ApJ, 704, 989

Alexander R. D., Pascucci I., 2012, MNRAS, 422, L82

Alexander R. D., Clarke C. J., Pringle J. E., 2006a, MNRAS, 369, 216

Alexander R. D., Clarke C. J., Pringle J. E., 2006b, MNRAS, 369, 216

Alexander R. D., Clarke C. J., Pringle J. E., 2006c, MNRAS, 369, 229

Andrews S. M., Williams J. P., 2005, ApJ, 631, 1134

Andrews S. M., Wilner D. J., Hughes A. M., Qi C., Dullemond C. P., 2010, ApJ, 723, 1241

Andrews S. M., Wilner D. J., Espaillat C., Hughes A. M., Dullemond C. P., McClure M. K., Qi C., Brown J. M., 2011, ApJ, 732, 42

Antoniucci S. et al., 2011, A&A, 534, A32

Armitage P. J., 2007, ArXiv Astrophysics e-prints

Armitage P. J., 2011a, ARA&A, 49, 195

Armitage P. J., 2011b, ARA&A, 49, 195

Armitage P. J., Hansen B. M. S., 1999a, Nature, 402, 633

Armitage P. J., Hansen B. M. S., 1999b, Nature, 402, 633

Armitage P. J., Livio M., Lubow S. H., Pringle J. E., 2002, MNRAS, 334, 248

Armitage P. J., Simon J. B., Martin R. G., 2013, ApJ, 778, L14

Artymowicz P., Lubow S. H., 1994, ApJ, 421, 651

Avenhaus H., Quanz S. P., Schmid H. M., Meyer M. R., Garufi A., Wolf S., Dominik C., 2014, ApJ, 781, 87

Bai X. N., 2011, ApJ, 739, 50

Balbus S. A., Hawley J. F., 1991a, ApJ, 376, 214

Balbus S. A., Hawley J. F., 1991b, ApJ, 376, 214

Bally J., Scoville N. Z., 1982, ApJ, 255, 497

Balsara D. S., 1995, Journal of Computational Physics, 121, 357

Bastian N., 2008, MNRAS, 390, 759

Bate M. R., Burkert A., 1997, MNRAS, 288, 1060

Bate M. R., Bonnell I. A., Price N. M., 1995, MNRAS, 277, 362

Beccari G. et al., 2010a, ApJ, 720, 1108

Beccari G. et al., 2010b, ApJ, 720, 1108

Bell C. P. M., Naylor T., Mayne N. J., Jeffries R. D., Littlefair S. P., 2013, MNRAS, 434, 806

Biazzo K., Alcalá J. M., Covino E., Frasca A., Getman F., Spezzi L., 2012, A&A, 547, A104

Binney J., Tremaine S., 1987, Galactic dynamics

Birnstiel T., Dullemond C. P., Brauer F., 2010, A&A, 513, A79

Birnstiel T., Andrews S. M., Ercolano B., 2012a, A&A, 544, A79

Birnstiel T., Andrews S. M., Ercolano B., 2012b, A&A, 544, A79

Bondi H., 1952, MNRAS, 112, 195

Bondi H., Hoyle F., 1944, MNRAS, 104, 273

Bouy H., Alves J., Bertin E., Sarro L. M., Barrado D., 2014, A&A, 564, A29

Brandt T. D. et al., 2014, ApJ, 786, 1

Brown J. M., Blake G. A., Qi C., Dullemond C. P., Wilner D. J., Williams J. P., 2009, ApJ, 704, 496

Bruderer S., 2013, A&A, 559, A46

Bruderer S., van der Marel N., van Dishoeck E. F., van Kempen T. A., 2014, A&A, 562, A26

Calvet N., Muzerolle J., Briceño C., Hernández J., Hartmann L., Saucedo J. L., Gordon K. D., 2004, AJ, 128, 1294

Calvet N. et al., 2005a, ApJ, 630, L185

Calvet N. et al., 2005b, ApJ, 630, L185

Casassus S. et al., 2013, Nature, 493, 191

Casertano S., Hut P., 1985, ApJ, 298, 80

Chauvin G. et al., 2014, ArXiv e-prints

Chiang E. I., Goldreich P., 1997, ApJ, 490, 368

Cieza L. A. et al., 2010, ApJ, 712, 925

Clarke C. J., 2007, MNRAS, 376, 1350

Clarke C. J., Owen J. E., 2013, MNRAS, 433, L69

Clarke C. J., Pringle J. E., 1993, MNRAS, 261, 190

Clarke C. J., Pringle J. E., 2004, MNRAS, 351, 1187

Clarke C. J., Gendrin A., Sotomayor M., 2001a, MNRAS, 328, 485

Clarke C. J., Gendrin A., Sotomayor M., 2001b, MNRAS, 328, 485

Craig J., Krumholz M. R., 2013, ApJ, 769, 150

Crida A., Morbidelli A., 2007, MNRAS, 377, 1324

Crida A., Morbidelli A., Masset F., 2006, Icarus, 181, 587

Currie T., Kenyon S. J., 2009, AJ, 138, 703

Dale J. E., Ercolano B., Bonnell I. A., 2012, MNRAS, 424, 377

Dale J. E., Ercolano B., Bonnell I. A., 2013a, MNRAS, 430, 234

Dale J. E., Ercolano B., Bonnell I. A., 2013b, MNRAS, 430, 234

D'Alessio P., Cantö J., Calvet N., Lizano S., 1998, ApJ, 500, 411

D'Antona F., Mazzitelli I., 1994, ApJS, 90, 467

Davies R. E., Pringle J. E., 1980, MNRAS, 191, 599

de Gregorio-Monsalvo I. et al., 2013, A&A, 557, A133

de Juan Ovelar M., Kruijssen J. M. D., Bressert E., Testi L., Bastian N., Cánovas H., 2012, A&A, 546, L1

de Juan Ovelar M., Min M., Dominik C., Thalmann C., Pinilla P., Benisty M., Birnstiel T., 2013, A&A, 560, A111

De Marchi G., Panagia N., Romaniello M., 2010, ApJ, 715, 1

De Marchi G., Panagia N., Romaniello M., Sabbi E., Sirianni M., Prada Moroni P. G., Degl'Innocenti S., 2011a, ApJ, 740, 11

De Marchi G., Panagia N., Romaniello M., Sabbi E., Sirianni M., Prada Moroni P. G., Degl'Innocenti S., 2011b, ApJ, 740, 11

De Marchi G., Panagia N., Sabbi E., 2011c, ApJ, 740, 10

De Marchi G., Panagia N., Sabbi E., 2011d, ApJ, 740, 10

De Marchi G., Beccari G., Panagia N., 2013a, ApJ, 775, 68

De Marchi G., Panagia N., Guarcello M. G., Bonito R., 2013b, MNRAS, 435, 3058

De Marchi G., Panagia N., Guarcello M. G., Bonito R., 2013c, MNRAS, 435, 3058

De Marchi G. et al., 2011e, ApJ, 739, 27

De Marchi G. et al., 2011f, ApJ, 739, 27

Dullemond C. P., Dominik C., 2005a, A&A, 434, 971

Dullemond C. P., Dominik C., 2005b, A&A, 434, 971

Dullemond C. P., Hollenbach D., Kamp I., D'Alessio P., 2007a, Protostars and Planets V, 555

Dullemond C. P., Hollenbach D., Kamp I., D'Alessio P., 2007b, Protostars and Planets V, 555

Dutrey A. et al., 2008, A&A, 490, L15

Edgar R., Clarke C., 2004, MNRAS, 349, 678

Ercolano B., Drake J. J., Raymond J. C., Clarke C. C., 2008, ApJ, 688, 398

Ercolano B., Clarke C. J., Drake J. J., 2009, ApJ, 699, 1639

Ercolano B., Clarke C. J., Hall A. C., 2011a, MNRAS, 410, 671

Ercolano B., Clarke C. J., Hall A. C., 2011b, MNRAS, 410, 671

Ercolano B., Mayr D., Owen J. E., Rosotti G., Manara C. F., 2014, MNRAS, 439, 256

Espaillat C. et al., 2010a, ApJ, 717, 441

Espaillat C. et al., 2010b, ApJ, 717, 441

Espaillat C. et al., 2014, ArXiv e-prints

Fedele D., van den Ancker M. E., Henning T., Jayawardhana R., Oliveira J. M., 2010a, A&A, 510, A72

Fedele D., van den Ancker M. E., Henning T., Jayawardhana R., Oliveira J. M., 2010b, A&A, 510, A72

Font A. S., McCarthy I. G., Johnstone D., Ballantyne D. R., 2004, ApJ, 607, 890

Forgan D., Rice K., 2009, MNRAS, 400, 2022

Fressin F. et al., 2013, ApJ, 766, 81

Gammie C. F., 1996, ApJ, 457, 355

Garufi A. et al., 2013, A&A, 560, A105

Ghosh P., Lamb F. K., 1979a, ApJ, 232, 259

Ghosh P., Lamb F. K., 1979b, ApJ, 234, 296

Goddard Q. E., Bastian N., Kennicutt R. C., 2010, MNRAS, 405, 857

Gorti U., Hollenbach D., 2009a, ApJ, 690, 1539

Gorti U., Hollenbach D., 2009b, ApJ, 690, 1539

Gorti U., Dullemond C. P., Hollenbach D., 2009a, ApJ, 705, 1237

Gorti U., Dullemond C. P., Hollenbach D., 2009b, ApJ, 705, 1237

Güdel M. et al., 2007, A&A, 468, 353

Guilloteau S., Dutrey A., Piétu V., Boehler Y., 2011a, A&A, 529, A105

Guilloteau S., Dutrey A., Piétu V., Boehler Y., 2011b, A&A, 529, A105

Gullbring E., Hartmann L., Briceño C., Calvet N., 1998, ApJ, 492, 323

Haisch Jr. K. E., Lada E. A., Lada C. J., 2001, ApJ, 553, L153

Hall S. M., 1997, MNRAS, 287, 148

Hartmann L., 2009, Accretion Processes in Star Formation: Second Edition. Cambridge University Press

Hartmann L., Calvet N., Gullbring E., D'Alessio P., 1998, ApJ, 495, 385

Hayashi C., 1981a, Progress of Theoretical Physics Supplement, 70, 35

Hayashi C., 1981b, Progress of Theoretical Physics Supplement, 70, 35

Heller C. H., 1995, ApJ, 455, 252

Herczeg G. J., Hillenbrand L. A., 2008a, ApJ, 681, 594

Herczeg G. J., Hillenbrand L. A., 2008b, ApJ, 681, 594

Hernández J. et al., 2007, ApJ, 662, 1067

Hillenbrand L. A., Hartmann L. W., 1998, ApJ, 492, 540

Hollenbach D., Johnstone D., Lizano S., Shu F., 1994, ApJ, 428, 654

Hoyle F., Lyttleton R. A., 1939, Proceedings of the Cambridge Philosophical Society, 35, 405

Hubber D. A., Batty C. P., McLeod A., Whitworth A. P., 2011, A&A, 529, A27

Hubber D. A., Allison R. J., Smith R., Goodwin S. P., 2013a, MNRAS, 430, 1599

Hubber D. A., Falle S. A. E. G., Goodwin S. P., 2013b, MNRAS, 432, 711

Ilgner M., Nelson R. P., 2006, A&A, 445, 205

Indebetouw R. et al., 2013, ApJ, 774, 73

Isella A., Carpenter J. M., Sargent A. I., 2009, ApJ, 701, 260

Isella A., Pérez L. M., Carpenter J. M., 2012, ApJ, 747, 136

Johansen A., Youdin A., Klahr H., 2009, ApJ, 697, 1269

Johnstone D., Hollenbach D., Bally J., 1998a, ApJ, 499, 758

Johnstone D., Hollenbach D., Bally J., 1998b, ApJ, 499, 758

Kenyon S. J., Hartmann L., 1987, ApJ, 323, 714

Kenyon S. J., Hartmann L., 1995, ApJS, 101, 117

Kley W., 1999, MNRAS, 303, 696

Koenigl A., 1991, ApJ, 370, L39

Koepferl C. M., Ercolano B., Dale J., Teixeira P. S., Ratzka T., Spezzi L., 2013a, MNRAS, 428, 3327

Koepferl C. M., Ercolano B., Dale J., Teixeira P. S., Ratzka T., Spezzi L., 2013b, MNRAS, 428, 3327

Kraus A. L., Ireland M. J., Hillenbrand L. A., Martinache F., 2012, ApJ, 745, 19

Kruijssen J. M. D., 2012, MNRAS, 426, 3008

Kruijssen J. M. D., Maschberger T., Moeckel N., Clarke C. J., Bastian N., Bonnell I. A., 2012, MNRAS, 419, 841

Lada C. J., Lada E. A., 2003, ARA&A, 41, 57

Lada C. J., Wilking B. A., 1984, ApJ, 287, 610

Lada C. J., Margulis M., Dearborn D., 1984, ApJ, 285, 141

Lada C. J. et al., 2006, AJ, 131, 1574

Landau L. D., Lifshitz E. M., 2010, Mechanics. Elsevier Butterworth-Heinemann

Lee A. T., Cunningham A. J., McKee C. F., Klein R. I., 2014, ApJ, 783, 50

Liffman K., 2003, PASA, 20, 337

Lin D. N. C., Papaloizou J., 1979, MNRAS, 186, 799

Lodato G., Price D. J., 2010, MNRAS, 405, 1212

Lodato G., Pringle J. E., 2007, MNRAS, 381, 1287

Lodato G., Rice W. K. M., 2004, MNRAS, 351, 630

Lodato G., Meru F., Clarke C. J., Rice W. K. M., 2007, MNRAS, 374, 590

Longmore S. N. et al., 2014, Protostars and Planets VI, ??

Lubow S. H., D'Angelo G., 2006, ApJ, 641, 526

Luhman K. L., Allen P. R., Espaillat C., Hartmann L., Calvet N., 2010, ApJS, 186, 111

Lynden-Bell D., Pringle J. E., 1974, MNRAS, 168, 603

Lyo A. R., Ohashi N., Qi C., Wilner D. J., Su Y. N., 2011, AJ, 142, 151

Malmberg D., de Angeli F., Davies M. B., Church R. P., Mackey D., Wilkinson M. I., 2007, MNRAS, 378, 1207

Malmberg D., Davies M. B., Heggie D. C., 2011, MNRAS, 411, 859

Mamajek E. E., 2009, in T. Usuda, M. Tamura, M. Ishii, eds, American Institute of Physics Conference Series. American Institute of Physics Conference Series, Vol. 1158, pp. 3–10

Manara C. F., Robberto M., Da Rio N., Lodato G., Hillenbrand L. A., Stassun K. G., Soderblom D. R., 2012a, ApJ, 755, 154

Manara C. F., Robberto M., Da Rio N., Lodato G., Hillenbrand L. A., Stassun K. G., Soderblom D. R., 2012b, ApJ, 755, 154

Manara C. F., Testi L., Natta A., Rosotti G., Benisty M., Ercolano B., Ricci L., 2014, A&A, 568, A18

Manara C. F., Beccari G., Da Rio N., De Marchi G., Natta A., Ricci L., Robberto M., Testi L., 2013, A&A, 558, A114

Mann R. K., Williams J. P., 2010, ApJ, 725, 430

Masset F., 2000a, A&AS, 141, 165

Masset F., 2000b, A&AS, 141, 165

Mayor M., Queloz D., 1995, Nature, 378, 355

Mayor M. et al., 2011, ArXiv e-prints

McCaughrean M. J., O'dell C. R., 1996, AJ, 111, 1977

Miotello A., Robberto M., Potenza M. A. C., Ricci L., 2012, ApJ, 757, 78

Moeckel N., Armitage P. J., 2012, MNRAS, 419, 366

Moeckel N., Bally J., 2007, ApJ, 656, 275

Moeckel N., Throop H. B., 2009, ApJ, 707, 268

Mohanty S., Jayawardhana R., Basri G., 2005, ApJ, 626, 498

Mohanty S., Ercolano B., Turner N. J., 2013, ApJ, 764, 65

Monaghan J. J., 1997, Journal of Computational Physics, 136, 298

Monaghan J. J., Lattanzio J. C., 1985, A&A, 149, 135

Morishima R., 2012, MNRAS, 420, 2851

Morris J. P., Monaghan J. J., 1997, Journal of Computational Physics, 136, 41

Movshovitz N., Bodenheimer P., Podolak M., Lissauer J. J., 2010, Icarus, 209, 616

Murray J. R., 1996, MNRAS, 279, 402

Muzerolle J., Hartmann L., Calvet N., 1998, AJ, 116, 455

Muzerolle J., Hillenbrand L., Calvet N., Briceño C., Hartmann L., 2003, ApJ, 592, 266

Muzerolle J., Allen L. E., Megeath S. T., Hernández J., Gutermuth R. A., 2010, ApJ, 708, 1107

Natta A., Testi L., Muzerolle J., Randich S., Comerón F., Persi P., 2004, A&A, 424, 603

Natta A., Testi L., Randich S., 2006, A&A, 452, 245

O'dell C. R., 1998, AJ, 115, 263

O'dell C. R., Wen Z., Hu X., 1993a, ApJ, 410, 696

O'dell C. R., Wen Z., Hu X., 1993b, ApJ, 410, 696

Olczak C., Pfalzner S., Spurzem R., 2006, ApJ, 642, 1140

Olczak C., Kaczmarek T., Harfst S., Pfalzner S., Portegies Zwart S., 2012, ApJ, 756, 123

Owen J. E., 2014, ApJ, 789, 59

Owen J. E., Clarke C. J., 2012a, MNRAS, 426, L96

Owen J. E., Clarke C. J., 2012b, MNRAS, 426, L96

Owen J. E., Ercolano B., Clarke C. J., Alexander R. D., 2010a, MNRAS, 401, 1415

Owen J. E., Ercolano B., Clarke C. J., Alexander R. D., 2010b, MNRAS, 401, 1415

Owen J. E., Ercolano B., Clarke C. J., 2011a, MNRAS, 412, 13

Owen J. E., Ercolano B., Clarke C. J., 2011b, MNRAS, 412, 13

Owen J. E., Clarke C. J., Ercolano B., 2012a, MNRAS, 422, 1880

Owen J. E., Clarke C. J., Ercolano B., 2012b, MNRAS, 422, 1880

Owen J. E., Hudoba de Badyn M., Clarke C. J., Robins L., 2013, MNRAS, 436, 1430

Paardekooper S. J., Mellema G., 2006, A&A, 453, 1129

Padoan P., Kritsuk A., Norman M. L., Nordlund Å., 2005, ApJ, 622, L61

Pelupessy F. I., Portegies Zwart S., 2012, MNRAS, 420, 1503

Pfalzner S., 2008, A&A, 492, 735

Pfalzner S., Umbreit S., Henning T., 2005a, ApJ, 629, 526

Pfalzner S., Vogel P., Scharwächter J., Olczak C., 2005b, A&A, 437, 967

Pfalzner S., Tackenberg J., Steinhausen M., 2008, A&A, 487, L45

Piétu V., Dutrey A., Guilloteau S., Chapillon E., Pety J., 2006, A&A, 460, L43

Pinilla P., Benisty M., Birnstiel T., 2012a, A&A, 545, A81

Pinilla P., Benisty M., Birnstiel T., 2012b, A&A, 545, A81

Pinilla P., Birnstiel T., Ricci L., Dullemond C. P., Uribe A. L., Testi L., Natta A., 2012c, A&A, 538, A114

Pollack J. B., Hubickyj O., Bodenheimer P., Lissauer J. J., Podolak M., Greenzweig Y., 1996, Icarus, 124, 62

Preibisch T. et al., 2005, ApJS, 160, 401

Price D. J., Monaghan J. J., 2007, MNRAS, 374, 1347

Rahman M., Matzner C. D., Moon D. S., 2013, ApJ, 766, 135

Ribas Á., Merín B., Bouy H., Maud L. T., 2014, A&A, 561, A54

Ricci L., Robberto M., Soderblom D. R., 2008, AJ, 136, 2136

Rice W. K. M., Wood K., Armitage P. J., Whitney B. A., Bjorkman J. E., 2003, MNRAS, 342, 79

Rice W. K. M., Armitage P. J., Wood K., Lodato G., 2006, MNRAS, 373, 1619

Robberto M. et al., 2013, ApJS, 207, 10

Rosenfeld K. A., Chiang E., Andrews S. M., 2014, ApJ, 782, 62

Rosenfeld K. A. et al., 2012, ApJ, 757, 129

Rosotti G. P., Ercolano B., Owen J. E., Armitage P. J., 2013, MNRAS, 430, 1392

Ruden S. P., 2004, ApJ, 605, 880

Ruffert M., 1997, A&A, 317, 793

Salpeter E. E., 1955, ApJ, 121, 161

Sargent A. I., Beckwith S., 1987, ApJ, 323, 294

Scally A., Clarke C., 2001, MNRAS, 325, 449

Shakura N. I., Sunyaev R. A., 1973a, A&A, 24, 337

Shakura N. I., Sunyaev R. A., 1973b, A&A, 24, 337

Shu F., Najita J., Ostriker E., Wilkin F., Ruden S., Lizano S., 1994, ApJ, 429, 781

Shu F. H., Adams F. C., Lizano S., 1987, ARA&A, 25, 23

Sicilia-Aguilar A., Henning T., Hartmann L. W., 2010, ApJ, 710, 597

Sicilia-Aguilar A., Henning T., Kainulainen J., Roccatagliata V., 2011, ApJ, 736, 137

Sicilia-Aguilar A., Kim J. S., Sobolev A., Getman K., Henning T., Fang M., 2013, ArXiv e-prints

Siess L., Dufour E., Forestini M., 2000, A&A, 358, 593

Silva-Villa E., Adamo A., Bastian N., 2013, ArXiv e-prints

Skrutskie M. F., Dutkevitch D., Strom S. E., Edwards S., Strom K. M., Shure M. A., 1990a, AJ, 99, 1187

Skrutskie M. F., Dutkevitch D., Strom S. E., Edwards S., Strom K. M., Shure M. A., 1990b, AJ, 99, 1187

Soderblom D. R., Hillenbrand L. A., Jeffries R. D., Mamajek E. E., Naylor T., 2013, ArXiv e-prints

Springel V., Hernquist L., 2002, MNRAS, 333, 649

Stolte A. et al., 2010, ApJ, 718, 810

Stone J. M., Norman M. L., 1992, ApJS, 80, 753

Strom K. M., Strom S. E., Edwards S., Cabrit S., Skrutskie M. F., 1989a, AJ, 97, 1451

Strom K. M., Strom S. E., Edwards S., Cabrit S., Skrutskie M. F., 1989b, AJ, 97, 1451

Throop H. B., Bally J., 2008, AJ, 135, 2380

Toomre A., Toomre J., 1972, ApJ, 178, 623

Turner N. J., Drake J. F., 2009, ApJ, 703, 2152

Turner N. J., Fromang S., Gammie C., Klahr H., Lesur G., Wardle M., Bai X. N., 2014, ArXiv e-prints

van der Marel N. et al., 2013, Science, 340, 1199

Varnière P., Tagger M., 2006, A&A, 446, L13

Walch S., Naab T., Whitworth A., Burkert A., Gritschneder M., 2010, MNRAS, 402, 2253

Weidenschilling S. J., 1977a, MNRAS, 180, 57

Weidenschilling S. J., 1977b, Ap&SS, 51, 153

Weintraub D. A., Sandell G., Duncan W. D., 1989, ApJ, 340, L69

Williams J. P., Cieza L. A., 2011a, ARA&A, 49, 67

Williams J. P., Cieza L. A., 2011b, ARA&A, 49, 67

Youdin A. N., Shu F. H., 2002, ApJ, 580, 494

Zhang K., Isella A., Carpenter J. M., Blake G. A., 2014, ApJ, 791, 42

Zhu Z., Nelson R. P., Hartmann L., Espaillat C., Calvet N., 2011, ApJ, 729, 47

Zhu Z., Nelson R. P., Dong R., Espaillat C., Hartmann L., 2012, ApJ, 755, 6

Acknowledgements

First of all, I would like to thank Barbara for believing in me since the first time we met (actually, even from the first e-mail I wrote her), for pushing me constantly in my work and guiding me through all the difficulties that every research work has, and for being always there every time I needed her. And thanks to all the group (present, past and future - I'm looking at you Dominika!), especially Til, Jim, David, Martin, I have learned so much from all of you. Thank you Daniel, George, Dennis (I'm sure I have not learned yet how to spell it correctly) - I enjoyed working together with you. I would like to thank all of my collaborators, in particular James. Thank you to Leonardo in particular and all the other participants of the star formation coffee at ESO, for teaching me that there is much more beyond an observation than what my little mind thought, thank you to Veronica for all of your coffees - including the star formation one at the USM, that I 'd also like to thank. Thank you to all the other students that I spent these years with - I think in particular to Carlo, Marco, Alex, Annalisa, Anna, Judith.

I would also like to thank all the great friends that I found these years here in Munich - thank you Lucia, Giovanni, Thomas, Isa, Marco, Anna, Vito, Andrea, Stephan, and all the other ones.

And thank you mum and dad - how would have we done, without knowing that we could always rely on you? Thank you Teresa - for making my life perhaps a bit more complicated, but much more beatiful. And finally, the latest and greatest thank to my Margherita.